# Rabconnectin3α promotes stable activity of the H+-pump on synaptic vesicles in hair cells

by

Zev B. Einhorn

A dissertation in partial fulfillment of the requirements for the degree of Doctor of Philosophy

Presented to the Neuroscience Graduate Program

Oregon Health & Science University

School of Medicine

November 2012

School of Medicine

Oregon Health & Science University

---

CERTIFICATE OF APPROVAL

---

This is to certify that the Ph.D. dissertation of

ZEV EINHORN

has been approved on November 9, 2012

---

Advisor, Teresa Nicolson, PhD

---

Member and Chair, Laurence Trussell, PhD

---

Member, Phil Stork, MD

---

Member, Peter Mayinger, PhD

---

Member, Craig Jahr, PhD

# Table of Contents

List of Figures ..... iv

Acknowledgements..... vi

Abstract ..... viii

**Chapter 1 – Introduction** ..... 1

**Chapter 2 – Determining subtle auditory deficits in mutant zebrafish** ..... 13

Summary ..... 14

Introduction ..... 15

Methods ..... 16

Results ..... 21

Determination of response rates to the acoustic tap and specificity of the acoustic stimulus ..... 22

Determining the best frequency of response and sound pressure level ..... 22

Proof of principle: the *stardust* mutant ..... 24

*Stardust* mutants exhibit normal startle movements ..... 25

*Stardust* mutants show abnormal response to pure-tone stimuli . 26

Conclusion ..... 27

Similarities between auditory and vestibular hair cells ..... 27

Verification of an improved method for assaying auditory escape behaviors ..... 28

**Chapter 3 - Cloning, Structure, and Localization of Rabconnectin3α** ..... 37

Summary ..... 38

Introduction ..... 39

Methods ..... 41

Results ……... 45

Positional mapping of *stardust* and generation of *rabconnectin3α* cDNA ……. 45

Tissue expression profile of *rbc3α* mRNA …… 47

Rbc3α is distributed within synaptic regions of the hair cell …….. 48

Conclusion ……. 54

The tissue distribution of Rbc3α indicates its synaptic utilization 55

The distribution of Rbc3α in the hair cell is synaptic ……..…… 56

**Chapter 4 - Rabconnectin3α promotes stable activity of the $H^+$-pump on synaptic vesicles in hair cells** ……. 65

Authors ……... 65

Acknowledgements ……..…… 65

Summary …… 66

Introduction ……... 67

Methods ……. 69

Results ……... 76

*Rbc3α* mutant hair cells fail to properly acidify synaptic vesicles . 76

Proper synaptic localization of V-ATPase subunits requires Rbc3α ……... 79

Synaptic composition is normal in *rbc3α* mutants …….. 82

Synaptic activity is reduced in *rbc3α* mutants …….. 84

Conclusion ……. 90

**Chapter 5 – Conclusion** …… 103

Summary of main findings ……... 103

A model for Rbc3 at the synaptic vesicle ……... 103

Rbc3α in auditory and visual behaviors ……. 104

Rbc3α selectively enhances synaptic vesicle acidification ……. 108

Rbc3α does not organize the hair-cell synapse …… 110

References …….. 114

# List of Figures

Figure 1.1 Transmission at the hair-cell synapse ……... 10

Figure 2.1 Experimental setup to determine the auditory escape behavioral response of larval zebrafish …… 32

Figure 2.2 Wild-type but not deafness mutant *pcdh15*$^{R360X}$ larvae respond to acoustic tap and strong pure-tone stimuli …… 33

Figure 2.3 Determination of the best frequency and sound pressure level of the larval AEBR ……... 34

Figure 2.4 Homozygous *stardust/rbc3*$\alpha$ mutants have normal motor activity (5 dpf) ……... 35

Figure 2.5 Homozygous *stardust/rbc3*$\alpha$ mutants have auditory and vestibular deficits (5 dpf) ……... 36

Figure 3.1 Positional mapping and cloning of *rbc3*α …….. 59

Figure 3.2 Expression of *rbc3*α …….. 61

Figure 3.3 Rbc3α constructs used for expression experiments …… 62

Figure 3.4 Rbc3α localizes to synaptic regions in the hair cell ……. 63

Figure 4.1 Rbc3α is required for proper acidification of basal vesicles ……... 95

Figure 4.2 A C-terminal fragment of Rbc3$\alpha$ does not inhibit acidification ……... 97

Figure 4.3 Cytosolic V1 sectors are redistributed in *rbc3*$\alpha$ mutants …… 98

Figure 4.4 Loss of Rbc3α function does not affect hair-cell synaptic components ……..…… 100

Figure 4.5 The rate and fidelity of stimulus-dependent spiking of lateral-line afferent neurons is reduced in *rbc3*$\alpha$ mutants …….. 101

Figure 5.1 Rbc3α at the hair-cell synapse …….…….. 112

**Acknowledgments**

I thank Dr. Teresa Nicolson for her generous and thoughtful guidance and contributions to my thesis work over the last 6 years. Teresa has been willing to think deeply about the scientific problems that I proposed, and enabled me to complete many experiments in her laboratory. I appreciate her driving the lab members to coordinate with each other and become each other's teachers. This thesis would not be possible without the contributions of several colleagues within Dr. Nicolson's laboratory, including Dr. Josef G. Trapani who performed all the electrophysiology experiments and Dr. Qianyong Liu who was instrumental in the identification of zebrafish mutant lines.

I thank my committee members, Dr. Laurence Trussell, Dr. Peter Mayinger, Dr. Philip Stork and Dr. Craig Jahr. Each of the members offered helpful scientific suggestions as well as encouraged me to stay focused. In addition, I would like to thank the Neuroscience Graduate Program Directors, Dr. Gary Westbrook and Dr. Peter Gillespie as well as our Coordinator, Liz Lawson for doing so much to make the graduate experience possible.

Finally, I would like to thank my best friends in Graduate School, Daniel Lioy-Ryan and Kateri Spinelli who loved me and let me love them and showed me the way to be a better scientist, and my family members who have always been excited for me.

## Abstract

Nearly 2 of every 1,000 children have congenital deafness. To date, more than more 60 genetic loci have been identified that contribute to nonsyndromic forms of inherited deafness. In order to understand how these genes affect hearing and balance, the Nicolson laboratory in collaboration with a large Tübingen Consortium has identified several genes important for the function of the hair cell, the sensory detector of the auditory, vestibular and lateral-line organ systems in mutagenized zebrafish. This thesis characterizes a new player, Rabconnectin3α, and its previously unknown contribution to hearing and synaptic vesicle acidification in hair cells. Chapter 1 gives a background of the literature of hearing with regard to operation of the hair cell and the use of a zebrafish as a genetic model of deafness. Chapter 2 follows the experimental set-up of a new testing procedure for discriminating hearing deficits in zebrafish and presents the role of Rabconnectin3α in zebrafish hearing. Chapter 3 presents data on the cloning and identification of a mutant zebrafish line containing genetic lesions in the gene *rabconnectin3α*, and also characterizes its tissue and subcellular distribution. Chapter 4 describes the contribution of Rabconnectin3α to the stable activity of the Vacuolar-type Proton Pump in hair cells, and defines its role in proper acidification of the lumen of the synaptic vesicle. Taken together, this thesis highlights the importance of Rabconnectin3α to hearing and balance.

# Chapter 1 - Introduction

*The hair-cell synapse is specialized for continuous release of synaptic vesicles*

Sensory hair cells of the auditory system transduce sound signals into graded electrical changes (reviewed in Nouvian et al., 2006). Similarly, sensory hair cells of the vestibular system detect and transduce forces produced by gravity and linear and angular acceleration of the head. The graded depolarization of the hair cell opens voltage-gated Cav1.3 channels that allow the sustained entry of $Ca^{2+}$ (Zenisek et al., 2003), triggering synaptic vesicle release of neurotransmitter onto afferents (Nouvian et al., 2006). The hair cell is capable of continuous exocytosis during sustained presentations of sound. In order to accomplish this, the hair cell has evolved various synaptic specializations, for example, the Cav1.3 channels. A cartoon diagram of the hair-cell synapse and several molecular players that were identified by our laboratory are displayed in Figure 1.1.

Of all its specializations, however, a prominent structural element of the hair-cell synapse is the presynaptic ribbon body, which appears as an electron dense body surrounded by tethered synaptic vesicles under an electron microscope (Lenzi et al., 1999). The role of the ribbon is still under investigation, but it might contribute to the replenishment of spent synaptic vesicles (Snellman et al., 2011), coordinating multi-vesicular release (Buran et al., 2010) in order to ensure rapid and faithful transmission of the encoded sound signal, or organize the synapse (Sheets et al., 2011). While we know the main component of the

ribbon is the protein Ribeye/CtBP2 (Schmitz et al., 2000, Zenisek et al., 2003), we have limited understanding of the players that govern the life cycle of a synaptic vesicle in hair cells (Zanazzi and Matthews 2009). How, for instance, are synaptic vesicles brought to the ribbon, filled with neurotransmitter, and ultimately released?

Recently, the small GTPase Rab3 was isolated in association with synaptic ribbons (Uthaiah and Hudspeth 2010). In chicken hair cells, immunolabeled Rab3 has a punctate staining pattern that overlaps with Ribeye at both the light and ultrastructural levels (Uthaiah and Hudspeth 2010). Intriguingly, Rab3 is also involved in the localization of the active zone protein Bruchpilot at presynaptic densities, or T-bars, of the Drosophila neuromuscular junction (Graf et al., 2009). This finding is notable because Drosophila T-bars have ribbon-like similarities at the ultrastructural level (Binnington and Lane 1982). While the molecular repertoire utilized by central and ribbon-type synapses differ (Zanazzi and Matthews 2009), vesicle trafficking at ribbon-type synapses may rely on Rab3 as it does at central synapses (Wang et al., 1997). Rab3 has 4 isoforms, a – d, which are regulated by Rab3 GTPase Exchange Protein (GEP) and Rab3 GTPase Activating Protein (GAP); (Wada et al., 1997, Fukui et al., 1997). Rab3 GEP and Rab3 GAP regulate the GTP- and GDP- binding states of Rab3, respectively. In its activated GTP-bound state, Rab3 translocates to the synaptic vesicle via geranylgeranylation, and can play a role in synaptic plasticity and synaptic vesicle release (Mahoney et al., 2006, Pavlos et al., 2010). Therefore, the role of Rab3 in ribbon synapse development and its possible contribution to

vesicle trafficking to the ribbon synapse is of great interest. Similarly, the regulators of Rab3 are also of interest as they too affect the trafficking of vesicles to the synapse (Tanaka et al., 2001, Niwa et al., 2008).

*The role of Rabconnectin3α is poorly understood*

The protein Rabconnectin3α (Rbc3α) was first purified from the rat hippocampus in a screen for interacting partners with Rab3 GEP and GAP on synaptic vesicles (Nagano et al., 2002). Originally, Rbc3α was proposed to act as a protein scaffold on synaptic vesicles that could coordinate Rab3 regulation by Rab3 GEP and Rab3 GAP. The Rbc3α protein is large, highly conserved, and has multiple WD-40 domains that may represent protein interaction sites based on the ability of other WD-40 domain containing proteins to have multiple interacting partners (Wall et al., 1995). Additionally, Rbc3α dimerizes with non-homologous Rbc3β to form the Rbc3 complex (Kawabe et al., 2003). The complex was also identified as solely present in neural tissues by Western Blot methods. One concern with the above studies is that the affinity purified antibodies used for immunolocalization and Western Blot experiments in the original studies were not validated for specificity. In addition, a clear demonstration that the Rbc3 complex has a role at the synapse was lacking. The only *in vivo* evidence that the complex regulates $Ca^{2+}$-dependent release comes from an experiment in which a C-terminal fragment of the Rbc3α protein was overexpressed in PC12-cell culture and the exocytosis of secretory granules was modestly reduced (Sakisaka and Takai 2005). To date, there have been no

further functional studies regarding the relationship between either Rbc3 complex and Rab3, or Rab3 regulators GEP and GAP prior to our examination (Einhorn et al., 2012).

The first clear biological functional study of the Rbc3 complex came from a genetic screen for genes that affect the acidification of various organelles within larval retinal and ovarian tissues of *Drosophila* (Yan et al., 2009); several mutant alleles of both *rbc3α* and *β* as well as mutant alleles within subunits of the Vacuolar-type ATPase (V-ATPase, or proton pump) were isolated in the screen. The authors predicted that the Rbc3-deficient phenotype might be due to mis-regulation of the Vacuolar-type ATPase (V-ATPase, which is also called the proton pump). Supporting this prediction, the researchers found that an exogenously expressed version of Rbc3β interacted with the E and H subunits of the V-ATPase. In the affected mutant fly tissues, endocytosis and Notch signaling were impaired as an indirect result of de-acidifcation of endosomal compartments. These findings were also observed in various mammalian cell-culture experiments (Sethi et al., 2010). The similarity of the Rbc3 phenotype across species and cell-types argues against Rbc3 as a brain-specific complex (Nagano et al., 2002, Kawabe et al., 2003), but it does not rule out a synaptic function for the complex.

In order to identify additional candidate pathways in which Rbc3α might serve a function, a proteomics based approach was undertaken to find interactors with Rbc3α (Li et al., 2012). In this study, the authors confirmed the association between Rbc3α and Rbc3β and also between Rbc3α and several

subunits of the V-ATPase. In contrast, the authors did not find Rab3, Rab3 GEP, or Rab3 GAP (Li et al., 2012). We also examined the experimental data and noted that Rbc3α might interact with several synaptic-vesicle associated proteins: Syntaxin 1-b, NSF, and Synaptojanin-1 which are involved in exocytosis, vesicle recycling, and endocytosis (reviewed in Südhof 2004), respectively. Additionally, Synaptojanin-1 and NSF are required for proper hair-cell synaptic activity in the zebrafish larvae (Trapani et al., 2009, Mo and Nicolson 2011), and Syntaxin 1 is present at the hair-cell synapse (Ramakrishnan et al., 2009). Collectively, the various studies of Rbc3α merit further clarification with regard to its association with Rab3 as well as further investigation of its role in shaping the activity of the V-ATPase.

The mechanisms by which Rbc3α contributes to the synapse are becoming clear (Einhorn et al., 2012). The activity of the V-ATPase on synaptic vesicles results in the creation of the proton electro-chemical gradient that drives the filling of synaptic vesicles with neurotransmitter (reviewed in Edwards 2007). It is possible that the loss of functional Rbc3α disrupts V-ATPase activity on the vesicle, thereby reducing neurotransmitter uptake. With regard to hearing, hair cells utilize the Vesicular glutamate transporter 3 (Vglut3, Obholzer et al., 2008, Seal et al., 2008, Ruel et al., 2008), which also relies on the proton electro-chemical gradient for its transport activity (reviewed in Edwards 2007). Therefore the loss of Rbc3α could ultimately impair transmission at the hair-cell synapse.

*Hearing in zebrafish lacking Rbc3α*

The search for the unique molecular players that orchestrate the demanding operations of the hair cell is ongoing. This is in part due to limited quantities of biological material from which proteome- and transcriptome-level experiments can be conducted (Gillespie and Hudspeth 1991). In spite of the limited understanding of the molecular anatomy of the hair cell, several important players have been identified through the mapping of inherited forms of deafness and vestibular dysfunction in human subjects and animal models (hereditaryhearingloss.org).

To this end, large-scale genetic screens of *N*-ethyl-*N*-nitrosourea (ENU)-mutagenized zebrafish were performed to isolate genes that contribute to hearing and balance by a consortium of researchers (Granato et al., 1996, Nicolson et al., 1998). Larvae were selected that were morphologically normal, displayed no obvious motor deficits, responded to touch, but had impaired auditory escape behavioral responses (AEBR) during an acoustic stimulus. In addition, mutant larvae exhibited obvious balance deficits such as upside-down swimming, or circling. From the genetic screen, several lines were isolated that carry mutations that specifically affect the synaptic performance of hair cells. These synaptic players include Cav1.3 (Sidi et al., 2004), Vglut3 (Obhholzer et al., 2008), Synj1 (Trapani et al., 2009), NSF (Mo and Nicolson et al., 2011) and Rabconnectin3α (Rbc3α, Einhorn et al., 2012).

Zebrafish larvae are advantageous as an experimental system for the genetic dissection of hearing and balance (Nicolson 2005). First, unbiased

genetic screens of zebrafish larvae for auditory/vestibular mutants successfully identified several genes critical for the function of the hair cell (Nicolson et al., 1998). These isolated mutant lines also included several alleles of the gene *rbc3α* (Einhorn et al., 2012). Screens were performed by assaying larvae for the presence of an AEBR when presented with an acoustic tap generated by the researcher on the side of the petri dish. The AEBR is a simple, well-defined behavior that in adult zebrafish requires a 60 dB higher sound pressure to activate than does the auditory brainstem response, measured by electrophysiological methods (Higgs et al., 2002). The AEBR is produced by a monosynaptic connection between an auditory hair cell of the inner ear and a giant hindbrain neuron called the Mauthner cell. When activated, the Mauthner cell mediates the motor circuitry that produces a stereotyped escape behavioral response (Zottoli, 1977, Kohashi et al., 2008). Because the Mauthner-mediated escape response is activated by both touch and acoustic stimuli, it is possible to ensure that an impaired AEBR is not the result of defects downstream of hearing due to the presence of a normal touch response. Taken together, the AEBR provides a simple, quantifiable measure of auditory function and can be performed on a large scale (Zeddies et al., 2005, Nicolson et al., 1998).

Additionally, larval hearing develops quickly between 4 and 5 days post fertilization (Zeddies et al., 2005) and therefore allows the functional examination of genes that are otherwise lethal in deficient adults. Finally, zebrafish are advantageous to examine hair cell function because they contain not only the inner ear organs that detect sound (the sacculus), gravity (the utricle), and

rotation of the head (the three cristae), they also have a third sensory organ system called the lateral-line organ, which detects water movement over the ear and body of the animal (reviewed in Dambly-Chaudière et al., 2003). The lateral-line organ is readily accessible to *in vivo* examination without the constraints of tissue culture because the hair cells are superficially located along the head and trunk of the animal. Furthermore, the lateral-line organ is also organized in simple rosettes that have 10 - 12 hair cells per organ, and only 3 to 5 ribbons per hair cell at 5 dpf (Sheets et al., 2011), which reduces the complexity of the system being observed. The lateral-line organs makes afferent and efferent connections with superficial ganglia located proximal to the ear and are also easily accessible for electrophysiological assays in an intact animal. As such, the lateral-line organ provides an approachable system with which to dissect the operation of the hair cell, despite the evolutionary divergence between the inner-ear and lateral-line organs (Ghysen and Dambly-Chaudière et al., 2007).

*Goal of hair-cell research*

Our aim is to identify and characterize novel components of the hair-cell synapse. In this study I investigated hearing- and balance- defective zebrafish, and particularly alleles of the mutant *stardust*, which encode nonsense mutations in the gene *rabconnectin3α*. In Chapter 2, I describe improved methods to determine subtle hearing impairments in larval zebrafish. In Chapter 3, I describe the mutations that underlie the various *rbc3α* alleles and examine synaptic distribution of the protein in hair cells. In Chapter 4, I examine the functional

significance of the interactions between Rbc3α and the V-ATPase and Rbc3α and Rab3. From our collective data, we find that Rbc3α plays a role in the local assembly of the V-ATPase on synaptic vesicles in hair cells and is necessary for proper hair-cell synaptic transmission, and ultimately auditory and vestibular behaviors.

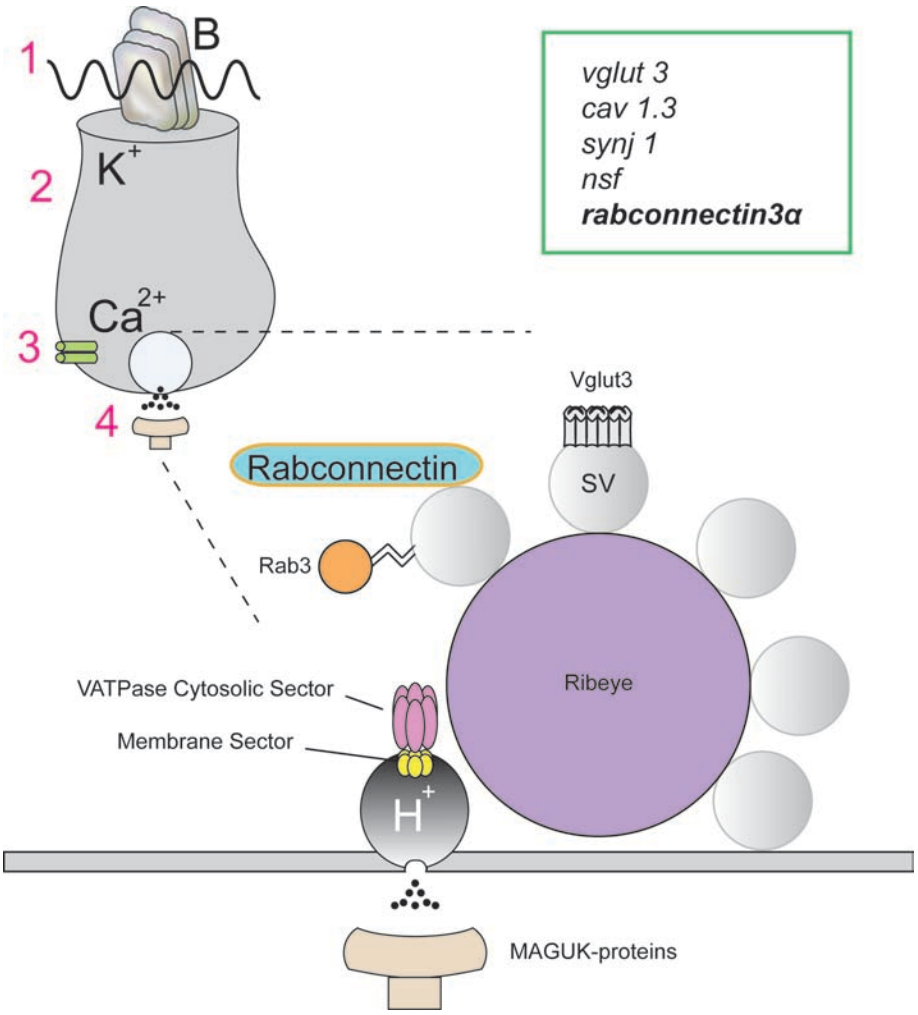


Figure 1.1 Transmission at the hair-cell synapse

Step 1: The hair cell has a mechanosensitive transduction apparatus within the apical stereocilia bundles (B). When vibratory stimuli, such as sound, pass over the apical bundles, the bundles are deflected and the mechanotransduction elements open. Step 2: This results in graded depolarizations of the hair cell. Step 3. Voltage-gated Cav1.3 channels (depicted in green) that are clustered at the synapse, allowing the entry of $Ca^{2+}$ that triggers synaptic vesicle release in Step 4. With regard to this study, the major molecular players at the hair-cell

ribbon synapse are illustrated in the bottom of the diagram between the dashed lines. Ribeye is the major component of the ribbon body (depicted in purple) and is surrounded by synaptic vesicles (SV). The small GTPase Rab3 (depicted in orange) translocates to synaptic vesicles in its activated, GTP-bound state. Its role at the ribbon synapse is unknown. Synaptic vesicles in hair cells are loaded with the neurotransmitter glutamate through the actions of the Vesicular glutamate transporter 3 (Vglut3). Vglut3 relies on a proton electrochemical gradient to drive its transport activity. The proton gradient ($H^+$) is established by the holoenzyme V-ATPase, which is composed of a cytosolic sector (lavender) and a membrane sector (yellow). The V-ATPase is regulated by the Rabconnectin3 complex (blue), which was originally found to be a synaptic vesicle scaffold upon which Rab3 might be regulated. When synaptic vesicles release their neurotransmitter contents, afferent neurons (beige) transmit to higher-order neural tissues the encoded sound signals. In zebrafish hair cells, post-synaptic densities can be immunolabeled with antibodies directed against MAGUK-domain containing proteins. The upper right box is a list of zebrafish mutants isolated in forward genetic screens for aberrant auditory/vestibular behaviors that were identified as containing genetic lesions in components of the synaptic-transmission machinery within the hair cell.

# Chapter 2 - Determining subtle auditory deficits in mutant zebrafish

Zev Einhorn and Teresa Nicolson

**Summary of Chapter**

Larvae were screened for auditory and vestibular behavioral deficits in response to a light acoustic tap on the side of a petri dish. Several of the mutations underlying the aberrant auditory/vestibular behaviors within various mutant lines were subsequently identified. Curiously, many balance-defective mutants are able to perform auditory escape behavioral responses (AEBR) when presented with the acoustic tap stimulus. The robust auditory function in the various vestibular mutant lines is puzzling, considering the shared transcript expression profiles of many of the lesioned genes in both auditory and vestibular hair cells. I hypothesized that the acoustic tap activates the AEBR at levels well above a threshold response rate of 50% and that as a consequence, testing for subtle hearing deficits by the behavioral assay is confounded by excessively strong stimulation. I reasoned that pure-tone stimulus presentations could be better controlled and adjusted to levels that are detectable over a dynamic range by wild-type larvae. Therefore, I modified existing methods to present pure-tone stimuli over a dynamic range of suitable pure-tone frequencies and sound pressure levels for behavioral testing. In this Chapter, I describe the successful implementation of the pure-tone test. With the improved method I discriminated a subtle hearing impairment in the vestibular mutant stardust, which had not been detected previously. Thus the improved method validates the hypothesis that in some instances, mutations that perturb the performance of the vestibular system can also have subtle effects on auditory system functionality.

## Introduction

Zebrafish are an excellent model system in which to study the key components of the hair-cell machinery. Thousands of lines of ENU-mutagenized zebrafish were screened with a behavioral assay for auditory/vestibular dysfunction (Nicolson et al., 1998). From this screen, several lines of recessive auditory/vestibular mutants were isolated that contained lesions in genes that specifically affect the operation of the hair cell. The behavioral screen consisted of a simple assay for the AEBR following presentation of an acoustic tap stimulus. The AEBR is a behavior that is well-defined at the anatomical level (Korn and Faber 2005), in which only a few synaptic connections underlie the response. Hair cells in the sacculus are activated by acoustic vibrations and transmit encoded sound signals along the statoacoustic nerve to a large reticulospinal neuron called the Mauthner-cell. When activated, the Mauthner-cell excites contralateral motor neurons and inhibits ipsilateral motor neurons through parallel spinal networks. As a result, the larva performs a characteristic C-turn flexure that reorients the animal in order to escape a potential threat, such as a predator. The assay is capable of determining an auditory phenotype in profoundly deaf animals and can be scaled for large screens.

Although the auditory behavioral screen was seemingly robust, it had a confounding result; several mutant lines appeared to have obvious balance defects, but the animals still responded at near wild-type rates to the acoustic tap, suggesting no auditory defect. This result is surprising considering the similarities of the auditory and vestibular hair cells, and would argue that the acoustic tap

stimulus protocol was not sensitive enough to detect subtle auditory dysfunction. The ability to discriminate subtle hearing deficits requires behavioral testing with auditory stimuli that are at the lower range of detection. In addition, the acoustic tap is difficult to control because the content is inherently multispectral and focal and may mimic a particularly aversive threat such as an oncoming predator. Therefore, I adapted an existing method for testing the AEBR (Zeddies et al., 2005, Prober et al., 2006). I presented pure-tone stimuli from a non-focal source to larvae over a range of sound pressure levels, and with the aid of a semi-automated apparatus captured and analyzed the larval escape response. I found that pure-tone stimuli could be adjusted to levels that covered a dynamic range of response within wild-type animals, and were therefore suitable for testing animals with subtle auditory deficits. Using this method, I was able to discriminate subtle auditory deficits within the vestibular-mutant *stardust*.

**Methods**

*High-speed video capture of auditory escape response*

Wild-type and mutant *rbc3*$\alpha$ larvae at 5 dpf were placed in a standard petri dish filled with E3 buffer. AEBRs induced by a light tap generated by the researcher to the side of a dish were imaged using a FASTCAM PCI512 high speed CCD camera (Photron). Images were captured at 1000 fps (512X512 pixels). Several larvae (*n* = 5 each genotype) were imaged simultaneously on a Zeiss Axiovert 100 microscope and analyzed by ImageJ software.

*Experimental apparatus*

Experiments were performed in a Zebrabox (Figure 2.1, Viewpoint Lifesciences). Larvae at 5 dpf were placed in 200 µl of E3 buffer in a standard translucent 96-well microplate (Corning Life Sciences). On command, the plate was vibrated by a Type 4810 shaker (Brüel & Kjær) in the dark inside a Zebrabox monitoring system (ViewPoint Life Sciences). Pure-tone stimuli delivered by the shaker were generated with VideoTrack version 3 software (ViewPoint Life Sciences) and amplified by STR-DG510 sound system (Sony). Sound pressures (SPL) were determined by placing a hydrophone (WP-23502- P16; Knowles Electronics) at the bottom of each well and recording voltage amplitudes with a TDS 1002B oscilloscope (Tektronix). According to the manufacturer datasheet, the hydrophone does not attenuate in frequency ranges from 100-1200 Hz. Voltages were then compared with an acoustic calibrator at 94 dB and 1 kHz in air (model 521; AcoPacific). Voltages were converted to decibels using 1 µPa as a reference pressure, the standard for US Naval measurement of pressure under water. The sound pressure levels at all frequencies were measured repeatedly. Every doubling of the voltage was the equivalent of an increase in 6 dB. Other groups reported that in small wells the measured sound pressure level (SPL) was not affected by the volume of water (Zeddies et al., 2005), arguing that the small wells had an acoustic impedance similar between air and water. In our hands, however, the addition of water increased the voltage readout on the oscilloscope and thus efforts were made to use 200 µl as a standard volume for all wells. The

pressure varied to some extent across the testing platform, +/- 3 dB, and therefore only center wells were used for measurement and behavioral testing.

Stimuli were presented for 100 ms at 400, 600, 800 and 1000 Hz with pressure levels of 132, 138, or 146 dB. Behavioral responses were recorded using a Dragonfly2 Camera CCD (Point Grey Research) and binned into 2 s timeframes with the VideoTrack software. According to the VideoTrack user manual, the operating procedure for the VideoTrack system uses an analogue voltage signal over time to scan a rapid image. I chose a frame rate of 10 images/second. Each point (800*600) in the image has a luminosity value (0-255, 8-bit dynamic range) that is converted to a digital value. The video image is converted to a binary image, where each pixel is black (0) or white (1). This allows the VideoTrack software to detect the animal from the background after contrast thresholding is obtained. Camera and VideoTrack settings were as follows: 100 ms shutter speed, 10 dB gain, 10 fps frame rate, 12 pixels detection sensitivity, 50 pixels burst activity threshold, and 10 pixels freeze behavior. An infrared light source continuously illuminated the larvae. For quantification of the auditory escape behavioral response (AEBR), six trials were performed per larvae with 3 minutes of rest between trials for a given stimulus. Larvae were placed in central wells in order to limit differences in sound pressure levels between the edges of the plate and more central wells. A response was scored as positive if an animal generated burst activity above a 50 pixel change.

*Optimization of the ZebraBox Apparatus*

Before beginning the experiments to determine the auditory function of various vestibular-mutant lines, I optimized several parameters of the ZebraBox apparatus. I set the detection threshold settings within the software to select for large changes in pixel luminosity that would better represent true larval AEBRs and would ignore small spontaneous movements that represented base-line activity. In addition, larvae were housed in the dark before and during testing in order to facilitate pigment-cell expansion, thus generating stronger contrasts between the animals and the surrounding white background. To account for possible movement artifacts, I performed a user-generated acoustic tap on the side of the testing platform and did not detect movement within water-only wells by manual inspection. Similarly, I conducted tests for the presence of movement artifacts generated by pure tones over a range of frequencies from 400-1200 Hz at 146 dB. This frequency range represents the best frequency of response by larvae (Zeddies 2005). At 100 Hz the platform vibrated in a visible manner, but at frequencies ≥ 400 Hz I did not detect movement of the platform. Therefore, the lowest frequency I used for experimentation was 400 Hz. I then examined the spontaneous activity of larvae due to concerns that large spontaneous movements could confound the detection of true AEBRs. In several instances, the spontaneous activity of some larvae was considerably higher than 20%. These larvae were excluded from the final analysis. I found that raising animals in the dark and limiting their exposure to light had the effect of reducing spontaneous activity (Prober et al., 2006). Under these dark conditions, the rate of spontaneous movement from moderately active larvae was measured at 6.9%

on one day of experimentation. Finally, I performed initial tests in the ZebraBox system with the wild-type larvae at 5 dpf. I presented a strong stimulus of 146 dB at 1000 Hz to the animals and then compared the manual observations with the results generated by the VideoTrack software. I observed that the software often misaligned the responses of half the larvae into the time bin preceding the stimulus, thus reducing the number of recorded AEBRs. I suspected that a combination of a slow video frame rate and the operation conducted by the software resulted in the misalignment of the stimulus and the recorded response. I found that increasing the minimal time bin from one to two seconds while simultaneously presenting the stimulus in the middle of the interval, resolved the effects of desynchronization. As a whole, the parameters I selected were optimal for the detection of the AEBR of larvae when presented with pure-tone stimuli.

I tested the response of larvae to repeated presentations of a strong stimulus to check for any habituation. I presented wild-type larvae with a series of 1000 Hz tones at 146 dB with a lengthy inter-stimulus interval of 180 s. Larvae responded above a threshold of 50 % for the first 15 trials (data not shown), but after the 16$^{th}$ trial, larvae failed to reach threshold response rates. Therefore, in order to minimize habituation I limited further testing to 6 trials per sound pressure presented and allowed the larvae to rest 10 minutes before presentation of the next progressively stronger stimulus.

*Statistical analysis*

Results are presented as the mean ± SEM. The statistical significance was assessed using the Student's *t* test or One-Way ANOVA followed by Bartlett's test for equal variances ($p < 0.05$).

## Results

ENU-mutagenized zebrafish lines were initially screened for auditory and vestibular deficits with a simple behavioral assay: a light acoustic tap (a mechanical force generated by administrating a push against the side of a dish with a forceps) was used to elicit a startle escape response. Several lines of mutants did not respond to the acoustic tap stimulus and were likely to have profound reduced sensory impairment in the mechano-sensitive organs (Nicolson et al., 1998). In contrast several mutant lines responded to the acoustic tap stimulus, but displayed clear balance defects—such as failure to maintain a dorsal upright posture—and were suspected to have subtle hearing deficits. Therefore I modified an existing method to test the larval AEBR with a semi-automated apparatus that generated pure-tone stimuli over a range of sound pressure levels, including levels that were detectable over a dynamic range by wild-type animals. A diagram of the ZebraBox apparatus and test procedure is presented in 2.1.

*Determination of response rates to the acoustic tap and specificity of the acoustic stimulus*

In order to test if the acoustic tap stimulus was too strong to detect subtle changes in auditory function, I examined if the AEBR was elicited above a threshold response rate of 50%. Wild-type 5 dpf larvae responded with a rate of 72.2 ± 10% to an acoustic tap stimulus in the ZebraBox apparatus ($n$ = 12, Fig. 2.2), well above 50%. In contrast, the deafness mutant *pcdh15*$^{R360X}$ (Nicolson et al., 1998) presented a significantly reduced response rate of 5.5 ± 3% ($n$ = 9, Fig. 2.2, wild-type vs. *pcdh15*$^{R360X}$ $p < 0.0001$). The spontaneous activity of *pcdh15*$^{R360X}$ animals was measured at 5.5 % in the absence of an acoustic stimulus, suggesting that the response of mutant *pcdh15*$^{R360X}$ during presentation of the stimulus represents background activity. These data indicate that the acoustic tap robustly elicits an AEBR in wild-type larvae well above threshold levels of activation and therefore may be too strong of a stimulus for assays of subtle auditory deficits.

*Determining the best frequency of response and sound pressure level*

In order to discriminate subtle hearing deficits, I searched for pure-tone stimuli that would elicit larval AEBR rates below a threshold of 50 %. Previous studies show that the best frequency range for activation of the larval AEBR is from 300 - 1200 Hz (Zeddies et al., 2005). I presented wild-type larvae with tones at 400, 600, 800, and 1000 Hz at a moderate 138 dB sound pressure level for a duration of 100 ms ($n$ = 11). I found no significant differences in the response

rates at each of the frequencies tested (Fig. 2.3; 400 Hz 19 ± 5%; 600 Hz 27 ± 6 %, 800 Hz 22 ± 5%, 1000 Hz 42± 12%%; one-way ANOVA; F(1.5, 43) = 8.7; $p > 0.05$). However, I observed a possible trend towards an increase in the response rate at 1000 Hz. Therefore, I selected 1000 Hz as the frequency for further testing of the AEBR. In order to identify a dynamic range of larval responses to a 1000 Hz tone stimulus, I tested wild-type larvae at several sound pressure levels. Preliminary experimentation indicated that sound pressure levels below 132 dB gave highly variable response rates in wild-type larvae, and these results were difficult to interpret due to statistically insignificant separation between true responses and background spontaneous movements. As such, I found that 132 dB was the lowest sound pressure level I could use for testing. Larvae responded at rates of 22 ± 6% at 132 dB, while at 138 dB larvae responded at 43 ± 6%, and at 146 dB larvae responded at a rate of of 71 ± 5% (Fig. 2.3). The response rate of wild-type larvae did not increase when I doubled the sound pressure from 146 dB to ~ 154 dB (data not shown). An explanation for the narrow range of a full response rate is lacking at this time. The weak response rate at 132 dB and 1000 Hz suggested that pure-tone stimuli could be adjusted to levels that would be useful for discriminating subtle hearing deficits. In order to validate the findings and ensure that the pure-tone stimulus did not activate the tactile escape response, I tested the deafness *pcdh15*$^{R360X}$ mutant at 1000 Hz and 146 dB ($n = 12$) and found a response rate of 6.9 ± 3% compared to a wild-type rate of 60.6 ± 10% (Fig. 2.2, $p < 0.0001$), indicating that the strongest

pressure presented for a pure-tone stimulus did not activate the tactile escape response.

*Proof of principle: the* stardust *mutant*

The unambiguous delineation between wild-type and deafness mutants by behavioral testing with pure-tone stimuli shows that the ZebraBox apparatus is useful for identifying profound auditory deficits in mutants. However, my goal was to use the system for determining subtle auditory deficits in balance-defective mutants that displayed robust AEBRs to the acoustic tap stimulus. Using the optimized conditions discussed above, I tested the balance-defective mutant *stardust* for auditory defecits. *Stardust* alleles contain various nonsense mutations in the gene *rabconnectin3α* (Einhorn et al., 2012). [The impact of the loss of *stardust* on the operation of the hair cell is discussed in detail in subsequent chapters.] Mutant *stardust* larvae are morphologically normal and do not display any obvious degeneration or necrosis. Mutant larvae perform an escape response to both touch and acoustic tap stimuli produced by tapping on the tank or petri dish. However, during the escape response, mutants have an aberrant body-axis orientation while swimming and fail to maintain an upright position, indicating a vestibular defect. In addition, they do not inflate their swim bladder, lack spontaneous eye movements, and their melanocytes do not contract when exposed to bright light (data not shown). Collectively, these responses suggest that both the visual and vestibular systems are impaired, but no auditory deficit had yet been found. This is surprising given the presence of

*rabconnectin3α* transcripts in hair cells of both the auditory and vestibular organs (Chapter 3).

Stardust *mutants exhibit normal startle movements*

Before presenting mutant *stardust* larvae with the pure-tone stimulus, I had to test for any downstream motor deficits that would confound interpretations of auditory escape behaviors. I therefore inspected the larval swimming and turning behaviors during the escape response to an acoustic tap stimulus. I compared multiple still frames of the escape reflex of 5 dpf wild-type siblings and homozygous stardust mutants carrying the putative strong allele, rbc3α$^{Q850X}$. [I describe the positional cloning of the alleles of *stardust* in Chapter 3, but they are given as follows: *rbc3α*$^{Q850X}$, *rbc3α*$^{Y2059X}$, or *rbc3α*$^{Y2447X}$ ]. At rest, wild-type larvae were oriented dorsal side up with respect to gravity, while rbc3α$^{Q850X}$ mutants were supine on the bottom of the dish with their ventral side exposed (Fig. 2.4A; n = 5 each). This lack of an upright position is similar to the postural defects seen in other balance-defective mutants (Nicolson et al., 1998). In response to a tap stimulus, wild-type and mutant larvae performed C-bends or counter turns and then swam several body lengths away (>3.5 mm). After short bouts of swimming, the wild-type larvae resumed a dorsal upright position, whereas the mutants were lying on their sides. These coordinated motor behaviors indicate that, like wild-type larvae, the *stardust* mutants are physically capable of performing an escape response.

Stardust *mutants show abnormal response to pure-tone stimuli*

I used the modified AEBR test as a quantitative behavioral assay of *stardust* auditory function and found that, consistent with previous results, the percentage of larvae that performed an AEBR to a tap stimulus was not significantly different between WT and *rbc3α*$^{Q850X}$, *rbc3α*$^{Y2059X}$, or *rbc3α*$^{Y2447X}$ animals (Fig. 2.5; $n$ = 24 animals each; $p < 0.05$, unpaired Student's $t$ test). To understand the contribution of *rbc3α* to detection of sensory stimuli, I measured the AEBR in response to pure-tone stimuli. At 132 dB, both *rbc3α*$^{Q850X}$ and *rbc3α*$^{Y2059X}$ mutants had fewer responses than WT animals ($p < 0.05$). However, mutants containing the *rbc3α*$^{Y2447X}$ allele were not statistically different from WT animals in response. At a higher SPL of 138 dB, only *rbc3α*$^{Q850X}$ animals had fewer responses than WT (WT, 43 ± 6%; *rbc3α*$^{Q850X}$, 18 ± 3%, $p < 0.001$). At the highest SPL tested, 146 dB, all three mutants performed worse than WT animals (WT, 71 ± 5% and *rbc3α*$^{Q850X}$, 54 ± 6%, $p < 0.05$; WT, 64 ± 4% and *rbc3α*$^{Y2059X}$, 45 ± 4%, $p = 0.0013$; WT, 67 ± 5% and *rbc3α*$^{Y2447X}$, 50 ± 6%, $p < 0.05$). The reduced AEBRs of mutant larvae indicate that hearing is impaired but not abolished. The results from this auditory test are also consistent with the observation that mutant larvae are still capable of producing a startle response. Taken together, the results from the behavioral testing of *rbc3α* mutant alleles indicates that pure-tones are better stimuli than the acoustic tap for determining subtle auditory deficits. Furthermore, the improved method was capable of discriminating differences between the alleles of *rbc3α*.

## Conclusion

The AEBR is a well-studied behavior that has been used as a measurement of auditory function in larval zebrafish. I find that the acoustic tap elicits high rates of response when presented to wild-type larvae and several lines of vestibular mutants. Because of the robustness of response to the acoustic tap, the discrimination of subtle auditory deficits is unfeasible, despite the likelihood that various vestibular mutant lines have impaired hearing. I observed, for example, that the vestibular mutant *stardust*, which was suspected to have a subtle hearing deficit, showed no dysfunction using the acoustic tap stimulus. Therefore, I modified existing methods to better assay the AEBR as a measurement of auditory function. I optimized pure tones to present to larvae in order to moderately elicit the AEBR in wild-type animals. As a result, I was able to test and measure the response of indeterminate auditory/vestibular mutant *stardust* with sound stimuli that closer approximate the limit of detection in wild-type animals. With the improved selection of sound stimuli I was able to distinguish subtle auditory deficits of, and differences between, the alleles of the vestibular mutant *stardust*. As a whole, these experiments underscore the molecular and operational similarities between hair cells of the vestibular and auditory organs.

### *Similarities between auditory and vestibular hair cells*

Through experimentation with pure-tone stimuli at moderate sound pressures, I was able to identify that the mutant stardust had moderate hearing

loss in addition to its obvious balance phenotype. Thus, I established an improved methodology that has sensitivity to test hearing impairment in vestibular mutant lines with subtle auditory deficits. An important question is why various vestibular mutant lines have indeterminate hearing loss, despite shared anatomical and molecular similarities between the auditory and vestibular sensory hair cells. I speculate that zebrafish are particularly reliant on hair-cell mediated sensory input from the vestibular system in order to maintain their balance. This is in contrast with mammals that have redundant input from proprioceptors in their limbs. For example, the loss of Vglut3 in mammals causes profound sensory hearing loss, but no striking balance deficits, while zebrafish mutants have severe deafness and balance defects (Obholzer et al., 2008, Ruel et al., 2008, Seal et al., 2008). This interspecies difference suggests that perturbations to hair-cell function profoundly impact the ability of zebrafish to maintain their balance because they lack sufficiently redundant mechanisms.

*Verification of an improved method for assaying auditory escape behaviors*

The validity of using the modified behavioral test as an assay of auditory function depends on both experimental testing parameters and careful examination of the effect of loss of gene function. Of particular concern is the use of a downstream locomotor output to measure upstream sensory performance. Any behavior is inherently complex, though the Mauthner-cell mediated locomotor response to aversive auditory stimuli is well defined (Korn and Faber et al., 2005, Kohashi et al., 2008). If a mutation affects downstream behaviors

independently of sensory performance, then the assay will be unreliable. I examined the vestibular mutant *stardust*, which exhibits defective swimming and postural maintenance, indicating impaired balance. Mutant *stardust* larvae lack spontaneous eye movements, which precludes testing the vestibular function of the animal with established assays of the vestibular-induced ocular reflex (Mo et al., 2010). The lack of spontaneous eye movements could also indicate a general motor activity deficit that would invalidate the use of the AEBR assay. To ensure that downstream locomotor activity is normal in the mutant *stardust*, I performed control experiments to test the Mauthner-cell mediated locomotor response during presentation of an acoustic tap. I captured the behaviors with high-speed video and observed robust C-turns in wild-type larvae and in mutant stardust animals. These results indicate that loss of the gene rbc3$\alpha$ did not developmentally or functionally perturb the Mauthner-cell mediated locomotor response, though I did not examine whether the response was minutely delayed (Kohashi et al., 2008). Furthermore, mutant stardust larvae had relatively normal coordination of their swimming (post C-turn observations), despite displaying misoriented body-axes, indicating that motor activity was overall apparently normal. Therefore, caution should be taken that individual mutant lines are evaluated for their ability to generate escape responses before conclusions are made of auditory function.

I evaluated several other testing parameters to determine the most suitable conditions for testing the larval AEBR in the ZebraBox apparatus. Movement of larvae in the startle assay is dependent on many factors, including

raising conditions, inter-stimulus interval, number of trials and lighting (Kimmel et al., 1974, Bang et al., 2002, Zeddies et al., 2005). Several reports indicate that raising density greatly affects the sensitivity of larvae to auditory stimuli and could result in desensitization (Burgess and Granato et al., 2008, Buck et al., 2012). In this study, larval raising density was not accounted for, and dishes contained between 45-60 larvae. Future studies will take care to lower larval density. Individual larvae were placed in wells for > 10 minutes before testing, though the process of transfer may desensitize animals. Another concern was habituation, I found that up to 15 trials were sufficient for determining the capability of larvae to respond to sound stimuli at 146 dB 1000 Hz, but more than 15 trials resulted in habituation. While inter-stimulus intervals of 45 seconds or longer did not result in habituation in other studies (Buck et al., 2012), I chose longer periods of 180 seconds. I also limited the experimental presentation to 6 trials per pressure level and waited > 10 minutes before presentation of progressively stronger stimuli. Taken together, habituation was not a concern in the AEBR protocol.

Finally, large spontaneous movements are a considerable concern as they could alter the detection of true startle responses. Larvae exposed to light for long periods are more active (Prober et al., 2006). Therefore larvae were raised in the dark and only exposed to light for brief periods to transfer them from the raising dish to the testing plate. As a result, I observed reduced rates of large spontaneous movements, though some wild-type larvae were still highly active and were subsequently excluded from the final analysis.

Because I am assaying the AEBR as a measure of auditory function, I was careful to minimize the contribution of non-auditory sensory systems to the escape response. Several studies indicate that the lateral line does not contribute significantly to the AEBR (Buck et al., 2012, Zeddies et al., 2005). The lateral line is primarily tuned to a frequency range of 50 – 100 Hz, and moreover, is maximally activated in the horizontal direction (Kindt et al., 2012). I placed the shaker beneath the testing platform in order to generate pure tones in the vertical orientation at frequencies ≥ 400 Hz, and thus should minimize the contribution of the lateral line to the AEBR in the behavioral testing. In addition, I did not observe obvious movement of the liquid within individual wells during tone generation, indicating that the energy required for activation of the tactile escape response is unlikely to be produced. Finally, fellow researcher Weike Mo examined the vestibular mutant *rock solo* with the current AEBR testing method. *Rock solo* lacks an otolith above the utricular hair cells, and as a result has severe balance defects (Mo et al., 2010). However, mutant *rock solo* animals exhibit a robust response to the acoustic tap stimulus (Mo et al., 2010), suggesting that the utricle does not contribute to audition. This result is in agreement with previous work that indicates that the utricle is primarily a vestibular organ (Riley and Moorman 2000), while the sacculus primarily contributes to hearing (Zeddies et al., 2005, Buck et al., 2012, Kohashi et al., 2008). Collectively, these results indicate that the system reliably elicits escape responses generated by auditory and not other sensory stimuli.

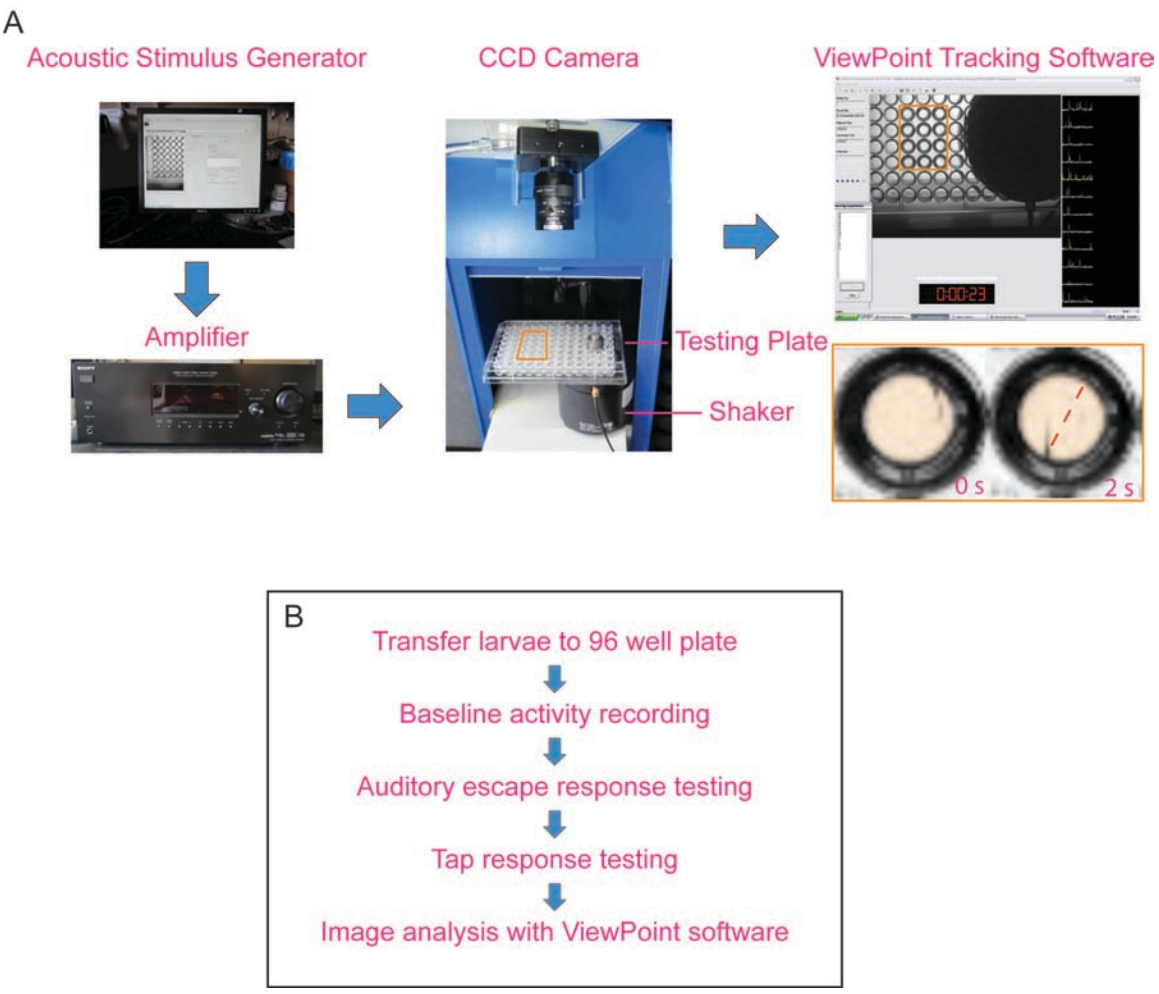


Figure 2.1 Experimental setup to determine the auditory escape behavioral response of larval zebrafish

***A***, Acoustic stimuli were generated with the ViewPoint software, amplified and produced by a shaker. Images were monitored by a CCD camera with an infrared filter. Movement was detected and analyzed with ViewPoint software. The orange box outlines the 12 wells that are used for testing, and an example of an AEBR in WT before and after stimulus presentation is shown in lower right. ***B***, The testing procedure used in the auditory pure tones, or acoustic tap, behavioral escape response assays.

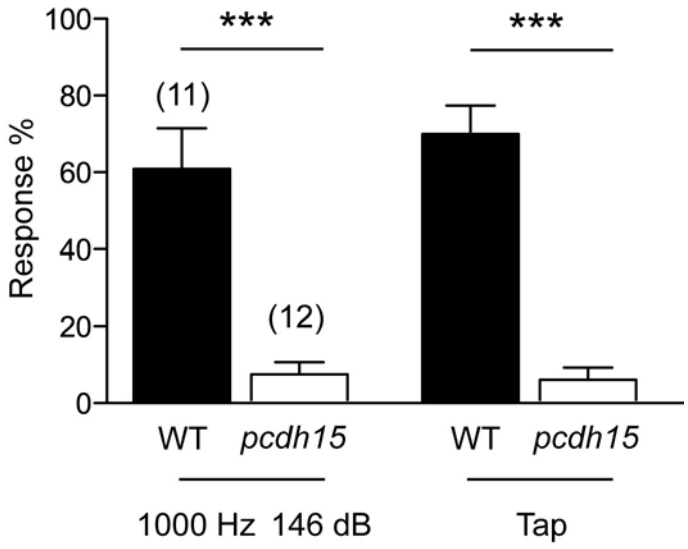


Figure 2.2 Wild-type but not deafness mutant *pcdh15*$^{R360X}$ larvae respond to acoustic tap and strong pure-tone stimuli

The percentage of WT or mutant *pcdh15*$^{R60X}$ larvae responding to either a mechanical tap stimulus or a tone of 1000 Hz at 146 dB SPL. Mean ± S.E.M. presented. Student's *t* test was performed, $p < 0.0001$. Numbers in parentheses above bar graphs equal the number of larvae tested.

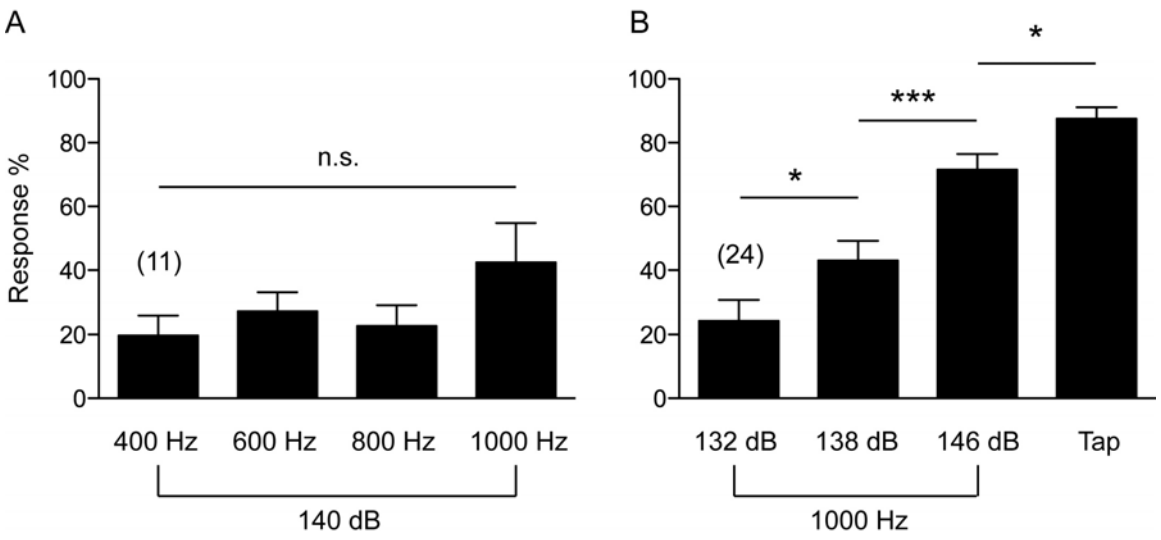


Figure 2.3 Determination of the best frequency and sound pressure level of the larval AEBR

***A***, The percentage of WT larvae responding to different pure-tones at 400, 600, 800 and 1000 Hz frequencies at 140 dB SPL. Tones were presented for 100 ms. The mean ± S.E.M. for  larvae at 5 dpf are plotted. Each experiment consisted of six trials for each frequency with an inter-stimulus interval of 180 s (see Materials and Methods). The difference between means was not statistically significant, One-Way ANOVA. ***B***, The percentage of WT larvae responding to a tone of 1000 Hz at various sound pressure level (SPL) in the wells (132, 138, and 146 dB SPL), or to an acoustic tap stimulus. Each 6 dB change represents a doubling of voltage applied to the shaker. Student's *t* test was performed, * = $p < 0.05$, *** = $p < 0.001$. Numbers in parentheses above bar graphs equal the number of larvae tested.

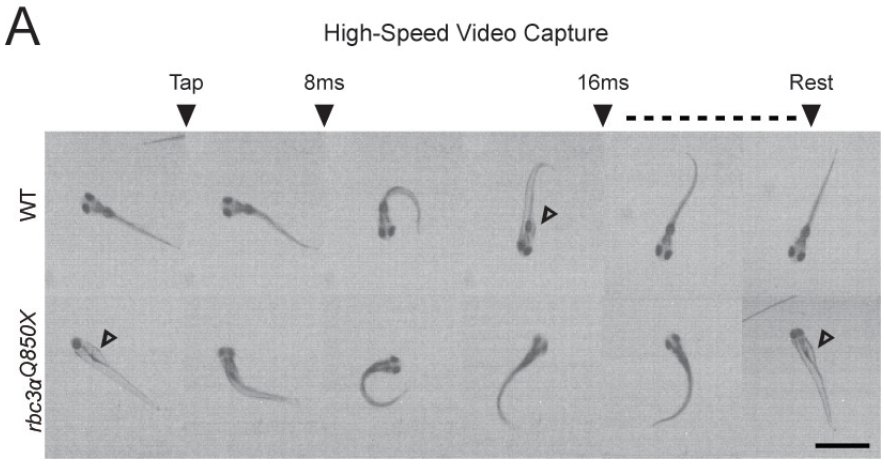


Figure 2.4 Homozygous *stardust/rbc3*$\alpha$ mutants have normal motor activity (5 dpf)

***A***, High-speed video capture of wild-type and mutant *rbc3*$\alpha^{Q850X}$ larval escape response to an acoustic tap (scale bar, 2 mm). Arrowheads denote exposed ventral side of larvae.

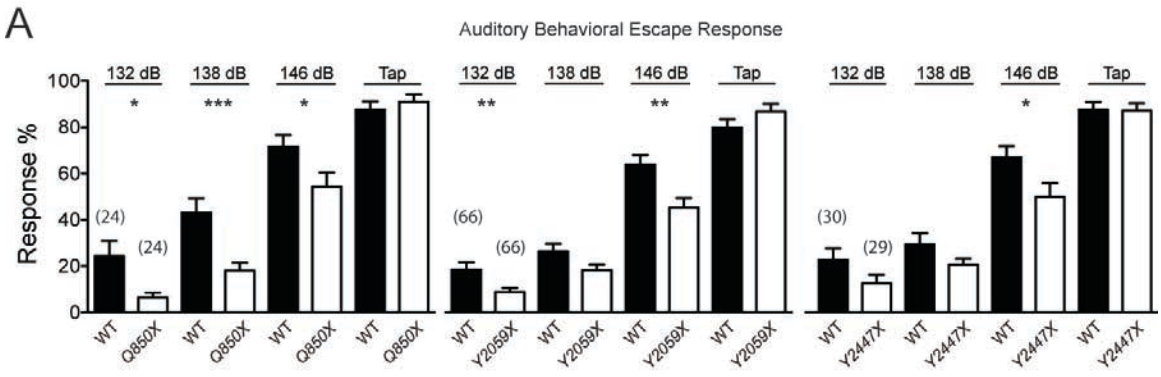


Figure 2.5 Homozygous *stardust/rbc3*$\alpha$ mutants have auditory and vestibular deficits (5 dpf)

***A***, Quantification of escape responses in larvae exposed to either a tap or 1 kHz frequency tone at 132, 138 and 146 dB. (n ≥ 24). Error bars represent standard error of means. Numbers in parentheses above histogram bars represent the number of larvae tested.

# Chapter 3 - Cloning, Structure, and Localization of Rabconnectin3α

Zev Einhorn, Qianyong Liu and Teresa Nicolson

**Summary of Chapter**

Rabconnectin3α (Rbc3α) is a large, highly conserved protein with multiple protein interacting partners (Kawabe et al., 2003, Yan et al., 2009, Li et al., 2012). While it was originally hypothesized to be a synaptic-vesicle scaffold upon which Rab3 regulation might occur (Nagano et al., 2002), its more clearly established role is as a regulator of the Vacuolar-type ATPase (V-ATPase), which pumps protons into various subcellular organelles. In this Chapter, I describe the positional cloning of the zebrafish auditory/vestibular-defective mutant *stardust*, and subsequently identify the gene *rbc3α* as lesioned in the various alleles of *stardust*. I also examine for the first time the effects of loss of Rbc3α throughout an entire organism as well as clone the first full-length cDNA of *rbc3α*. I detail the spatio-temporal expression pattern of the gene throughout the nervous system of the larva, including sensory hair cells. Finally, by performing a structure and localization analysis of exogenously expressed Rbc3α and various truncated versions of the protein tagged by a fluorescent reporter, I determine that the protein has a synaptic-vesicle like distribution within hair cells. I also find that the N-terminal half of the protein is sufficient for its enhanced vesicular translocation. Taken, together these results suggest that Rbc3α associates with synaptic vesicles and contributes to hearing and balance at the sensory receptor cell of the auditory/vestibular systems.

## Introduction

Rbc3α and its protein partner Rbc3β form the Rbc3 complex (Kawabe et al., 2003). Both proteins are conserved across species and contain multiple WD-40 domains that are putative sites for protein-protein interactions (Nagano et al. 2002, Kawabe et al., 2003). Rbc3α also shares weak similarity with the yeast Rav1 protein, which also regulates the assembly of the V-ATPase holocomplex (Kane 2006). The Rbc3 complex associates with synaptic vesicles in the rat hippocampus and was originally conjectured to be a scaffold upon which Rab3 GEP and GAP regulate Rab3 activity at the vesicle (Nagano et al., 2002). Additionally, the complex was detected exclusively in the brain although its biological function was not revealed. In contrast, later studies described its function as a regulator of the V-ATPase from insects to vertebrates and across diverse cell-types (Yan et al., 2009, Sethi 2010), but did not detail the protein or transcripts' tissue and subcellular distributions. Therefore, an examination is merited that addresses both the tissue distribution of the transcript and protein, as well as the biological function of Rbc3α.

Rab3 shapes synaptic plasticity and a post-docking step of synaptic vesicles to the active zone (Südhof 2004). However, the only evidence indicating that Rbc3α plays a role in $Ca^{2+}$-dependent exocytosis comes from a study examining the effects of exogenously expressed fragments of the protein on secretion of granules in PC12 cells (Sakisaka and Takai 2005). It was found that a C-terminal fragment of the protein (amino acids 2495 – 3036 of human, corresponding to amino acids 2499 – 3062 of zebrafish) resulted in a modest

reduction in exocytosis. However, these results did not demonstrate a clear synaptic function for the Rbc3 complex.

The first clear biological function of Rbc3α and Rbc3β was discovered in a mosaic genetic screen of Drosophila mutants that exhibited defects in the acidification of various intracellular organelles (Yan et al., 2009). The findings in several alleles of mutant rbc3α and rbc3β were confirmed by later studies that collectively support a role for the Rbc3 complex as a regulator of intracellular acidification through direct protein interactions with the V-ATPase (Sethi et al., 2010, Li et al., 2012). In contrast, Rab3 GEP, GAP and Rab3 isoforms were not found in a protein-interaction search for interactors with Rbc3α (Li et al., 2012). Based on these collective findings, I predict that Rbc3α performs a synaptic function by regulating V-ATPase activity at the synapse (Takamori et al., 2006, Uthaiah and Hudspeth 2010).

In order to test this prediction I examined the *stardust* auditory/vestibular zebrafish mutants, which harbor various nonsense mutations in the alleles of the gene *rbc3α* (Einhorn et al., 2012). In this Chapter, I first detail the isolation and cloning of the mutations within *stardust*. Then, in order to determine the tissues underlying the *stardust* auditory/vestibular phenotype, we examine the tissue distribution of *rbc3α* in pre- and post-hearing zebrafish larvae. Finally, we clone a full-length cDNA for structure-localization experiments and determine the distribution within hair cells of the Rbc3α protein and the necessary domains for its synaptic location. Taken together, our results indicate that Rbc3α has a synaptic distribution in hair cells, which argues for a synaptic function.

## Methods

*Primary Antibodies for Immunohistochemistry and fluorescence labeling*

Rabbit polyclonal Vglut3 antibody (1:1000 dilution) was described in (Obholzer et al., 2008). Serum and affinity-purified rabbit polyclonal antibodies against the C-terminus (CGADGTLKMRVLPDRYNIPASIFQIL) of *Danio rerio rbc3α* were generated by Protein-tech (Chicago, IL). Additionally, serum and affinity-purified chicken polyclonal antibodies against the C-terminus (Open Biosystems) were also generated. Antibodies were tested at concentrations of 1:100, 1:500, or 1:1000 on wild-type and homozygous mutant *rbc3α*$^{Q2447X}$ larvae. Different permeabilization treatments were tested, including acetone or 0.1% Triton-X. Labeling for the serum antibodies of both rabbit and chicken was strong in the kinocilia and plasma membranes of hair cells, but was identical in wild-type and mutant *stardust* control larvae and therefore lacked specifity. Affinity-purified antibodies did not label either wild-type or mutant control larvae.

*Molecular Biology*

For determination of mutant *stardust* alleles, mRNA was extracted from day 5 zebrafish larvae by standard methods. First-strand cDNA was generated from transcripts with the SuperScript III First-Strand Synthesis System (Invitrogen). Total RNA was extracted from larvae and poly(A) RNA was enriched using the MicroPoly(A)Purist kit (Invitrogen). RT-PCR was performed using total RNAs isolated from whole zebrafish larvae at 5 dpf.

The following zebrafish *rbc3α* specific primers were designed to cover the predicted zebrafish *rbc3α* sequence based on ESTs from Ensembl Zebrafish Assembly version 8 and 9 (Transcripts: ENSDART00000087935 and ENSDART000000149158), *rbc3α* 1 (5'- atgcatctgcaccaggtgctgacggg -3'), *rbc3α* 1517 aa Reverse (5'- cacctgtgcatgttcggggcc -3'), *rbc3α* 1408 aa Forward (5'- gttgccggtcgagatggtggacg -3'), and *rbc3α* End Reverse (5'- ttagaggatctggaatatactggccg -3'). The primers were used to verify the predicted *rbc3α* sequence and for generation of cDNA template. 5' RACE-ready cDNA was generated by reverse transcribing mRNA with the SMARTer RACE cDNA amplification kit (Clontech). Touchdown PCR was then performed on 5'RACE-ready cDNA with Advantage 2 Polymerase Mix (Clontech). 2μl of larval cDNA was used as a template. Primers used were Universal Primer Mix (SMARTer RACE) and Rbc3α Rev - 286 bp (CCAAACAAACGTCACAAGCAACTGAATTAC). Touchdown melting temperatures were as follows: 5 cycles at 75° C then 30 cycles at 72° C. A strong DNA band of ~1kB in length was detected by gel electrophoresis and extracted and purified for DNA. Following purification, Nested PCR was performed using the purified PCR amplicon, Nested Universal Primer A (SMARTer RACE kit) and *rbc3α* Rev – 286 primer with 30 cycles at a melting temperature of 58° C. A strong band at 500 bp was detected, extracted and sequenced using the *rbc3α* Rev – 286 primer. 87 nucleotides (29 amino acids) were read between the predicted methionine start codon and the 5' end of the incomplete transcript for *rbc3α.*

Partial *rbc3α* ds-cDNAs were generated by PCR using primers targeting first (1-1517 aa) and second (1408-3062) halves of the predicted full-length transcript (forward primer 5- atgcatctgcaccaggtgctgacggg-3; reverse primer 5- cacctgtgcatgttcggg -3; forward primer 5- gttgccggtcgagatggtggacg -3; reverse primer 5- ttagaggatctggaatatactggccg-3) and were sequenced with internal primers. Full-length *rbc3α* (Genbank accession number is pending) was generated by TA cloning both halves of ds-cDNAs into TOPO 2.1 PCR vectors (Invitrogen), restriction-enzyme digestion with AgeI and NotI enzymes (NEB), and re-ligation of fragments with T4 DNA Ligase (NEB).

Expression constructs were generated with Multisite Gateway Technology (Invitrogen, Kwan et al., 2007). In brief, full-length *rbc3α* (ATG-3062) was PCR amplified with Gateway compatible attB sites (forward primer 5- ggggacagctttcttgtacaaagtggccatgcatctgcaccaggtgctgacggg -3; reverse primer 5- ggggacaactttgtataataaagttgcttagaggatctggaatatactggccg -3) and recombined to generate 3'entry vector p3E-*rbc3α*, then p3E-*rbc3α* was recombined with p5E-*6.5myosin6b* minimal promoter (Mo and Nicolson, 2011), pME-*GFP,* and the pDestination 395 vector to generate -*6.5kb_myosin6b:gfp-rbc3α;clcm2:gfp*. Constructs were then micro-injected (50 ng/µl) along with Tol2 transposase mRNA at the one-cell stage of embryos. The following primers were used for the generation of various truncated versions of *rbc3α* within the Gateway system: ATG (forward primer 5-gggacagctttcttgtacaaagtggccatgcatctgcaccaggtgctgacggg -3), 715 (reverse primer 5- ggggacaactttgtataataaagttgctcagagaatcagctcactgtagatcgc -3), 850X (reverse

primer 5-ggggacaactttgtataataaagttgcctatgtgttcgagccgcactgg -3), 1217 (reverse primer 5-ggacaactttgtataataaagttgctcatcctccaagaggcagggtgactgc-3),1517 (reverse primer 5-ggggacagctttcttgtacaaagtggccgcacctgtgcatgttcggggcc -3), 1408 (forward primer 5-ggggacagctttcttgtacaaagtggccgttgccggtcgagatggtggacg-3), and (forward primer 5- ggggacagctttcttgtacaaagtggctcccacctctgcccctgcaca-3), 2304 (forward primer 5-ggggacagctttcttgtacaaagtggctcccacctctgcccctgcaca -3).

*In situ hybridization*

Digoxygenin-labeled riboprobes were generated with the DIG Labeling Kit (Roche) from a previously published *rbc3α* probe CB952, (Thisse et al., 2001). In situ hybridization was performed as described previously (Söllner et al., 2004) with 200 ng of probe. Larvae at 72 hours post fertilization (hpf) were imaged as whole-mounts. Larvae at 4 days post fertilization (dpf) were cryosectioned into 12 μm slices using standard methods. Larvae were viewed on a Zeiss Axio bright-field microscope (Oberkochen) using either a 10X or 20X dry lens objective. Images were captured with an AxioCam MRc5 color digital camera using Axiovision software and exported as TIFF files to Adobe Photoshop or ImageJ (US National Institutes of Health) for analysis.

*RT-PCR of neuromasts and yolk epithelium*.

Neuromasts along the head and trunk of Tübingen wild-type larvae were extracted by a suction pipette and aspirated into cold lysis buffer from Cells-to-cDNA kit II (Ambion). First strand cDNA synthesis was performed using Sprint-

RT Complete-Oligo(dT) 18 kit (Clontech Laboratories). cDNAs were amplified by PCR using ChoiceTaq Blue Master Mix (Denville Scientific) with primers pairs targeting *cadherin23* (forward 5' cagtagttgcaggctccaca 3' and reverse 5' tgggctgctaactccagatt 3'), *rbc3α* 2902-3602 (forward 5' gcagcagttgatcatcacgggcggcaggaaggg 3' and reverse 5' gaggatctggaatatactggccggaatgttgtagcggtcggg 3'), *rbc3α* bp 2964-3'UTR (forward 5' catggcctcatgcactcattcagcacc 3' and reverse 5' cgtggggcgaggtgcgagata 3'). Water was used as a negative template control.

*Generation of transgenic strains*

Animals were microinjected with Tol2 mRNA and *-6.5myosin6b: gfp-rbc3α 2304-3062,clcm2:gfp*. F0 animals were screened to generate F1 transgenic animals *Tg(-6.5myosin6b: gfp-rbc3α 2304-3062,clcm2:gfp)*.

## Results

*Positional mapping of* stardust *and generation of* rabconnectin3α *cDNA*

To identify the genetic lesions in *stardust* alleles, a meiotic recombination map was generated by scoring recombination events in 385 homozygous mutant larvae with microsatellite markers. A large critical interval of 3.7 Mb was defined based on the Zv8 assembly of the zebrafish genome. The critical interval contained 60 candidate genes, including *rbc3α* (also known as *dmxl2;* 3.1A). To identify lesions within candidate genes, total mRNA was reverse transcribed from extracts of homozygous larvae. I then performed PCR from amplified cDNA and

sequenced amplicons from several candidates, despite incomplete assembly and coverage of the genomic region within the critical interval. Three alleles of *stardust* contained nonsense mutations in the gene *rbc3α* (Fig. 3.1 B). A fourth allele failed to generate cDNA from *rbc3α* transcripts, but control *vglut1* transcript was detected (data not shown).

The alleles of *stardust* were fortuitously located in assembled regions of the zebrafish genome, but the remainder of the genomic region containing the full-length *rbc3α* gene was incomplete. In brief, the 5' methionine start codon and a middle section of the transcribed sequence of *rbc3α* were missing. In order to generate full-length cDNA for future structure-function experiments, I determined the rest of the coding sequence zebrafish *rbc3α*. To begin I used the N-terminus of human Rbc3α (amino acids 1 – 22) as a search query in the UCSC genome browser for *Danio rerio* and found an unpredicted fragment with the putative methionine start codon, (Zv7_NA3030, 22 predicted amino acids). I confirmed it was the start codon by performing 5' rapid amplification of cDNA ends (5'RACE) with *rbc3α* specific reverse primers. Because the 3' end of the transcribed gene was available in the assembly, I then performed RT-PCR using total RNA from 5dpf larvae with *rbc3α* specific primers to generate partially overlapping amplicons that covered the entirety of the predicted coding sequence of the *rbc3α* gene. I found new exons 18, 19, 20 and 26 as well as alternative splicing of exon 9 (Fig. 3.1 C). As a result of these experiments, I found that the predicted Rbc3α protein has 3062 amino acids if all exons are included (Fig. 3.1 B and D). There was approximately 72% identity between predicted zebrafish and human

Rbc3α proteins, confirming the identity of the zebrafish *rbc3α* gene (Fig. 3.1 E). To my knowledge, these efforts resulted in the first full-length cDNA of *rbc3α*. In contrast to many zebrafish genes, I was unable to find any duplicates of *rbc3α* in the current assembly of the zebrafish genome. Based on the findings, I designated the three alleles of *stardust* containing stop codons, according to their amino acid locations as follows: Q850X, Y2059X, and Y2447X (Fig. 3.1 B).

*Tissue expression profile of* rbc3α *mRNA*

The behavioral deficits of mutant *stardust* larvae indicate that Rbc3α plays an important role in hearing and balance. I hypothesized that the auditory and vestibular cell-types that underlie the behavioral phenotype of the mutant *stardust* was the sensory hair cell. To begin the examination, I reviewed previous expression data generated by a large-scale collection of embryonic and larval expressed genes (Thisse et al., 2001). Transcripts for *rbc3α* are present as early as gastrulation and by larval stages the transcripts are primarily expressed throughout the nervous system (Thisse et al., 2001). These temporal and spatial distribution patterns suggest that the transcript is widely utilized by a variety of tissues throughout the embryo and later stage larvae. This finding argues against the finding that Rbc3α is solely expressed in the brain (Nagano et al., 2002).

Due to poor resolution of the large-scale expression collection (Thisse 2001), I was unable to determine if hair cells also expressed the *rbc3α* transcript. However, a micro-array analysis of hair-cell transcripts in the zebrafish, indicated high levels of *rbc3α* expression (McDermott et. al, 2007). Therefore, I examined

the expression pattern of *rbc3α* mRNA in the larva at pre- and post-hearing stages (3 and 4 dpf, respectively) using an RNA *in situ* probe against an internal portion of the *rbc3α* transcript to confirm the hair-cell expression. I detected transcripts in the eye, throughout the brain, and in the sensory epithelia of the ear and cranial ganglia at 3 and 4 dpf (Fig. 3.2 A and B). The labeling seen in the inner nuclear layer and ganglion cell layer of the retina raises the possibility that mutant visual deficits may also be present at early steps in sensory detection (See Chapter 2). Although I did not detect labeling of the lateral-line organ by *in situ* hybridization, I predicted that *rbc3α* was also expressed in lateral-line hair cells. Therefore, I used RT-PCR as an alternative detection method for detection of hair-cell transcripts in the lateral-line organ (Trapani et al., 2009; Trapani and Nicolson, 2011). I isolated superficial neuromasts of larvae and prepared cDNA, and then used primers against two different fragments of *rbc3α.* I amplified another known hair-cell gene, cadherin23 as a positive control (Fig. 3.2 C). I was able to amplify *rbc3α* from neuromast cDNA, a result that is consistent with *rbc3α* expression in hair cells of the lateral-line organ. The expression pattern of *rbc3α* suggests that defects in hair-cell function potentially underlie the aberrant auditory and vestibular behaviors of *rbc3α* mutants.

*Rbc3α is distributed within synaptic regions of the hair cell*

Previous work argues that Rbc3α regulates the V-ATPase and could also contribute to the synaptic vesicle cycle, though the latter had not been demonstrated definitively (Yan et al., 2009, Nagano et al., 2002, Sakisaka and

Takai 2005). Synthesizing these findings, I hypothesized that Rbc3α performs a synaptic function in hair cells through regulating the activity of the V-ATPase on synaptic vesicles. [ I examine V-ATPase regulation by Rbc3α in Chapter 4]. Before examining the activity of the V-ATPase on synaptic vesicles directly, I first asked whether Rbc3α was distributed within synaptic-vesicle regions of the hair cell, which would support the claim that the protein performs a role in the synaptic vesicle cycle (Nagano et al., 2002, Sakisaka and Takai 2005). In order to examine the distribution of the Rbc3α protein, I attempted to generate specific Rbc3α antibodies, but was unsuccessful (See Methods). Instead, I cloned full-length *rbc3α* [Genbank accession number pending], and exogenously expressed N-terminally tagged GFP-Rbc3α in hair cells using a minimal *myosin6b* promoter. A diagram of the various Rbc3α constructs and the experimental results are summarized in Figure 3.3. I observed that GFP-Rbc3α was localized to the basal end of hair cells in a crescent-like distribution pattern (Fig. 3.4 A, B). The localization of GFP-Rbc3α in live cells was similar to that of Vglut3, an integral membrane protein residing within basally localized synaptic vesicles (Fig. 3.4 C; Obholzer et al., 2008). The localization of Rbc3α near hair-cell synapses suggests a synaptic function for the protein as predicted by previous studies (Nagano et al., 2002, Sakisaka and Takai 2005).

The mechanism by which Rbc3α associates with synaptic vesicles is likely mediated by protein-protein interactions because there are no predicted integral membrane domains within the protein. However, zebrafish Rbc3α has multiple WD-40 domains that are possible sites for protein-protein interaction (Fig. 3.1 B

and 2 A, SMARTdatabase; Wall et al., 1995). Therefore, I performed a structure-localization analysis of exogenously expressed versions of truncated GFP-Rbc3α in order to determine which domains of the protein confer its enhanced translocation from the cytoplasm to synaptic vesicles within hair cells. Additionally, I wanted to confirm the previous finding that an exogenously expressed C-terminal fragment of Rbc3α inhibits $Ca^{2+}$ -dependent exocytosis (Sakisaka and Takai 2005).

Before I began the structure and localization analysis, I determined whether the various expression constructs were generally stable and detectable within the hair cell *in vivo*. My main concerns were that the levels of expression and transient nature of exogenous expression might affect the interpretation of the results. It was apparent that all the constructs were mosaically expressed in pre-hearing hair cells at variable levels of intensity between 2 to 3 dpf, with the exception of a stable C-terminal fragment discussed later. By post-hearing stages at 4 dpf, the transient expression was altogether indistinguishable from background fluorescence, which precluded further analysis at later larval stages. Because the *in vivo* analysis was temporally restricted from 2 to 3 dpf, I first ensured that synaptic vesicles were present and localized to synaptic regions as early as 2 dpf and therefore characteristic of post-hearing distributions. I immunolabeled larvae at 2 dpf for the synaptic vesicle protein Vglut3, and observed that the staining was present at the basal end of hair cells (data not shown). This result indicates that integral components of the synaptic vesicle are

present at synaptic regions within hair cells during the pre-hearing temporal window in which I performed a structure-localization analysis.

I was also concerned that other variables such as maturity of the cell, stability of the protein, and the level of expression might interfere with the interpretation of the localization experiments. For example, I observed that very young hair cells exhibited higher levels of GFP fluorescent signal with many of the expression constructs. These cells were identified by their round morphology, and in some cases, dividing nuclei, and were excluded from the analysis due to their immaturity. High levels of expression also saturate the number of sites on synaptic membranes upon which Rbc3$\alpha$ can attach. In my previous experience, the over-expression of various cytoplasmic proteins within hair cells (for example Rab3A, Rab3 GEP, or Rab7) results in cell-fill dispersal that does not represent endogenous protein distributions. Therefore, I excluded from the localization analysis those hair cells that appeared to have excessively strong expression.

The isolation of the *rbc3α*$^{Q2447X}$ allele of the mutant *stardust*, which contains a nonsense mutation at amino acid 2447, and is therefore missing the final six WD-40 domains, suggests that the C-terminal end of the protein performs an essential function. As mentioned previously, a C-terminal fragment of human Rbc3α (aa 2495 – 3036) was found to modestly inhibit $Ca^{2+}$-dependent exocytosis in PC12 cells (Sakisaka and Takai 2005). This C-terminal fragment contained the final six WD-40 domains in tandem, which could work in concert to mediate protein interactions (Wall et al., 1995). Additionally, Rbc3α interacts with components of the synaptic-vesicle machinery (Li et al., 2012), and altogether

the evidence raises the possibility that the protein has a synaptic function. I tested whether the corresponding zebrafish Rbc3α fragment acts in a dominant-negative manner as predicted, by expressing a slightly longer version of GFP-Rbc3α C-term 2304 – 3062 fragment (Fig. 3.4 D). Unlike my other expression constructs, I was able to obtain stable transgenic animals with this construct. I found wide-spread distribution of the C-terminal fragment (2304 – 3062 aa), and noted that the fluorescent signal was very high. Due to the level of expression, I was unable to validate whether the C-terminal 2304 – 3062 portion of the protein affects its distribution, but I was able to determine that the fragment is well tolerated by the hair cell. In contrast with my prediction (Sakisaka and Takai 2005), transgenic animals did not display obvious auditory/vestibular defects despite robustly expressing the transgene throughout every hair cell because of stable insertion of the transgene in progeny. This result suggests that the C-terminal fragment does not act in an obviously dominant-negative manner on auditory/vestibular behaviors. Future studies will be needed to address whether a modest transmission defect at the hair-cell synapse is present in the C-terminal fragment expressing transgenic animals.

I then proceeded to determine which portions of the Rbc3α protein are necessary, or sufficient for its basal synaptic localization. I first examined whether a larger C-terminal half of Rbc3α could enhance the basal localization of the protein because of the effects on behavior when the final 6 WD-40 domains are lacking in the mutant *rbc3α*$^{Q2447X}$ (See Chapter 2 rbc3αQ2447X allele behavior). When I exogenously expressed GFP-Rbc3α C-term 1408 – 3062, I observed that

the construct was transiently distributed throughout the hair cell, excluding the nucleus (Fig. 3.4 E and F), but did not exhibit gross over-expression. This result indicates that the C-terminus does not contain a portion of the protein that enhances synaptic translocation.

Next, I expressed a fragment containing the N-terminal (aa 1 – 1577) half of the Rbc3α protein, which contains the first six WD-40 domains. When transiently expressed in hair cells at low levels, the GFP-Rbc3α N-term 1-1577aa fragment appeared to have a slight basal enhancement (Fig. 3.4 G and H). In contrast, cells with higher levels of expression appeared to have widespread distributions of the construct (Fig. 3.4 I). Due to the difficulty in obtaining hair cells that would express the various constructs, I was unable to perform a quantitative analysis of apical and basal distributions. The enhanced basal localization of the N-terminal half of the protein in low-level expressing cells suggests that the N-terminal half contains a portion of the protein that enables Rbc3α to translocate to synaptic regions of the hair cell.

I then refined the search for specific domains that contribute to the association of the protein with synaptic regions by subdividing the N- terminal half of the Rbc3α protein further. In brief, I did not find a minimal portion of the Rbc3α protein that is sufficient for augmented synaptic translocation, suggesting that nearly the entire N-terminal half (1 – 1517 aa) of the protein is required (Fig. 3.3).

Finally, I wanted to express a truncated N-terminal version of Rbc3α (GFP-Rbc3α 1 – 850 aa), in order to test the behavior of a mimic of the strongest allele

*rbc3α*$^{Q850X}$; if the truncated protein was stably expressed in the hair cell, it might reflect the behavior of the endogenous truncated protein in the mutant *rbc3α*$^{Q850X}$. I found that the expression of the construct was transient and strong (Fig. 3.4 J and K), but because it was detectable it was evident that the truncated protein was not immediately degraded. This will be examined in future studies.

**Conclusion**

This study was the first to examine the functional effects of loss of *rbc3α* in a whole organism, the tissues underlying the behavioral deficits of mutant *stardust* animals, and the subcellular distribution of the exogenously expressed protein in hair cells. I positionally cloned various alleles of the auditory/vestibular mutant *stardust* and found they encode nonsense mutations in the gene *rbc3α*. Tissue expression experiments using *in situ* hybridization and RT-PCR were performed and transcripts of *rbc3α* were detected throughout the zebrafish larvae, particularly the nervous system and sensory tissues including the eye, ear, and lateral-line organs. These results indicate that early sensory receptor hair-cells are the cell-types underlying the auditory/vestibular phenotype of mutant *stardust* animals. In order to determine the structure and localization of the Rbc3α protein, I cloned the first full-length *rbc3α* cDNA and was then able to perform *in vivo* examination of the exogenously expressed protein by confocal microscopy. I found that the full-length GFP-tagged protein is distributed in synaptic regions of the hair cell, supporting its proposed role as a synaptic vesicle associated protein. In addition, I found that the N-terminal half of the protein (1 – 1517 aa), which

contains the first 6 WD-40 domains, is required for the enhanced translocation of Rbc3α to vesicular regions within the hair cell. Finally, I did not observe obvious auditory/vestibular dysfunction in zebrafish that transgenically express a C-terminal Rbc3α fragment (2034 – 3062 aa), which had been previously found to inhibit $Ca^{2+}$-dependent exocytosis (Sakisaka and Takai 2005).

*The tissue distribution of Rbc3α indicates its synaptic utilization*

We found that the expression of the *rbc3α* transcript was widespread throughout the zebrafish larva. This is meaningful because it was originally reported that Rbc3α protein is solely expressed in the brain (Nagano et al., 2002). This finding was challenged by subsequent observation that identified a contribution of Rbc3α to the intracellular acidification of diverse tissue types (Yan et al., 2009, Sethi et al., 2010). However, we also observed that the greatest intensity of transcript labeling was within neural tissues, which is compatible with its original identification as expressed in the mammalian hippocampus and the hypothesis that Rbc3α has a synaptic function (Nagano et al., 2002, Sakisaka and Takai 2005) The transcript's expression in the zebrafish hair cell indicates that the receptor cell-type contributes to the auditory/vestibular dysfunction observed in mutant *stardust* animals. Given the widespread expression of *rbc3α* that I detected in the nervous system, I speculate that the neural circuitry of the escape response might be subject to differences between the alleles, despite the ability of all alleles of the mutant to robustly respond to a light touch.

Based on the widespread expression of the protein and its importance in

intracellular acidification, and indirectly Notch signaling (Yan et al., 2009, Sethi 2010), one might predict that the loss of Rbc3α would have dramatic effects on the morphology of an affected animal. For instance, an examination of zebrafish lines with mutations in various V-ATPase subunits found that the retinal pigment epithelium of the affected animals degenerates and another cell-type, the melanocytes, appear translucent and ghostly (Nuckels et al., 2009). By comparison, I observed that the mutant *rbc3α* animals lack spontaneous eye movements and light adaptation responses in the otherwise normal appearing melanocytes, which is consistent with visual dysfunction. However, the melanocytes appeared otherwise normal in mutants and were replete with pigment in the subcellular melanophores. The selective importance of Rbc3$\alpha$ to hearing and visual behaviors may indicate that it is utilized in a similar manner by both systems. Syndromic forms of deafness and blindness are relatively common due to the considerable overlap between the systems (hereditaryhearingloss.org). One similarity, for instance, is the appearance of ribbon-type synapses by auditory and visual systems. It will require further investigation to determine why Rbc3$\alpha$ has a selective contribution to hearing and vision.

*The distribution of Rbc3$\alpha$ in the hair cell is synaptic*

I found that exogenously expressed Rbc3$\alpha$ protein translocates to synaptic regions of the hair cell, similar to its endogenous localization at central synapses (Nagano et al., 2002), and its association with components of the synaptic machinery (Li et al., 2012). But an important question remains as to how the

Rbc3α protein associates with synaptic vesicles without the presence of transmembrane helical domains. The attempts to dissect specific portions of the protein that are sufficient for vesicular translocation had limited success, though I observed that the N-terminal half of the protein is required. It was my hope that by isolating a small region of the protein required for its vesicular translocation and using it as bait, I could more precisely screen for protein interacting partners that were vesicular docking sites for Rbc3α. As it stands, I can only speculate how this might occur. A good starting point, however, is the V-ATPase itself as the site of docking due to multiple interactions between the V-ATPase holocomplex and the Rbc3 complex (Yan et al., 2009, Li et al., 2012). The V-ATPase holocomplex is estimated at 1 copy per synaptic vesicle, and no more than 2 (Takamori et al., 2006), and has multiple subunits of Atp6V1A, which is an interactor with Rbc3α (Li et al., 2012). Alternatively, Rbc3α might dock on the synaptic vesicle via Rab3 GEP, which can serves as both an exchange factor and stably associated adaptor of Rab3 (Niwa et al., 2008). Rab3 is present at 10 copies per synaptic vesicle (Takamori et al., 2006), and could enable Rbc3α to translocate at several sites. However, the association between Rbc3α and Rab3 GEP and Rab3 has not been repeated by other studies (Li et al., 2012).

Finally, I performed a structure-localization analysis of a transgenically expressed Rbc3α C-terminal fragment in hair cells in order to determine if the fragment acts in a dominant-negative manner on hearing and vestibular behaviors as predicted from its inhibitory effect on secretion (Sakisaka and Takai 2005). I did not, however, find evidence for this, though there are several

differences between this examination and previous work indicating a modest inhibition on $Ca^{2+}$-dependent exocytosis with the corresponding human C-terminal fragment (Sakisaka and Takai 2005). First, I used behavior as an assay, which is downstream of sensory detection. In contrast, the Sakisaka study measured secreted levels of growth hormone in PC12 cells as a readout of exocytosis. Further, the PC12 cells were stimulated with non-physiological levels of high $K^+$ solutions. In the future the laboratory researchers will perform lateral-line afferent recordings from stable transgenic animals expressing the C-terminal fragment of Rbc3α in the hair cell in order to determine if the fragment inhibits $Ca^{2+}$-dependent exocytosis.

Ultimately, the goal is to determine the contribution of various domains of Rbc3α on operation of the hair-cell synapse. Stable transgenic animals might allow better quantification of the protein's distribution. Not described in this study, I have also cloned the first full-length *rbc3β* cDNA in zebrafish and plan to conduct exogenous expression experiments in the hair cells of wild-type and mutant stardust animals in order to determine if it requires its protein partner Rbc3α for its synaptic-vesicle association (Kawabe et al., 2003). Conversely, one can knockdown Rbc3β and examine the effects on Rbc3α localization.

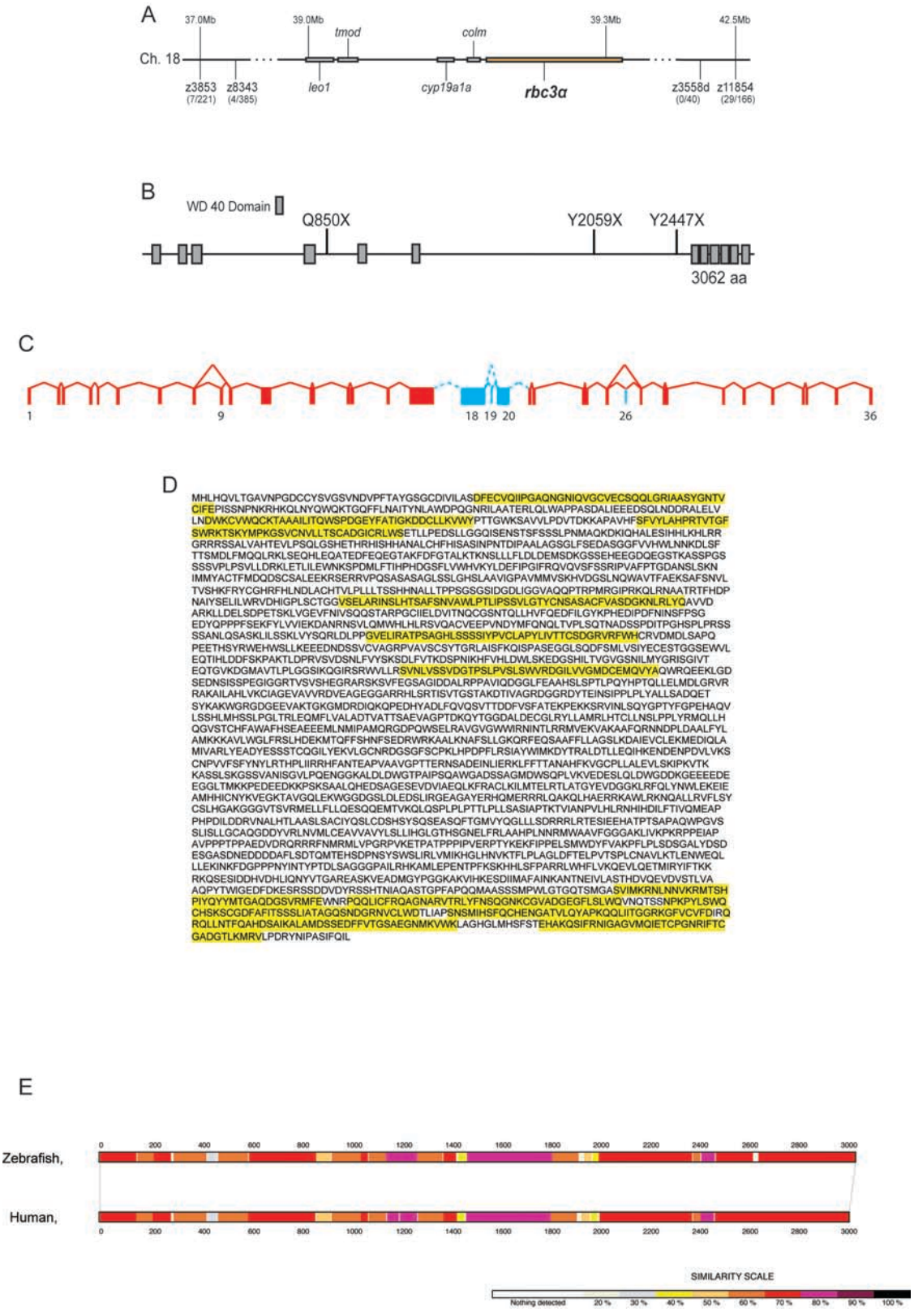


Figure 3.1 Positional mapping and cloning of *rbc3*α

***A***, Map of the critical interval containing *stardust* on chromosome 18. Flanking microsatellite markers are indicated below the bar. Not all predicted genes are shown. ***B***, Three alleles of *stardust* contain nonsense mutations in *rbc3*α. The 12 predicted WD-40 repeats of the Rbc3α protein are indicated by gray boxes. ***C***, Splice isoforms of *rbc3*α containing new exons 18, 19, 20 and 26 marked by blue boxes. Red boxes denote previously known exons. Numbers below red boxes indicate exon number. Unknown length of intronic sequences denoted by dashed blue lines. ***D***, Amino acid sequence of full-length protein predicted from zebrafish *rbc3*α. Yellow highlighted amino acids denote WD-40 predicted domains. ***E***, Alignment between human and zebrafish *Rbc3*α proteins indicate 72% identity between the homologs.

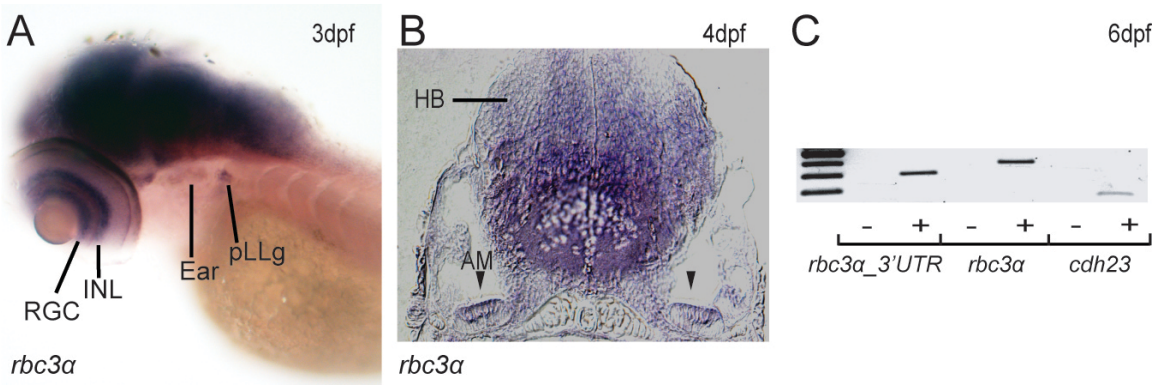


Figure 3.2 Expression of *rbc3*α

***A**, In situ* hybridization pattern of *rbc3*α transcripts at 3 dpf. ***B***, A coronal section through the hindbrain and inner ear at 4 dpf stained for *rbc3*α mRNA. Arrowheads denote macular hair cells. ***C***, PCR products for *rbc3*α and hair-cell specific *cdh23* amplified using cDNA isolated from lateral-line neuromasts of WT larvae at 6 dpf. AM, Anterior macula; HB, hindbrain; INL, inner nuclear layer; pLLg, posterior lateral line ganglion; RGC, retinal ganglion cell.

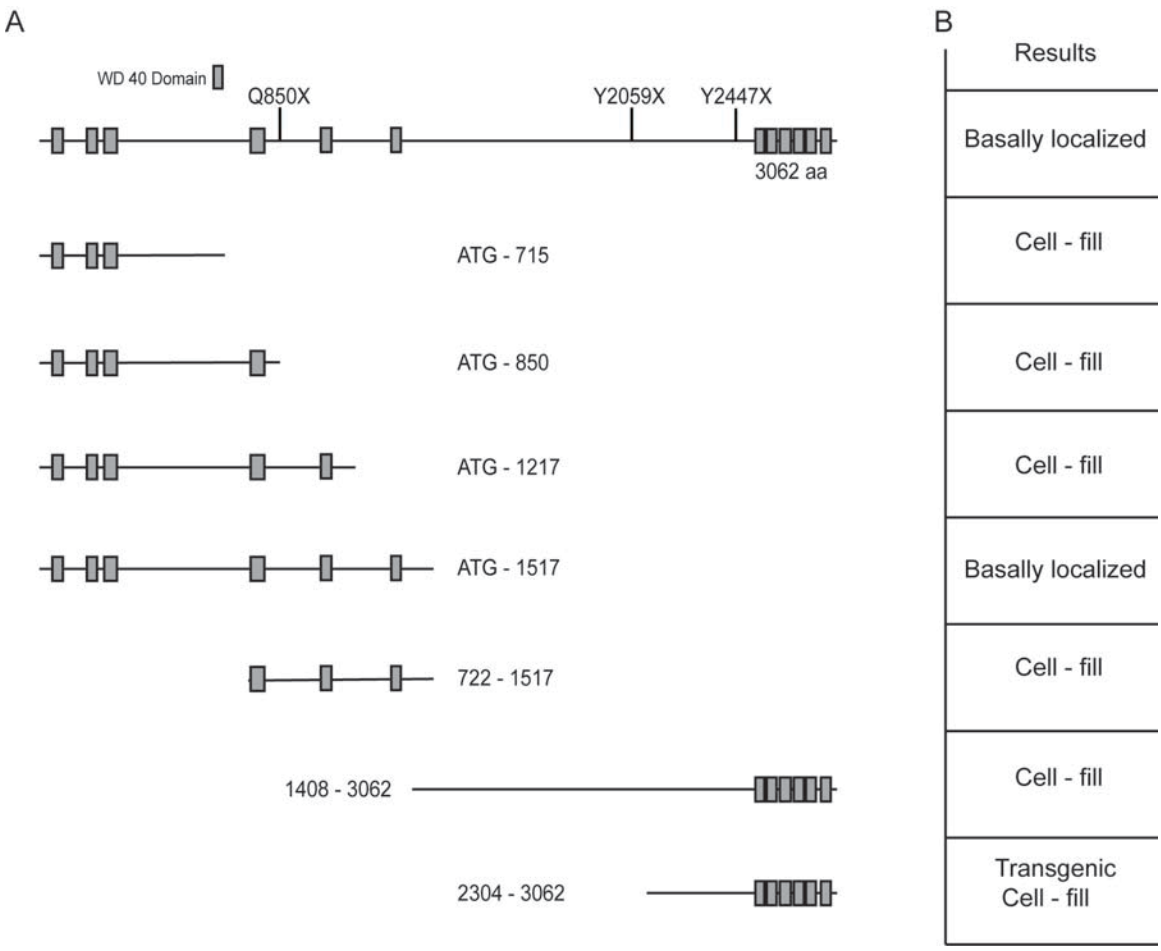


Figure 3.3 Rbc3α constructs used for expression experiments

***A**, Diagram of full-length Rbc3*α and various truncated constructs used for structure-localization analysis. Amino acids of *stardust* alleles denoted above full-length protein. The 12 predicted WD-40 repeats are indicated by gray boxes. ***B**,* Summary of results of various constructs used for structure-localization analysis.

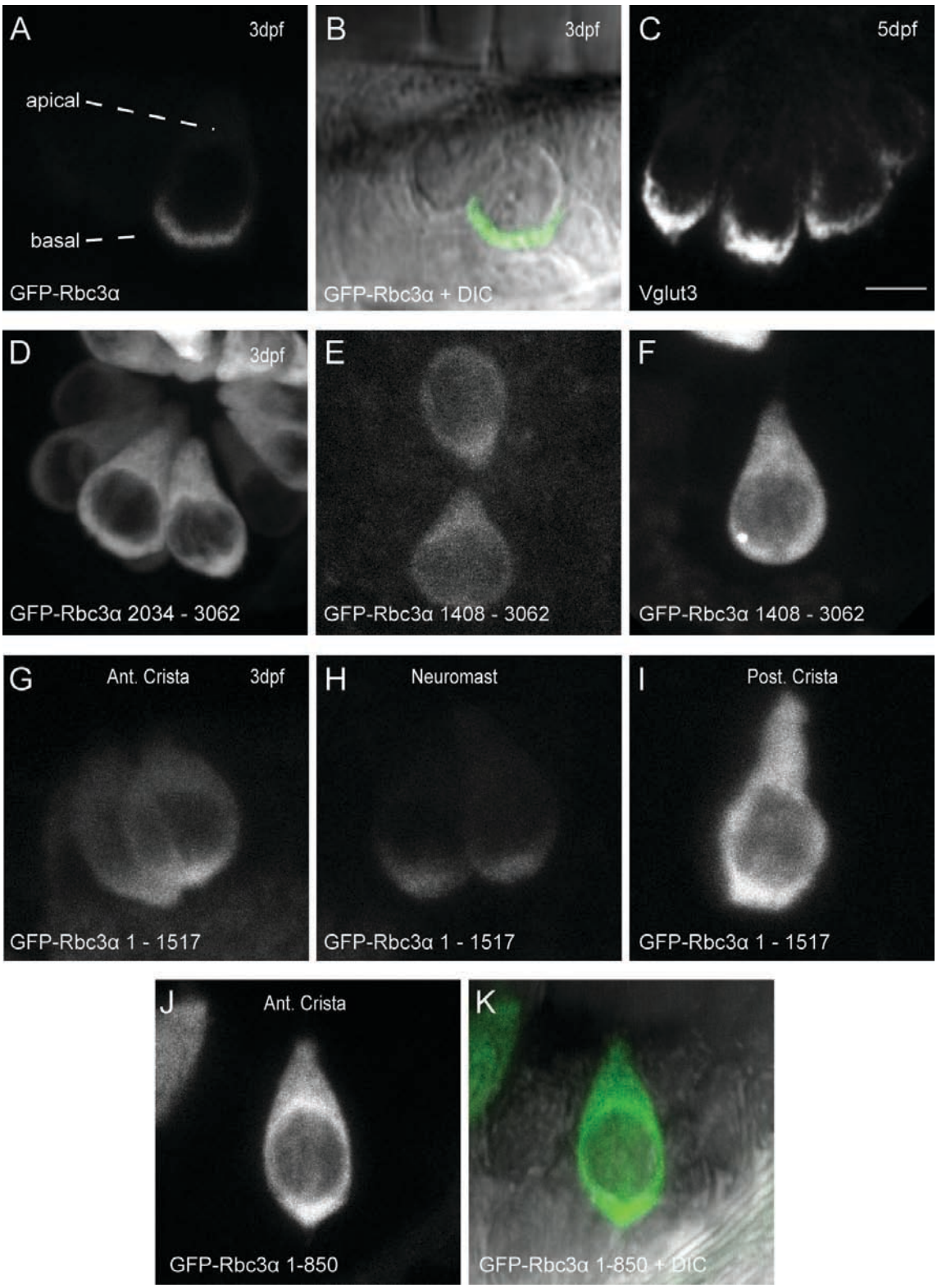


Figure 3.4 Rbc3α localizes to synaptic regions in the hair cell

***A***, ***B***, Confocal *Z*-projection of transient expression of *Tg(−6.5myo6b:GFP–rbc3α)* plasmid in an ampullary hair cell at 3 dpf. Rbc3α–GFP expression localized to the base of hair cells. ***C***, Example of labeling of synaptic vesicles with anti-Vglut3 antibody in inner ear hair cells (5 dpf). ***D***, C-terminal fragment of *Tg(−6.5myo6b:GFP–rbc3α 2034-3062aa*) is widely distributed in neuromast of transgenic hair cell at 3dpf. ***E***, Examples of transient GFP-Rbc3α 1408-3062aa labeling in neuromast with low expression, ***F,*** or in a neuromast with high expression (3 dpf). ***G***, Example of low-expression in ampullary hair cell of N-terminal fragment Rbc3α 1-1517 aa. ***H,*** Example of low-expression in neuromast hair cell of N-terminal fragment Rbc3α 1-1517 aa, or ***I***, example of high-expression posterior crista (3 dpf). ***J***, ***K***, N-terminal version of Rbc3α (GFP-Rbc3α 1 – 850 aa) expressed in a neuromast. Scale bar, 4 μm. Note individual images were adjusted to different gains in order to illustrate localization better due to variability in intensity between constructs.

# Chapter 4 - Rabconnectin3α promotes stable activity of the $H^+$-pump on synaptic vesicles in hair cells

**Authors:**

Zev Einhorn, Josef G. Trapani, Qianyong Liu and Teresa Nicolson

**Acknowledgements:**

This study was supported in part by NIH R01 DC006880. We thank the members of the Tübingen 2000 Screen Consortium for their assistance in isolating the *rbc3α* alleles.

**Chapter Summary**

Acidification of synaptic vesicles relies on the Vacuolar-type ATPase (V-ATPase), which provides the electrochemical driving force for neurotransmitter exchange. The regulatory mechanisms that ensure assembly of the V-ATPase holoenzyme on synaptic vesicles are unknown. Rabconnectin3α (Rbc3α) is a potential candidate for regulation of V-ATPase activity because of its association with synaptic vesicles and its requirement for acidification of intracellular compartments. Here, we provide the first evidence for a role of Rbc3α in synaptic vesicle acidification and neurotransmission. In this study, we characterized mutant alleles of *rbc3α* isolated from a large-scale screen for zebrafish with auditory/vestibular defects. We showed in Chapter 2 that Rbc3α is localized to basal regions of hair cells where synaptic vesicles are present. To determine whether Rbc3α regulates V-ATPase activity, we examined the acidification of synaptic vesicles and localization of the V-ATPase in hair cells. In contrast to wild-type hair cells, we observed that synaptic vesicles had elevated pH and a cytosolic subunit of the V-ATPase was no longer enriched in synaptic regions of mutant hair cells. As a consequence of defective acidification of synaptic vesicles, afferent neurons in rbc3α mutants had reduced firing rates and reduced accuracy of phase-locked action potentials in response to mechanical stimulation of hair cells. We also find no evidence that Rbc3α is a regulator of Rab3, nor strong evidence that Rab3 is a component of the ribbon body as previously conjectured. Collectively, our data suggest that Rbc3α modulates synaptic transmission in hair cells by promoting V-ATPase activity in synaptic vesicles.

## Introduction

Forward genetic screens for hearing and balance mutants in zebrafish and mouse knock-outs have identified several of the molecules important for synaptic transmission in hair cells (Nicolson et al., 1998; Leibovici et al., 2008; Obholzer et al., 2008; Trapani et al., 2009). One such protein is *vesicular glutamate transporter 3* (Vglut3), which loads neurotransmitter glutamate into synaptic vesicles through a voltage gradient (Fremeau et al., 2002; Obholzer et al., 2008; Ruel et al., 2008; Seal et al., 2008), which is initially established by concentrating protons into the lumen of the synaptic vesicle by the V-ATPase, and as a result, robust V-ATPase activity is critical for proper synaptic transmission (Schenk et al., 2009; Goh et al., 2011). However, relatively little is known about how synaptic vesicles acquire the V-ATPase in its fully assembled and active state.

The V-ATPase holoenzyme is a complex that contains a cytosolic (V1) sector and a membrane (V0) sector that are each composed of multiple subunits. The cytosolic and membrane sectors are largely pre-assembled and can reversibly disassociate (Smardon et al., 2002, Trombetta et al., 2003; Smardon and Kane, 2007). Regulated assembly of the V-ATPase holoenzyme is an efficient mechanism for modulating V-ATPase activity (Toei et al., 2010). Whether regulated holoenzyme assembly also shapes V-ATPase activity on synaptic vesicles is unknown.

Rbc3$\alpha$ is a potential candidate for regulating the assembly of the V-ATPase holoenzyme on synaptic vesicles for several reasons. Recent work has

shown that the Rbc3 complex is essential for acidification of intracellular compartments in *Drosophila* ovarian tissue and mammalian cell-lines (Yan et al., 2009; Sethi et al., 2010). Moreover, Rbc3β biochemically interacts with insect V1 subunits E and H, as evidenced by co-immunoprecipitation experiments (Yan et al., 2009). Prior evidence also supports a role in synaptic vesicle function for the Rbc3 complex: Rbc3α and β subunits were originally identified from purified synaptic vesicle fractions and antibodies against Rbc3α labeled synaptic regions of the rat hippocampus (Nagano et al., 2002; Kawabe et al., 2003). Finally, an examination of the Rbc3α protein's interactome in the murine hippocampus supported the association between Rbc3α and the V-ATPase, particularly the V-ATPase cytosolic subunit Atp6V1A, (Li et al., 2012). Taken together, these data raise the possibility that the Rbc3 complex modulates V-ATPase activity on synaptic vesicles by promoting holoenzyme assembly.

In addition to a putative role in synaptic vesicle acidification, Rbc3α might also contribute to the synaptic vesicle's life cycle in other important ways. The protein was first purified in a screen for interactors with Rab3 GEP and GAP on synaptic vesicles (Nagano et al., 2002), and therefore was hypothesized to be a synaptic vesicle scaffold upon which Rab3 is regulated by GEP and GAP (Wada et. al, 1997, Fukui et al., 1997). The biological significance of Rbc3α's association with the synaptic vesicle, however, had not been determined prior to our work (Einhorn et al., 2012). It is possible that Rbc3α plays a role linking the ribbon to Rab3 signaling (Uthaiah and Hudspeth 2010). Additionally, several synaptic-vesicle associated proteins were also found to interact with Rbc3α (Li et

al., 2012): Syntaxin 1, Synaptojanin 1 and NSF. Finally, there is a modest inhibition of $Ca^{2+}$ -dependent secretion from the mis-expression of a human C-terminal fragment of the Rbc3α protein in PC12-cell culture (Sakisaka and Takai 2005). These findings raise the possibility of a potential contribution from Rbc3α to the synaptic vesicle cycle.

In this study, we examined the morphology and activity of hair-cell synapses of rbc3α mutant zebrafish to determine the function of Rbc3α in hair cells. Our observations indicate that rbc3α mutant hair cells have overall normal synaptic structure, but synaptic vesicles fail to fully acidify presumably due to fewer assembled V-ATPase holoenzymes. We propose that Rbc3α plays a role in modulating vesicular V-ATPase activity in hair cells that ultimately affects proper synaptic transmission that is essential for both auditory and vestibular function.

## Methods

### *Fish Strains*

Wild-type, mutant, and transgenic larvae were maintained in both Tübingen and Top Long Fin strains. Larvae were kept at 28.5 °C in the dark in E3 buffer during development. Mutants were identified in a large-scale ethyl-N-nitrosourea screen (Tübingen 2000 Screen Consortium). Both sexes were examined.

### *Molecular Biology*

Expression constructs were generated with Multisite Gateway Technology (Invitrogen, Kwan et al., 2007). In brief, *atp6v1aa* was PCR amplified with Gateway compatible attB sites (forward primer 5-ggggacaagtttgtacaaaaaagcaggctccgccaccatggatttttccaagctgcctaagatccga -3 ; reverse primer 5-ggggaccactttgtacaagaaagctgggtcgtcttccagggtgcggaaggaattctg-3) and recombined to generate 3'entry vector p3E- *atp6v1aa*, then p3E-*atp6v1aa* was recombined with p5E-*6.5myosin6b* minimal promoter (Mo and Nicolson, 2011) , pME-*GFP,* and the pDestination 395 vector to generate -*6.5kb_myosin6b:gfp- atp6v1aa;clcm2:gfp*. *atp6v0a1* contained in the pME18S-FL3 (ATCC) was PCR amplified with primers (forward primer 5 -ggggacagctttcttgtacaaagtggcgatgggggagctgtttcgcagcgagg-3 ; reverse primer 5-ggggacaactttgtataataaagttgcttattcttcagacttgccatccaga-3) and recombined with p3E. pME-*atp6v1aa* and p3E-*atp6v0a1* cloned to generate -*6.5myosin6b:atp6v1aa-GFP,clcm2:GFP* and -*6.5myosin6b:GFP-atp6v0a1,clcm2:GFP* constructs, respectively. Constructs were then micro-injected (50 ng/µl) along with Tol2 transposase mRNA at the one-cell stage of embryos.

*Generation of transgenic strains*

*Rbc3*$\alpha^{+/Q850X}$ animals were in-crossed and microinjected with Tol2 mRNA and -*6.5myosin6b:atp6v1aa-gfp;clcm2:gfp*. F0 animals were screened and crossed to *rbc3*$\alpha^{Q850X}$ to generate F1 transgenic animals *Tg(-6.5myosin6b:atp6v1aa-gfp,clcm2:gfp);rbc3*$\alpha^{Q850X}$.

*RT-PCR of neuromasts and yolk epithelium*.

Tissues from Tübingen wild-type larvae were extracted by a suction pipette and aspirated into cold lysis buffer from Cells-to-cDNA kit II (Ambion). Overlying yolk skin cells were dissected by fine tweezers. First strand cDNA synthesis was performed using Sprint-RT Complete-Oligo(dT) 18 kit (Clontech Laboratories). cDNAs were amplified by PCR using ChoiceTaq Blue Master Mix (Denville Scientific) with primers pairs targeting *rbc3*$\alpha$ bp 8726-9105 (forward 5' gcagcagttgatcatcacgggcggcaggaaggg 3' and reverse 5' gaggatctggaatatactggccggaatgttgtagcggtcggg 3'), or *atp6v1aa* bp 748-1299 (forward 5' ggagccttcggctgtggcaag 3' and reverse 5' ccagaacacctgcacaatac 3'). Water was used as a negative template control.

*Primary Antibodies for Immunohistochemistry and fluorescence labeling*

Rabbit polyclonal panMAGUK (1:500 dilution) and mouse monoclonal Ribeyeb (1:1000 dilution) antibodies were described in (Sheets et al., 2011). Rabbit polyclonal Vglut3 antibody (1:1000 dilution) was described in (Obholzer et al., 2008). Atp6V1A (a and b) proteins were targeted by rabbit polyclonal antibody, dilution 1 µg/ml (17115-1-AP, Proteintech Group). PanRab3 mouse antibody (1:1000 dilution, #107011, Synaptic Systems). Actin was labeled by incubation with Alexa488-Phalloidin (1:1000 dilution, Invitrogen).

*Whole-mount immunohistochemistry and fluorescent imaging*

Zebrafish larvae at 5 dpf were fixed in 4% paraformaldehyde and phosphate buffered saline with 0.02% Tween (PBS-T) overnight at 4°C, permeabilized with ice-cold acetone for 5 minutes, and blocked with PBS-T containing 1% bovine serum albumin (BSA) and 1% dimethyl sulfoxide (DMSO) for 2 hours room temperature. They were then incubated with primary antibodies in blocking buffer overnight at 4°C, washed several times in PBST, and incubated in blocking buffer with secondary antibodies conjugated to Alexa488 (Molecular Probes, Invitrogen) and DyLight 549 (Jackson ImmunoResearch). Images through the Z-plane were collected with Zeiss Axiovert ImagerM.1 microscope with an LSM700 confocal scanhead, Axiocam MrM camera, oil-immersion lens Zeiss Plan Apochromat 63X/1.4NA objective (Zeiss). 488 nm and 555 nm laserlines were used for excitation and laser intensities were adjusted to minimize photobleaching.

For quantification of the Atp6V1A (a and b), neuromasts IO1-3 and SO1-3 were used due to their exceptional preservation of morphology of the hair bundles after paraformaldehyde fixation. Top-down confocal images were collected through the Z plane of the entire neuromast (10-15 μm). Statistical subtraction was then performed with Metamorph software (Molecular devices) with a threshold set to 300 pixels. Single optical sections of 1 μm that were beneath the apical hair bundle were selected for analysis of apical compartments. Maximum *z*-plane projections of the basal end (3 μm optical section) were

selected for basal measurements. Total neuromast V1A signal was measured for maximal projections through the *z*-plane of the entire neuromast.

For quantification of the Rab3 and Vglut3 signal, L2 neuromasts were used for confocal microscopy. Maximal *z*-projections of the entire neuromast were performed (10-15 μm). Statistical subtraction was performed and neuromasts thresholded to 150 pixels and measured. For determination of Ribeyeb and panMAGUK overlap, Manders correlation coefficients were determined for maximal *z*-projections of L2 neuromasts using the plugin JACob of ImageJ (Bolte and Cordelières, 2006).

*Live cell imaging*

For live imaging, larvae at 5dpf were anesthetized in 0.01% tricaine and embedded in 1.5% low-melt agarose containing tricaine. Live-cell staining was performed with confocal microscopy using a water-immersion lens 60X/0.95NA objective. 488 nm and 555 nm laserlines were used for excitation. The entire neuromast was imaged for analysis with ImageJ. Hair cells that displayed very high expression of transgene constructs, including aberrant nuclear signal, were excluded from further analysis.

*LysoTracker staining of acidic compartments*

LysoTracker DND-99 dye (Invitrogen) at 100 nM concentration was used for labeling acidic compartments. Larvae were continuously incubated with dye, and then imaged (555/590 excitation/emission). Z-stacks of L2 neuromasts were used for comparison. Images were thresholded to 100 and measured with ImageJ. LysoSensor GREEN-DND-189 (Invitrogen) was added at 100 nM and emission was imaged at 505 nm.

*V-ATPase pharmacological inhibition*

Bafilomycin A1 inhibitor (Sigma) was added to the whole-larvae bath at a final concentration of 1 μM. Larvae were incubated for 5 minutes and washed repeatedly before imaging.

*Electrophysiology and Lateral-line Afferent Recordings.*

Our recording setup for both microphonics and action currents has been previously described (Obholzer et al., 2008; Trapani and Nicolson, 2010). To suppress muscle activity, larvae were anesthetized and then microinjected in the heart with 125 μM α-bungarotoxin. For extracellular current recordings, borosilicate glass pipettes were pulled (P-97, Sutter Instruments) with a long taper and had resistances between 5 and 15 MΩ in extracellular solution. Microphonic electrodes resembled standard patch pipettes with resistances from 1 to 5 MΩ in extracellular solution. Signals were obtained using an EPC 10 amplifier and Patchmaster software (Heka Electronic). Extracellular action currents were recorded from the soma of an individual lateral-line afferent neuron

with seal resistances ranging from 20 to 80 MΩ. The recordings were done in voltage-clamp mode, sampled at 50 µs/pt and filtered at 1 kHz. Microphonic potentials were performed in current-clamp mode and sampled at 100 µs/pt. An additional amplifier (Model 440, Brownlee Precision) was used for a total of 10,000X gain and 50 Hz filter of the voltage signal. For microphonics, the recording electrode was positioned (MPC-385, Sutter Instruments) adjacent to the neuromast at the height of the hair-cell stereociliary bundles. For action current recordings, the electrode was positioned within the posterior lateral-line ganglion. The neuromast innervated by the selected afferent neuron was then identified by incrementally moving the waterjet from neuromast to neuromast until phase-locked spiking was seen in response to stimulation of the innervated neuromast.

*Mechanical Stimulation.*

Stimulation of neuromast hair-cells was performed with a pressure clamp (HSPC-1, ALA Scientific) attached to a glass micropipette (tip diameter ~ 30 µm) filled with extracellular solution. The waterjet pipette was positioned (MP-265, Sutter Instruments) approximately 100 µm from a given neuromast and displacement of the kinocilia was verified by eye.

*Signal Analysis.*

Data were analyzed using custom software written in Igor Pro (Wavemetrics) and were plotted with Prism 5 (Graphpad). Average spike rate (spikes/second) was computed from the total number of spikes in 60 consecutive

one-second traces. Average spike latency from the start of each 60 cycle and the degree of synchrony between the stimulus wave and the action current response (calculated as vector strength) was performed as described previously (Trapani et al., 2009). Representative microphonic traces were the average of 200 consecutive 500-ms traces. Mean power spectral density (PSD) was then determined from the sum of individual PSDs for each of the 200 traces during the 200-ms stimulus portion of each trace.

*Statistical Analysis*

Average data are presented as the mean ± standard error (SEM). Statistical significance was determined using either a Student's two-tailed *t* test (paired or unpaired as appropriate), Mann-Whitney test, or analysis of variance (one-way ANOVA with Bonferonni's multiple comparisons test). Differences between groups were considered significant if *p* values were less than 0.05. Linear regression analysis was performed for R square. Statistical analyses were performed and graphs were constructed using Prism 5.0 software.

## Results

*Rbc3α mutant hair cells fail to properly acidify synaptic vesicles*

The Vglut3-like distribution pattern of GFP-Rbc3α in hair cells suggests a functional link between the protein and synaptic vesicles. Previous genetic evidence also argues for the importance of Rbc3α in the acidification of other intracellular compartments (Yan et al., 2009; Sethi et al., 2010). Therefore, we

predicted that the loss of Rbc3α would also affect synaptic vesicle acidification. To examine this possibility, we applied the acidotropic and cell-permeant fluorescent dye LysoTracker to whole larvae in order to label acidic compartments. Lysotracker has been used to examine synaptic vesicles in retinal bipolar termini (Abreu et al. 2008). In live hair cells of wild-type larvae, the fluorescent signal was greatest at the basal end of hair cells where synaptic vesicles reside (Fig. 4.1 A, B). Interestingly, at lower-gain settings, ring-like topologies or tori at the base of the hair cell became apparent (Fig. 4.1 A). To determine whether LysoTracker dye labeled acidic synaptic vesicles surrounding each ribbon body, we applied the dye to transgenic larvae stably expressing Ribeye b-GFP. The Ribeye b-GFP aggregates were surrounded by the LysoTracker-labeled tori, confirming that ribbon-associated vesicles were labeled. In addition, immunolabel of Vglut3 also surrounds Ribeye b positive puncta (data not shown, Obholzer et al. 2008). The remainder of the basally concentrated dye likely consists of various acidic organelles, including synaptic vesicle, lysosomes and endosomes though I did no further experiments to verify this possibility. We next examined live hair cells of mutant larvae to determine whether hair cells require Rbc3α for synaptic vesicle acidification. For comparison between genotypes, we restricted our analysis to neuromasts at the same position (L2) along the trunk. Basal LysoTracker signal of either rbc3α$^{Q850X}$, or rbc3α$^{Y2447X}$ mutants was greatly reduced compared to wild-type hair cells, but not between alleles (Fig. 4.1 B, C, E; WT 1332 ± 126 A.U. n = 12; *rbc3α$^{Q850X}$* 169 ± 20 A.U. n = 11; rbc3α$^{Y2447X}$ 168 ± 15 A.U. n = 11, one-way ANOVA; $F(2,31) = 74.8$; $p <$

0.0001). A similar observation of reduced Lysotracker signal was made for the mutant rbc3α$^{Y2059X}$ (data not shown). In addition, the fluorophore LysoSensor GREEN-DND-189 (LysoSensor) has been used to label phagosomes in microglia of zebrafish (Peri and Nusslein-Volhard 2009). We find that it also labels synaptic vesicles in wild-type hair cells more readily than mutant hair cells (data not shown). Together, these results indicate that proper synaptic vesicle acidification requires functional Rbc3α.

The residual labeling of mutant synaptic vesicles suggested that low levels of V-ATPase activity were still present. Therefore, to determine whether Rbc3α acts as a modulator of V-ATPase activity, we then applied the V-ATPase-specific inhibitor bafilomycin to both wild-type and rbc3α$^{Q850X}$ mutant animals. In hair cells of each genotype, basally localized LysoTracker signal was reduced to levels below that of untreated rbc3α$^{Q850X}$ mutants (Fig. 4.1 D, E; WT bafilomycin-treated 76 ± 16 A.U. n = 6; untreated *rbc3α$^{Q850X}$* 169 ± 20 A.U. n = 11; *rbc3α$^{Q850X}$* bafilomycin-treated 64 ± 13 A.U. n = 5; one-way ANOVA; F(2,19) = 8.7; $p$ = 0.002). This result supports a modulatory role rather than an absolute requirement for Rbc3α in vesicle acidification. We also noted that near the epithelial surface of hair cells, apical puncta were labeled with LysoTracker and were present in both wild-type and mutant hair cells. These puncta had levels that were similarly matched, suggesting that the decrease in mutant labeling was specific to basal compartments (Fig. 4.1 F; WT 183 ± 18 A.U. n = 6 larvae; rbc3α$^{Q850X}$ 232 ± 19 A.U. n = 9; rbc3α$^{Y2447X}$ 213 ± 15 A.U. n = 11; one-way ANOVA; F(2,23) = 1.5; $p$ = 0.234). Collectively, our results with LysoTracker

suggest that the function of Rbc3$\alpha$ is primarily to modulate the pH of synaptic vesicles in hair cells.

Because a C-terminal fragment of human Rbc3α (aa 2495 – 3036) inhibits $Ca^{2+}$ dependent exocytosis (Sakisaka and Takai 2005) and secretory granules are acidic organelles that also require the V-ATPase for their release, we tested whether a similar zebrafish fragment of the Rbc3α protein 2304 – 3062 inhibits synaptic vesicle acidification. We generated stable transgenic animals *Tg(-6.5myosin6b:gfp-rbc3$\alpha$ 2304-3062,clcm2:gfp)*, and noted high levels of the fluorescent signal within the hair cell (Fig. 3.5 Chapter 3). However, when we examined wild-type animals for an acidification change in the synaptic vesicles, we observed no correlation between LysoTracker signal and GFP signal (Fig. 4.2; R square = 0.054; $p$ = 0.21). This result suggests that the C-terminal fragment does not act in a dominant negative manner to inhibit synaptic vesicle acidification. Our results indicate that in PC12 cell growth hormone release experiments with Rbc3α C-terminal fragments, $Ca^{2+}$-dependent exocytosis is likely inhibited through an acidification-independent manner.

*Proper synaptic localization of V-ATPase subunits requires Rbc3$\alpha$*

Our results are consistent with a role for Rbc3α in modulating acidification of synaptic vesicles. We next set out to determine the molecular basis of this modulation. Given the interaction between various subunits of the Rbc3 complex and the V-ATPase in *Drosophila*, altered V-ATPase activity was a plausible explanation for defective acidification (Yan et al., 2009). We hypothesized that

Rbc3α promotes acidification of vesicles via regulation of the proton pump. Rbc3α may influence proton pump activity in several ways including trafficking, protein expression or degradation, or assembly of the V-ATPase holoenzyme (Toei et al., 2010).

To determine which mode of V-ATPase regulation might be affected by the loss of Rbc3α function, we examined the distributions and levels of subunits of the cytosolic (V1) and membrane (V0) sectors of the V-ATPase. To visualize the cytosolic sector, we labeled whole larvae with an anti-panV1A antibody, and counterstained for actin using Alexa488-Phalloidin. The specificity of the V1A antibody was confirmed as ionocytes, which express high levels of V-ATPase, were robustly labeled (Fig. 4.3 A, A'; Shiao et al., 2005; Horng et al., 2009). The V1A immunolabeling observed in hair cells was markedly enriched at basal regions in wild-type hair cells (Fig. 4.3 B, shown in purple), but in contrast, was evenly dispersed between apical and basal regions of rbc3α$^{Q850X}$ hair cells (Fig. 4.3 B'). To quantify the differences in V1A distribution between wild-type and mutant hair cells, we measured the ratio of apical-to-basal signal. We found that the ratio of apical-to-basal V1A signal was significantly increased in rbc3α$^{Q850X}$ hair cells (Fig 4.4 C; WT 0.54 ± 0.03 n = 15 neuromasts, 9 animals; rbc3α$^{Q850X}$ 0.92 ± 0.03 n = 13, 8 animals; $p < 0.0001$; unpaired Student's t test). To determine whether the increase in apical-to-basal ratio was due to a change in V1A expression, we measured the total fluorescence of V1A and found that the overall intensity of V1A labeling did not significantly differ between wild-type and mutant hair cells (Fig. 4.3 D; WT 937 ± 61 A.U. n = 15 neuromasts, 9 animals;

rbc3$\alpha^{Q850X}$ 889 ± 57 A.U. n = 13, 8 animals; *p* = 0.57; unpaired Student's t test). Thus, protein levels of the cytosolic V-ATPase subunit appear unaffected in mutant hair cells, while the distribution pattern indicates a possible defect in trafficking, assembly, or vesicle distribution.

Across species, defective assembly of the V-ATPase holoenzyme results in dispersed V1, but not V0, sectors away from normally acidified compartments (Seol et al., 2001; Smardon et al., 2002; Sautin et al., 2005). Therefore, we also examined the distribution of the membrane sector of the V-ATPase by transient expression of a GFP-tagged membrane subunit, V0A1a. Expression of GFP-V0A1a was not robust, however, a few inner-ear hair cells expressed GFP-V0A1a at sufficient levels for detection *in vivo*. Unlike the altered pattern of the V1A cytosolic subunit of the V-ATPase, the distribution of the GFP-tagged membrane V0A1a was similar in both wild-type and rbc3$\alpha^{Q850X}$ hair cells (Fig. 4.3 E, E'; n = 10 cells each). We observed higher levels of GFP signal near synaptic regions of the hair cells in both genotypes, suggesting that vesicular trafficking of the membrane V0A1a subunit is not perturbed in mutant hair cells. Normal localization of the membrane sector argues against a general trafficking defect of the proton pump.

To extend our *in vivo* analysis and confirm our findings with the pan-V1A antibodies, we also tagged a V1A subunit with GFP and examined stable transgenic expression of this cytosolic protein in live cells. In contrast to the V0A1a membrane subunit, the pattern of the cytosolic V1Aa-GFP subunit was altered in mutant hair cells. As seen with the immunolabeling experiments, wild-

type hair cells showed an enriched GFP signal at the basal end, whereas GFP signal was dispersed in mutants (Fig. 4.3 F, F'; WT 0.71 ± 0.04 apical-to-basal ratio n = 9 neuromasts, 9 animals; rbc3α$^{Q850X}$ 1.09 ± 0.06 n = 5 neuromasts, 5 animals; *p* = 0.0004, unpaired Student's t test). These findings point to a mechanism involving V-ATPase holoenzyme assembly, as opposed to aberrant trafficking or protein levels in hair cells that are Rbc3α-deficient.

Rbc3α may also play a role in shaping V-ATPase localization in other cell types, such as the previously mentioned ionocytes. We therefore isolated yolk epithelium, which includes numerous ionocytes, and then prepared extracts for RT-PCR of *v1aa* and rbc3α transcripts. We detected products for both cDNAs (data not shown), indicating that yolk epithelial cells also express the Rbc3α protein. While variability in cell-to-cell labeling within individuals of both genotypes made quantification of signal intensities difficult, the loss of Rbc3α did not appear to have an obvious impact on apical V1A localization in ionocytes (Fig. 4.3 A, A'). Consequently, pathways in ionocytes that assemble the V-ATPase holoenzyme at apical regions may have redundant mechanisms, or limited need for Rbc3α. Taken together, these results suggest that assembly defects of the V-ATPase in rbc3α mutants are primarily restricted to synaptic vesicles in hair cells.

*Synaptic composition is normal in* rbc3α *mutants*

The distribution of the Rbc3 complex and its interaction with regulators of the small GTPase Rab3 may indicate additional synaptic roles for the complex, such as Rab3-dependent trafficking (Nagano et al., 2002; Kawabe et al., 2003).

Additionally, Rab3 has a putative role as docking agent for synaptic vesicles with the ribbon body (Uthaiah and Hudspeth 2010), as observed in central synapses (Wang et al., 1997). Therefore, we assessed the distributions and levels of synaptic vesicle proteins by immunolabeling hair cells with antibodies that target Vglut3 and Rab3 (a-d isoforms, Obholzer et al., 2008). We found that both Vglut3 and Rab3 were basally enriched in wild-type and mutant rbc3α$^{Q850X}$ hair cells, and the intensity of labeling was not significantly different for either proteins (Fig. 4.5 A, B; Vglut3 WT 496 ± 29 A.U.; mutant 609 ± 51 A.U., n = 13 neuromasts, 7 animals each; $p$ = 0.09 Mann-Whitney Test; panRab3 WT 883 ± 31 A.U. and mutant 856 ± 62 A.U.; $p$ = 0.21 Mann-Whitney Test). In addition, wild-type and mutant efferent termini readily labeled with Rab3 (arrowheads Fig. 4.4 A, B). These observations further argue against a trafficking defect, or a decrease of the vesicle population at the synapse. We also did not observe in wild-type or mutant animals basally localized punctae of Rab3 in a manner similar to that reported in chicken hair-cells, which have Rab3/ribeye double-positive punctae (Compare Fig. 4.4, B with Fig. 6 A-C of Uthaiah and Hudspeth 2010). Occasionally, however, we observed Vglut3/Rab3 double-positive rings at the basal end of the wild-type hair cells ($n$ = 7 animals) that were reminiscent of the previously observed LysoTracker rings and are consistent with the observation that ribbons are surrounded by synaptic vesicles (Lenzi et. al 1999). We did not see these rings in mutant hair cells ($n$ = 2 out of 7 animals), but we were unable to examine enough animals to draw meaningful conclusions.

The Rbc3 complex may also play a role in the synaptic development of the lateral line, as it is necessary for processing the intracellular domain of Notch in other organisms (Yan et al., 2009; Sethi et al., 2010), and Rab3 has been implicated in the nucleation of the neuromuscular junction in Drosophila (Graf et al., 2009). We therefore labeled presynaptic ribbon bodies with an anti-Ribeye b antibody and labeled postsynaptic contacts with an antibody against MAGUK proteins (Fig. 4.4 D, E; Sheets et al., 2011). We observed that rbc3α$^{Q850X}$ mutants and wild-type hair cells contained Ribeye b and MAGUK-positive puncta with similar co-localization of both proteins (Fig. 4.4 F; Manders correlation coefficient WT 0.58 ± 0.05 *n* = 9, rbc3α$^{Q850X}$ 0.57 ± 0.04 *n* = 8; *p* = 0.87; unpaired Student's t test). We also did not observe obvious morphological defects nor cell death within the inner ear or neuromasts. Altogether, our observations suggest that the contribution of Rbc3$\alpha$ to the mutant auditory and vestibular behavioral phenotypes is not due to an obvious disruption in the development or morphology of hair-cell synapses.

*Synaptic activity is reduced in rbc3$\alpha$ mutants*

Hair cells transduce high frequency stimuli with temporal precision that is maintained during sustained periods of stimulation (reviewed in Nouvian et al., 2006). In order to support high rates of neurotransmitter release, a hair cell must ensure that synaptic vesicles are sufficiently acidified for optimal neurotransmitter filling. Considering the defective acidification of synaptic vesicles in rbc3$\alpha$ mutants, we hypothesized that reduced V-ATPase activity would result in

reduced synaptic transmission at mutant hair-cell synapses. In addition to reduced neurotransmitter release, it was not clear whether mechanotransduction might also be sensitive to changes in apical V-ATPase activity (Shiao et al., 2005; Wangemann, 2006). To determine if reduced V-ATPase activity had any effect on mechanotransduction, we first recorded microphonic potentials in the presence of bafilomycin. Drug treatment did not have an obvious effect on microphonic potentials (data not shown). Consistent with this observation, the amplitude of microphonic potentials and power spectra of the microphonic potentials were similar in response to 20 Hz stimulation of wild-type and rbc3α$^{Q850X}$ neuromasts (Fig. 4.5 A; WT n = 3; Mutant n = 6, 20 Hz p = 0.24; 40 Hz p = 0.93). The absence of effect on mechanotransduction is in agreement with our previous experiments, and it suggests that the defects in rbc3α mutant hair cells are largely synaptic.

In zebrafish larvae, an afferent neuron forms multiple synapses with groups of lateral-line hair cells that are all aligned with the same planar polarity in one or more neuromasts (Nagiel et al., 2008; Obholzer et al., 2008; Faucherre et al., 2009). It is not known whether single vesicles are released at each synapse during depolarization of lateral-line hair cells, as is the case for cochlear outer hair cells (Weisz et al. 2009), or whether multi-vesicular release occurs, as has been described for inner hair cells and bullfrog saccular hair cells (Glowatzki and Fuchs 2002; Li et al. 2009). Furthermore, in afferent neurons of mammalian inner hair cells, an EPSP at a single synapse generates a postsynaptic action potential (Rutherford et al. 2012). However, at the developmental stage used for our

recordings, the action potentials of a single afferent neuron may be generated following activation of presumably many more synapses. Thus, it is not known whether a single EPSP is sufficient or whether EPSPs from multiple synapses must summate in order to bring the afferent neuron to threshold in the lateral line.

In order to examine synaptic transmission of wild-type hair cells in the presence of bafilomycin and in *rbc3*α mutant hair cells, we recorded evoked action potentials from afferent neurons of the lateral line organ. First, we confirmed our findings with bafilomycin by examining afferent activity during stimulation of lateral line hair cells at 60 Hz before and after application of bafilomycin. Inhibition of the V-ATPase drastically reduced the firing rate of wild-type neurons (Fig. 4.5 B; WT: 27 ± 4 spikes/sec; bafilomycin: 5 ± 1 spikes/sec; n = 3 larvae; $p < 0.05$, paired Student's *t* test). These results strongly suggest that V-ATPase activity is necessary for proper synaptic transmission, presumably by establishing the proton and electrical gradient, which provides the driving force for neurotransmitter exchange.

We next examined synaptic transmission in rbc3α$^{Q850X}$ mutants by recording evoked activity of lateral-line afferent neurons and stimulating hair cells at two different frequencies: 20 and 60 Hz. At 60 Hz, the evoked firing rates of lateral-line afferent neurons were significantly reduced in rbc3α$^{Q850X}$ mutants (Fig. 4.5 B, C; WT: 22 ± 2 spikes /sec, n = 9; rbc3α$^{Q850X}$ 12 ± 3 spikes/sec, n = 9; $p < 0.05$; unpaired Student's *t* test). The reduced spiking rate observed in the mutants at 60 Hz stimulation is consistent with the notion that synaptic vesicles are underfilled and do not contain sufficient quantities of neurotransmitter that

reliably bring the afferent neuron to threshold. In contrast to 60 Hz, stimulation at 20 Hz did not result in a significant difference between wild-type and mutant afferent firing rates (WT: 14 ± 4 spikes/sec, n = 5; *rbc3α*$^{Q850X}$ 10 ± 3 spikes/sec, n = 7; p = 0.4; unpaired Student's t test). Presumably this difference in spiking rate at 20 versus 60 Hz in *rbc3α*$^{Q850X}$ larvae reflects the difference in the length of the cycle; at 20 Hz the 50 millisecond period results in a 25 millisecond depolarization of the hair cell, which is a longer period of time for synaptic vesicle fusion and subsequent release of neurotransmitter. Despite normal spiking rates at 20 Hz, reduced neurotransmitter release may nevertheless result in a longer temporal delay in reaching threshold of firing in afferent neurons. Indeed, there was a significant increase in the latency of firing in *rbc3α*$^{Q850X}$ larvae at both 20 and 60 Hz when compared to wild-type animals (Fig. 4.5 D; 20 Hz, WT: 0.16 ± 0.01, n = 5; *rbc3α*$^{Q850X}$ 0.30 ± 0.02, n = 7; p < 0.001; two-tailed unpaired Student's t test; 60 Hz, WT: 0.27 ± 0.02, n = 9; *rbc3α*$^{Q850X}$ 0.41 ± 0.04, n = 9; p < 0.01; two-tailed unpaired Student's t test). The shift in latency is consistent with defective acidification and consequent reduced concentration of neurotransmitter within the synaptic vesicles of *rbc3α* mutants.

Interestingly, the effects of bafilomycin treatment had a greater effect on firing rates than the loss of Rbc3α function (Fig. 4.5 B), similar to the results obtained from experiments with LysoTracker pH indicator dye (Fig. 4.1 D, E). Following prolonged incubation in bafilomycin, action potentials disappeared (data not shown). These results support the notion of a modulatory role for

Rbc3α leading to partial filling of vesicles in the mutants in contrast to the severe depletion of neurotransmitter in vesicles after bafilomycin treatment.

The reduction in spike rate at higher frequencies would also predict that a decrease in the fidelity of stimulus encoding would be present in the mutant larvae (Wittig and Parsons, 2008). We found that the fidelity of phase-locked spiking of the afferent neuron to the 60 Hz mechanical stimulus was decreased. Calculation of vector strength, an indication of the precision of responses to a given stimulus, was significantly reduced in rbc3α$^{Q850X}$ larvae (Fig. 4.5 E; WT: 0.87 ± 0.01, n = 9; rbc3α$^{Q850X}$ 0.78 ± 0.02, n = 9; $p < 0.001$; unpaired Student's *t* test). A reduction in the fidelity of phase locking further supports the hypothesis that a defect in Rbc3α leads to underfilled synaptic vesicles in mutant hair cells. We also determined the fidelity of phase locking at 20 Hz and observed a slight, but statistically insignificant difference between wild-type and mutant larvae (WT: 0.96 ± 0.01, n = 5; rbc3α$^{Q850X}$ 0.85 ± 0.05, n = 7; $p = 0.13$, unpaired Student's *t* test). This result indicates that for longer durations of stimulation such as 20 Hz cycle, normal spike rates and phase locking are still possible in rbc3α mutants despite a significant shift in latency.

An additional postsynaptic effect that could result from reduced release of neurotransmitter is a decrease in the rate of spontaneous spiking of the afferent neuron (Rutherford et al., 2012). We previously showed that spontaneous activity of afferent neurons in the lateral line is generated by hair-cell neurotransmission (Trapani and Nicolson, 2011). To determine whether spontaneous activity was affected in rbc3α$^{Q850X}$ mutants, we recorded afferent activity in the absence of

mechanical stimulation. We observed a reduction in the rate of spontaneous action potentials in rbc3α$^{Q850X}$ mutants with a significant increase in the mean interspike interval (WT: 83 ± 9 msec, n = 11; rbc3α$^{Q850X}$ 394 ± 141 msec, n = 7; $p < 0.05$; unpaired Student's *t* test).

Given that endosomes are thought to be a source for replenishing synaptic vesicles (Südhof, 2004), that endosomal maturation is defective in Rbc3α–deficient flies (Yan et al., 2009), and Rbc3α might interact with the recycling/endosomal machinery of the hair cell, such as Nsf and Synaptojanin-1 (Li et al., 2010), we next considered whether synaptic vesicle replenishment is impaired in rbc3α$^{Q850X}$ hair cells. Furthermore, like rbc3α mutants, a similar reduction in initial spike rate and phase locking was reported for *synj1* mutants, which have defects in synaptic vesicle recycling (Trapani et al., 2009). We therefore mechanically stimulated hair bundles with a sustained stimulus of 15 minutes at 60 Hz while recording the resulting evoked activity in the afferent neuron. We found that in contrast to *synj1* mutants, sustained stimulation did not further degrade the synaptic firing rate of rbc3α$^{Q850X}$ mutants (Fig. 4.5 C; 10 ± 5 spikes/sec; n = 4; p = 0.14; paired Student's *t* test). This result suggests that despite the reduced rate of spiking at 60 Hz, replenishment of synaptic vesicles at this same frequency is not defective in rbc3α$^{Q850X}$ hair cells. Altogether, our electrophysiology results are consistent with the synaptic defects identified by our cellular and molecular analyses, suggesting that synaptic activity is impaired as a result of de-acidified and underfilled synaptic vesicles in the hair cells of rbc3α mutants.

## Conclusion

Numerous studies have demonstrated that acidification of the lumen of synaptic vesicles is a necessary step in loading neurotransmitter into vesicles (Edwards, 2007; Schenck et al., 2009; Goh et al., 2011). In this study, we demonstrate that de-acidification of synaptic vesicles, either by genetic disruption of Rbc3α function or pharmacological inhibition of the proton pump, impairs synaptic transmission in hair cells. Our experiments indicate that proton gradients are reduced in mutant rbc3α synaptic vesicles and can be further dissipated by the proton pump inhibitor bafilomycin. Furthermore, blocking the proton pump drastically attenuates synaptic transmission in wild-type hair cells to levels below those in rbc3α mutants. Consistent with involvement of Rbc3α in synaptic vesicle acidification, the V1A cytosolic subunit of the V-ATPase was not concentrated in synaptic regions of mutant hair cells. Altogether, our data provide strong evidence for a defect in vesicle acidification that causes a reduction in the quantity of neurotransmitter in mutant synaptic vesicles. Thus, we propose that Rbc3α modulates synaptic activity in hair cells by promoting the assembly of the V-ATPase holoenzyme on synaptic vesicles, thereby regulating the vesicle's internal pH and, ultimately, its concentration of neurotransmitter.

Several observations suggest that the primary function of Rbc3α is synaptic in nature. First, GFP-Rbc3α localizes to the basal end of hair cells in a distribution pattern akin to synaptic vesicle proteins. This distribution pattern is also in agreement with the vesicular distribution pattern observed for Rbc3α in the rat CNS (Nagano et al., 2002). Next, the acidification defect affects basally

located structures such as synaptic vesicles in mutant hair cells, while apical membrane compartments appear to be unaffected. Finally, various V-ATPase subunits were enriched at the basal regions of wild-type hair cells, whereas mutant hair cells had a pronounced decrease in the basal localization of the cytosolic subunit V1A. Similar dispersal of various V1 sector subunits has been reported for conditions causing disassembly of holoenzyme (Seol et al., 2001; Smardon et al., 2002; Sautin et al., 2005), a finding that is consistent with the notion that Rbc3$\alpha$ regulates synaptic vesicle acidification via a mechanism involving assembly of the cytosolic and membrane components of the proton pump.

We also considered alternative possibilities that might account for a decrease in synaptic vesicle acidification. Changes in both protein levels and trafficking of the proton pump could lead to acidification defects. However, the aberrant redistribution of V1A cytosolic subunits in mutants appeared to not be due to a change in V1A protein levels as evidenced by the intensity of immunolabeling. A general trafficking defect was also not apparent, as we found that subcellular localization of synaptic vesicle proteins Rab3 and Vglut3, and exogenously expressed GFP-V0A1a was unchanged in mutant hair cells. Such results are inconsistent with either degradation of proton pump subunits or a trafficking defect of the V-ATPase complex (Hurtado-Lorenzo et al., 2006; Oehlke et al., 2011).

Overall, our results point to a modulatory role for Rbc3α as opposed to an absolute requirement for synaptic vesicle acidification. Defects of vesicle

acidification could be further compounded by inhibition of the proton pump with bafilomycin in the mutants. We also noted that while the V1A cytosolic subunit appeared dispersed in mutant hair cells, its distribution still partially overlapped with the synaptic vesicle region of the hair cell, potentially accounting for the remaining vesicular V-ATPase assembly. As mentioned previously, de-acidification of synaptic vesicles would be expected to reduce neurotransmitter filling in synaptic vesicles (Edwards, 2007). Supporting this prediction, *rbc3*α mutant afferents have reduced evoked and spontaneous synaptic firing rates. In addition, there was an increased latency in spike timing, and decreased phase locking of evoked action potentials in response to mechanical stimulation of hair cells. Still, the evoked firing rate of *rbc3*$\alpha$ mutant afferents was greater than that of wild-type afferents after the larvae were treated with bafilomycin. This result further suggests that mutant vesicles have partially-filled vesicles due to the remaining V-ATPase activity.

Aside from a role in synaptic vesicle acidification, the loss of Rbc3$\alpha$ could also impact synaptic transmission in other ways (Sakisaka and Takai 2005), including perturbing vesicle trafficking or vesicle fusion. Our examination of a Rbc3α C-terminal fragment indicates that the modest $Ca^{2+}$-dependent exocytosis inhibition observed in other studies is likely inhibited through an acidification-independent manner (Sakisaka and Takai 2005). The Rbc3 complex was originally proposed to act as a synaptic scaffold upon which Rab3 GEP and GAP regulate Rab3 activity (Nagano et al., 2002; Kawabe et al., 2003). Rab3 activity shapes exocytosis, Rab3-dependent cargo trafficking to the synapse, and

potentially nucleation of the synapse (Tanaka et al., 2001; Niwa et al., 2008; Graf et al., 2009, Uthaiah and Hudspeth 2010). Therefore, impaired Rab3 GEP and Rab3 activity might be disrupted in *rbc3α* mutants. However, the distribution of vesicular proteins Rab3 and Vglut3 and the apposition of pre- and postsynaptic components, Ribeyeb and MAGUK, respectively, were unchanged in *rbc3*α mutants. These findings argue against the idea that Rab3 activity is disrupted. Additionally, we did not observe Rab3 basal puncta in the hair cell as had been previously reported in chicken hair cells (Uthaiah and Hudspeth 2010), which could arise from either differences in species, or antibody reagents. Another possible role comes from recent evidence indicating that the V0 sector contributes to membrane fusion (Hiesinger et al., 2005; Sun-Wada et al., 2006; Peri and Nüsslein-Volhard, 2008; Di Giovanni et al., 2010). Whether synaptic vesicle fusion proceeds normally in the absence of functional Rbc3α requires further investigation, but data from *C. elegans* suggests that V0-mediated membrane fusion does not require V-ATPase holoenzyme assembly (Liégeois et al., 2006).

While the etiology resulting from the loss of V-ATPase activity in human patients is incomplete, mutations within subunits of the V-ATPase (V1B1 and V0A4) cause progressive sensorineural deafness accompanied by distal renal tubular acidosis (Karet et al., 1999; Stover et al., 2002). Assembly and trafficking of the V-ATPase in rat kidney cell-ines is disrupted by mutations that mimic human V1B1 lesions in the orthologous rat V1B1 subunits, suggesting a potential mechanism behind the human disease (Yang et al., 2006). Surprisingly, however,

V1B1 knockout mice are not deaf (Dou et al., 2003), suggesting that mice may have multiple mechanisms for ensuring the acidification of compartments, or sub-detectable expression levels of compensatory V1B2 subunit (Finberg et al., 2005). In zebrafish larvae, various V-ATPase subunit mutations cause gross morphological defects (Nuckels et al., 2009). In contrast to the severe consequences of V-ATPase mutations, the reduced V-ATPase activity phenotype seen in *rbc3α* mutants results in a more restricted phenotype of hearing impairment in zebrafish.

In summary, we have identified a novel role for Rbc3a in the acidification of synaptic vesicles in vertebrate hair cells. Rbc3α appears to modulate the activity of the V-ATPase holoenzyme on synaptic vesicles, most likely through a mechanism involving its assembly. Our study is the first step towards understanding how Rbc3α may act as both a synaptic vesicle scaffold and regulator of the V-ATPase. In the future, because Rbc3α interacts with Nsf and Synj-1 (Li et al., 2012), we plan to test compound mutants of *rbc3α* and *nsf* (Mo and Nicolson 2011), or *synj-1* (Trapani et al., 2009), to identify the site of intervention in the life cycle of the synaptic vesicle that is subject to Rbc3α regulation. For instance, we might find that another synaptic transmission gene when mutated, e.g. a mutation in *nsf*, potentiates, or suppresses, the mutant *stardust* phenotype.

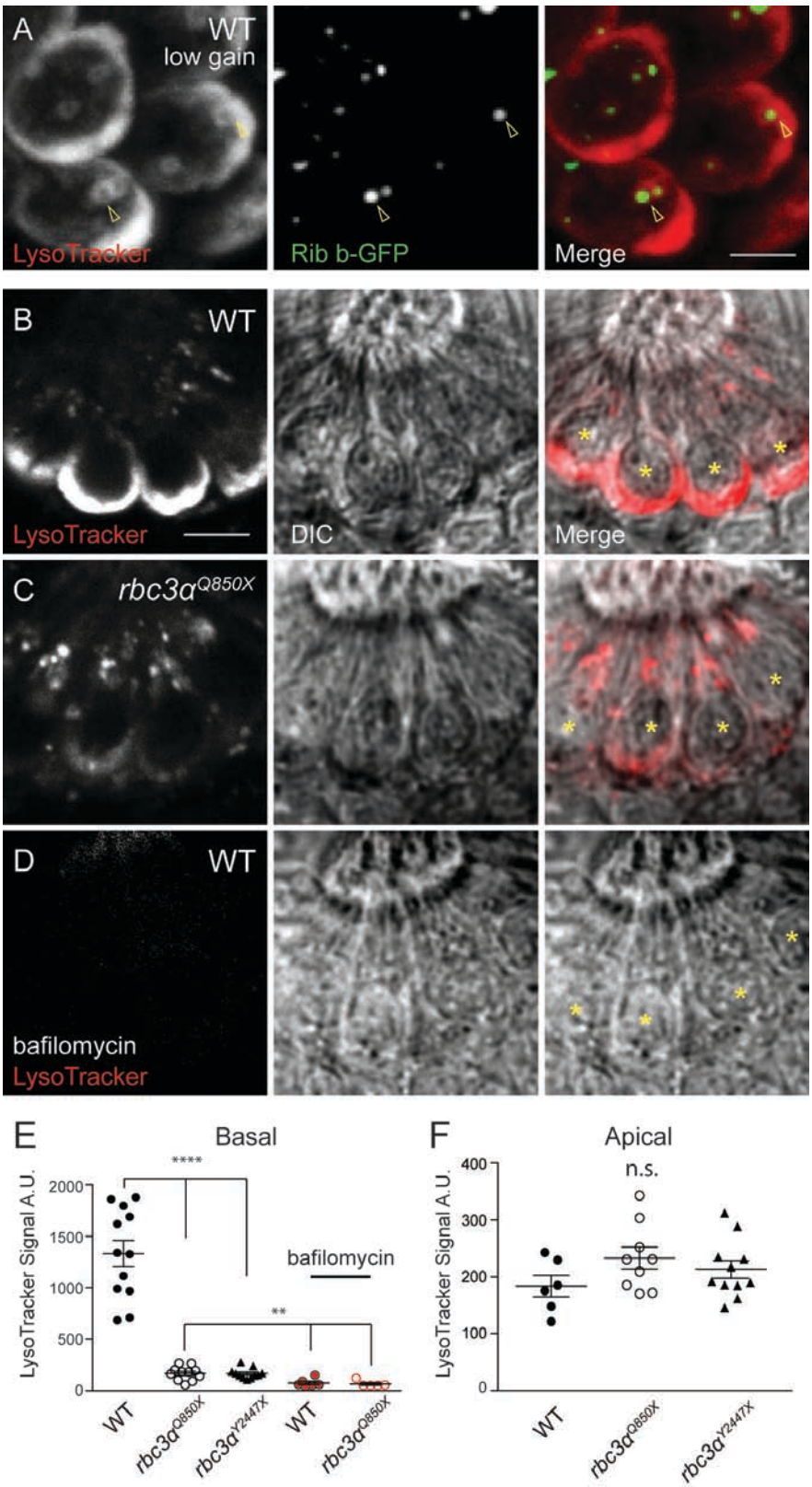


Figure 4.1 Rbc3α is required for proper acidification of basal vesicles

***A***, Confocal image of a *WT*$^{Tg(-6.5kb\_myo6b:Ribeye\ b\text{-}GFP)}$ lateral-line L2 neuromast labeled with LysoTracker vital dye. Arrowheads indicate Ribeye b-GFP puncta and surrounding synaptic vesicle pool. (Top-down view of hair cells and low gain were used to visualize tori. Scale bar, 2 μm). ***B, C***, LysoTracker labeling of L2 neuromasts in wild-type and mutant *rbc3*$\alpha^{Q850X}$ larvae at 5 dpf. ***D***, LysoTracker dye and 1 μM bafilomycin applied to a wild-type L2 neuromast. The oblique focal planes in B-D include the apical surface of each neuromast. Hair-cell nuclei are indicated by asterisks. Scale bar, 5 μm. ***E,*** Quantification of basal LysoTracker signal. Each data point represents the average signal of an entire neuromast for WT and rbc3α$^{Q850X}$, rbc3α$^{Y2447X}$ mutants (one-way ANOVA, $F(2,31) = 74.8$, $p < 0.0001$) and for untreated *rbc3*$\alpha^{Q850X}$ and Bafilomycin-treated WT and *rbc3*$\alpha^{Q850X}$ mutants (one-way ANOVA, $F(2,19) = 8.7$, $p = 0.002$). Mean fluorescent signals were significantly different between wild-type and mutant neuromasts. ***F***, Quantification of apical LysoTracker staining WT and rbc3α$^{Q850X}$, and rbc3α$^{Y2447X}$ (one-way ANOVA, $F(2,23) = 1.5$, $p = 0.234$).

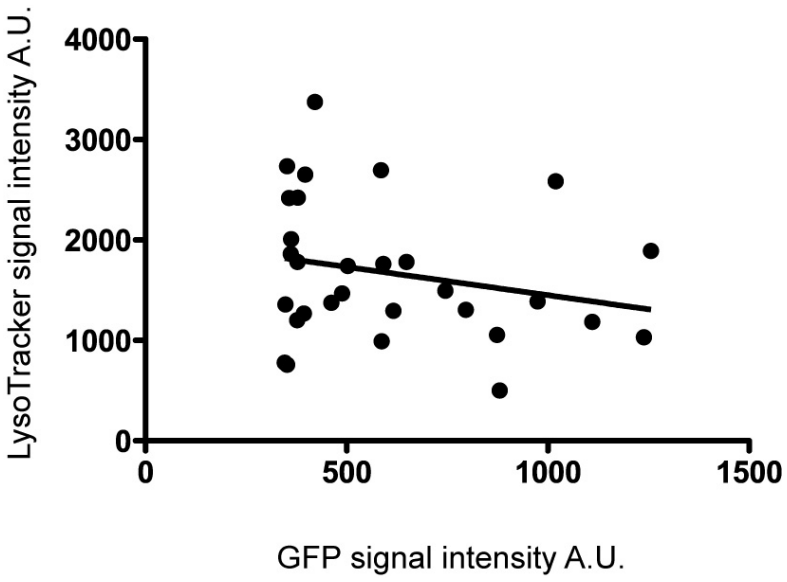


Figure 4.2 A C-terminal fragment of Rbc3$\alpha$ does not inhibit acidification

Correlation plot of LysoTracker intensity versus GFP intensity in hair cells that expresses *Tg(-6.5myosin6b:gfp-rbc3$\alpha$ 2304-3062).*

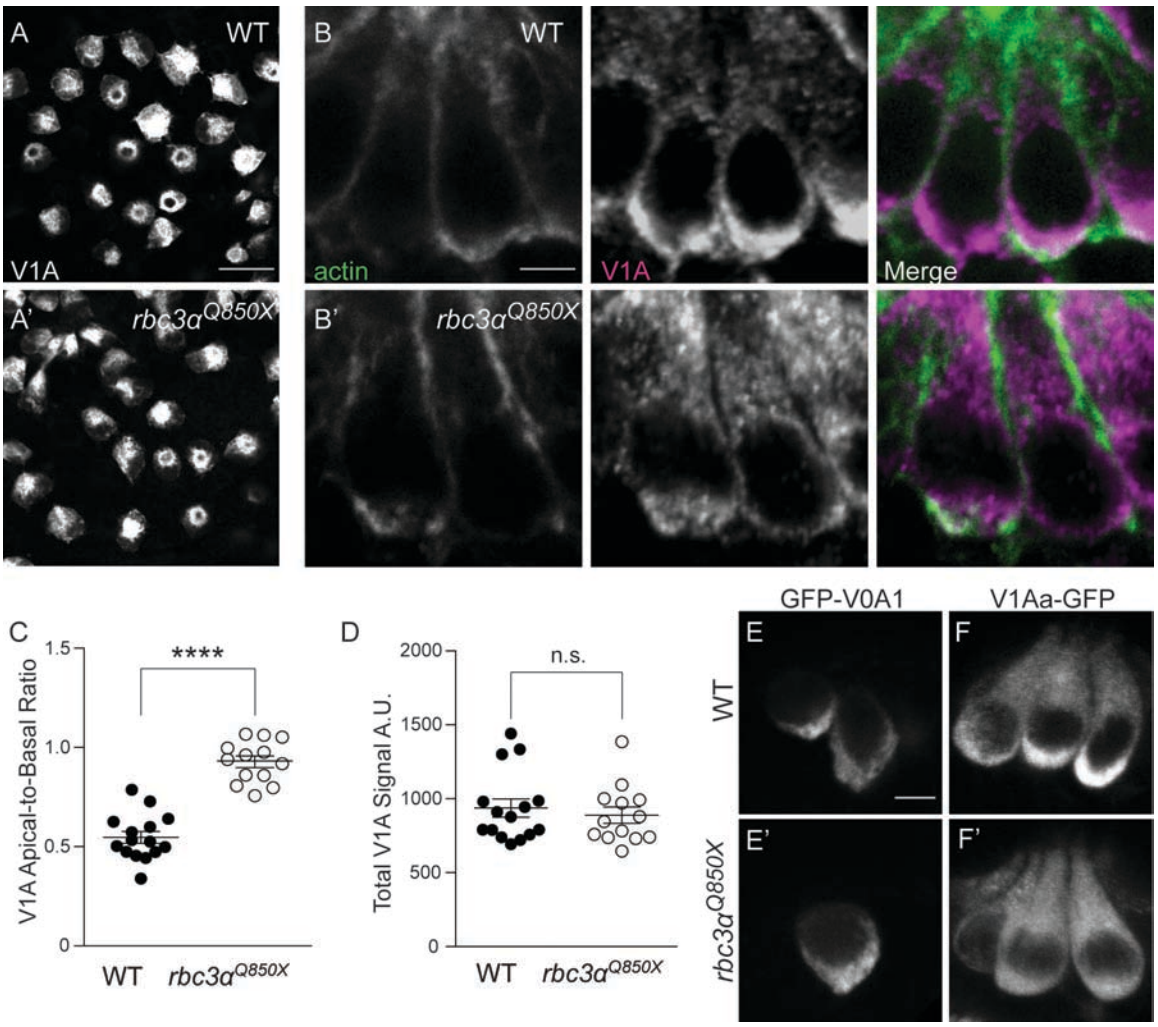


Figure 4.3 Cytosolic V1 sectors are redistributed in *rbc3α* mutants

***A, A'***, Positive control for Atp6V1A immunolabeling (V1A a and b cytosolic subunits) of yolk ionocytes in wild-type and mutant larvae. (Scale bar, 20 μm). ***B, B'***, Side view of wild-type and rbc3α$^{Q850X}$ lateral-line hair cells labeled with Alexa488-phalloidin and V1A antibody. Labeling of V1A cytosolic subunits was enhanced at the base of wild-type, but not mutant hair cells. (Scale bar, 3 μm). ***C***, Enhanced apical-to-basal ratio of V1A immunofluorescent signal in rbc3α$^{Q850X}$

mutants (WT n = 15 neuromasts, 9 animals; rbc3$\alpha^{Q850X}$ n = 13, 8 animals; p < 0.0001; unpaired Student's t test). ***D***, Average V1A fluorescent signal of whole neuromasts (WT n = 15 neuromasts, 9 animals; rbc3$\alpha^{Q850X}$ n = 13, 8 animals *p* = 0.57; unpaired Student's t test). ***E, E'***, Transient expression of V0a1 subunit using *Tg(myo6b:GFP-Atp6V0A1a)* plasmid in ampullary hair cells at 3 dpf. Note strong basal signal in both wild-type and mutant hair cells. ***F, F'***, Stable transgenic expression of V1aa subunit in *Tg(myo6b:GFP-Atp6V1Aa)* larvae. Side view of L2 neuromast at 5 dpf. Note stronger basal signal in wild-type (***F***) than mutant hair cells (***F'***) (WT n = 9 neuromasts, 9 animals; rbc3$\alpha^{Q850X}$ n = 5 neuromasts, 5 animals; *p* = 0.0004, unpaired Student's t test). Scale bar, 4 μm.

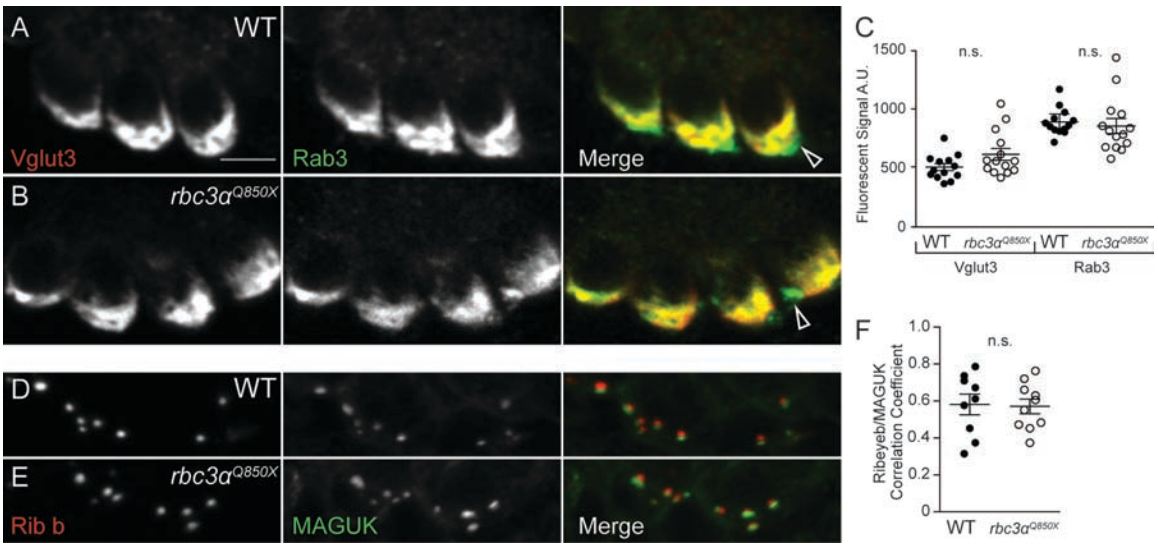


Figure 4.4 Loss of Rbc3α function does not affect hair-cell synaptic components

***A, B***, Confocal *z*-projections of L2 neuromasts labeled with anti-panRab3 and anti-Vglut3 antibodies in either wild-type (***A***), or *rbc3α*$^{Q850X}$ (***B***) larvae at 5 dpf. (Scale bar, 4 μm.) ***C***, Quantification of immunofluorescent signal of Vglut3 (n = 13 neuromasts, 7 animals each; $p = 0.09$ Mann-Whitney Test) and panRab3 labeling ($p = 0.21$). ***D, E***, Labeling of L2 neuromasts with presynaptic Ribeye b and postsynaptic panMAGUK antibodies. ***F***, Overlap of panMAGUK and Ribeye b puncta. Each data point represents the correlation coefficient of a single neuromast (Manders correlation coefficient WT $n = 9$ neuromasts, rbc3α$^{Q850X}$ $n = 8$ neuromasts; $p = 0.87$; unpaired Student's t test). Error bars represent standard error of the means.

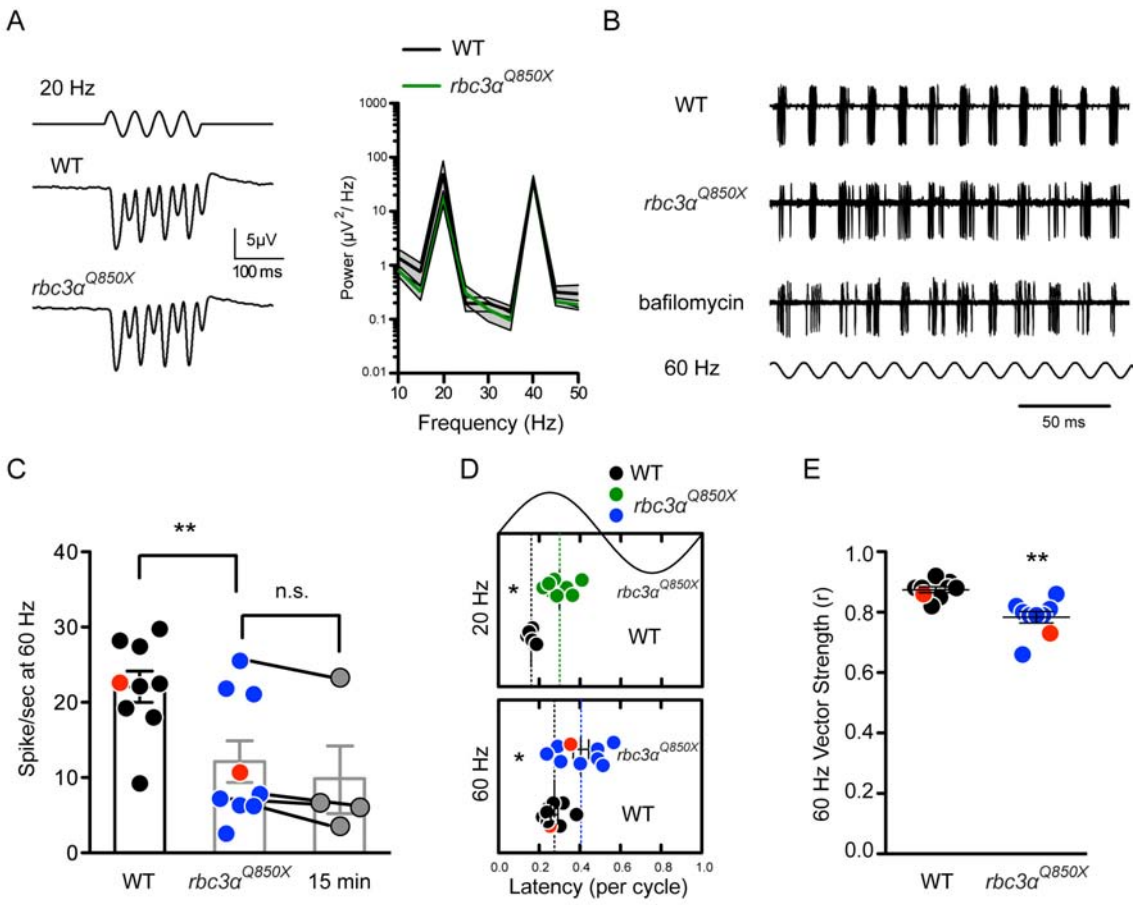


Figure 4.5 The rate and fidelity of stimulus-dependent spiking of lateral-line afferent neurons is reduced in *rbc3α* mutants

***A***, Left panel, average microphonic potentials recorded from wild-type (WT; middle) and mutant (*rbc3α*$^{Q850X}$; bottom) larvae in response to 20 Hz stimulation for 200 ms (top). Right panel, comparison of power spectra from microphonic potentials recording during the stimulus presentation from wild-type (n = 3) and *rbc3α*$^{Q850X}$ larvae (n = 6) for frequency components between 10 and 50 Hz. Note the large peaks at both the stimulus frequency (20 Hz) and the 2n frequency, 40 Hz. Error is represented by grey shaded area above and below solid lines. ***B***,

Traces of spikes recorded from afferent neurons during stimulation of hair cells at 60 Hz. Each panel is an overlay of 60 consecutive sweeps. Top: WT; middle: *rbc3*$\alpha^{Q850X}$; bottom: WT treated with bafilomycin; 60 Hz stimulus waveform shown beneath the three panels. ***C,D,E***, The activity of afferent neurons was recorded for 60 seconds during either continuous 60 Hz or 20 Hz stimulation. ***C,*** Plot of the quantified average spike rate for WT (black circles), *rbc3*$\alpha^{Q850X}$ (blue circles), and *rbc3*$\alpha^{Q850X}$ following 15 minutes of continuous 60 Hz stimulation (grey circles). The open bars represent the mean of the recordings for each condition. ***D***, Mean latency of spikes from the stimulus deflection (positive portion of the period of a 20 or 60 Hz cycle) for recordings from WT (black circles) and *rbc3*$\alpha^{Q850X}$ at 20 Hz (green circles) and *rbc3*$\alpha^{Q850X}$ at 60 Hz (blue circles). The dashed line indicates mean latency for each condition. ***E***, The vector strength of spiking for the same recordings shown in C and D for WT (black circles) and *rbc3*$\alpha^{Q850X}$ (blue circles). The red symbols in ***C, D***, and ***E*** are from the WT and *rbc3*$\alpha^{Q850X}$ recordings shown in *B*. Significance was determined by paired and unpaired Student's *t* test (as appropriate) and error bars represent standard error of means.

# Chapter 5 - Conclusion

## Summary of main findings

In this study, we linked the functional role of Rbc3α as a regulator of the V-ATPase with its previous characterization as a synaptic vesicle associated protein. We began our dissection of its role in a whole organism by discriminating a subtle auditory dysfunction in the auditory/vestibular mutant *stardust* with an improved upon assay of the auditory escape behavioral response. We then cloned several alleles of mutant *stardust* encoding nonsense mutations in the gene *rbc3α*. Transcripts of *rbc3α* were detected in hair cells of the auditory, vestibular and lateral-line organs and an exogenously expressed GFP-tagged Rbc3α protein was distributed in a synaptic vesicle-like manner in the hair cells. The synaptic vesicles of Rbc3α-deficient hair cells have elevated pH due to mis-assembly of the V-ATPase holoenzyme and as such, they lose their proton-chemical driving force for glutamate uptake. As a result of the probable reduction in vesicle filling with neurotransmitter, the fidelity of synaptic transmission at the hair-cell synapse is impaired. This in turn degrades the ability of the auditory and vestibular systems to respond to sound or head movements. In this chapter, I will discuss the larger implications of our findings, unresolved questions, and future directions.

### *A model for Rbc3 at the synaptic vesicle*

Our findings demonstrate that Rbc3α plays a critical role in the acidification of synaptic vesicles at the hair-cell synapse. In the absence of Rbc3α, the basal

end vesicles are de-acidified, while the apical organelles appear unaffected. We further suggest that Rbc3α is necessary for complete association of the V-ATPase holoenzyme on synaptic vesicles in hair cells as the cytosolic V1 sector, but not V0 sector, loses its enhanced basal-end localization in mutant *stardust* hair cells. We suggest that loss of Rbc3α-dependent acidification likely results in the dissipation of the driving force for neurotransmitter uptake into synaptic vesicles, which is consistent with the reduced synaptic activity at the hair-cell synapse. As such, the phenotype of Rbc3α-deficient animals is marked by auditory and vestibular deficits. Given this scenario, we have modeled the role of Rbc3α at the hair-cell synapse in Figure 5.1. This model highlights the importance of both Rbc3α in vesicle acidification and neurotransmitter filling and links the central findings of previous publications that the protein associates with synaptic vesicles and is important in controlling V-ATPase activity.

*Rbc3α in auditory and visual behaviors*

In Chapter 2 I showed that subtle auditory deficits in a class of vestibular mutants could not be discriminated with the acoustic tap despite the prevalence of shared gene expression between auditory and vestibular organs. In order to improve the reliability of the AEBR as a quantitative assay of auditory function, we used the vestibular dysfunctional mutant *stardust* as a test of our optimized high-throughput automated system with pure-tone presentations. We find that the mutant *stardust* has modestly impaired hearing, and even more so, we find the strongest allele of *stardust* had the worst performance in the acoustic startle

assay, thereby demonstrating the sensitivity of our system to discriminate subtle differences between alleles of the same affected gene. Our results are also consistent with the prediction that the shared gene expression profile of *rbc3α* in the auditory and vestibular hair cells should affect the performance of both systems when an animal is Rbc3α-deficient. Currently we do not have an explanation for why there are differences between the alleles. We speculate that in the larval AEBR, the downstream neuronal connection from the hindbrain Mauthner cell to the contralateral motor neurons and ipsilateral inhibitory neurons, might be differentially affected in each mutant background. The physiology of the hair-cell synapse appears similar in each allele at least. Another potential advantage of our improved behavioral protocol will be the ability to more precisely determine the tissues underlying behavioral deficits in various mutant lines. For instance, Rbc3α is expressed widely throughout the nervous system, including sensory hair cells (Einhorn et al., 2012). One could create transgenic animals in which *rbc3α* expression is restored in only hair cells, neurons, or both with tissue-specific promoters. Through tissue specific restoration, one can then use the behavioral assay to examine each step along the escape circuit to explain potential differences between alleles.

The selective importance of Rbc3α to visual and auditory/vestibular systems, but not touch sensation, also deserves further investigation. The selective phenotypes might reflect the commonalities between these tissues. Retinal bipolar cells and photoreceptors of the eye share an assortment of unique molecular specializations with the hair cell, and also have ribbon-type

synapses (Zanazzi and Matthews, 2009). Inherited forms of human deafness and blindness such as Usher syndrome are due to genetic lesions in the common molecular repertoire of the hearing and visual systems (hereditaryhearingloss.org). Perturbation of V-ATPase activity in retinal tissues is the most obvious explanation for the visual impairment exhibited by mutant *stardust* animals. Supporting this prediction, various V-ATPase mutants have visual deficits (Nuckels et al., 2009). Likewise, we predict that the various zebrafish V-ATPase mutants have impaired hearing and balance. We note however, that two recessive mutations in humans of the V-ATPase B1 and V0A4 subunits cause syndromic forms of sensorineural deafness and acidosis in the kidneys, but vision was not reported to be impaired (Karet et al., 1999, Stover et al., 2002).

In addition to the V-ATPase as a target of Rbc3α in the ear and eye, a number of other candidate proteins were found in a screen for interactors with Rbc3α that might affect both hearing and vision (Li et al., 2012). Several proteins were found that remodel the cytoskeleton and include Mtap1a, Nckap, Cyfip1 and 2. For instance, Mtap1a is genetic modifier of hearing in the mouse mutant *tubby*, which exhibits retinal degeneration and hearing loss (Ikeda et al., 2002). Intriguingly, both zebrafish mutant *stardust* and mutant *nevermind* larvae, which harbors mutations in the gene *cyfip2* (Pittman et al., 2010), have impaired vision (Baier et al., 1996). *Rbc3α* mutants lack spontaneous eye movements and light adaptation responses in melanocytes, suggesting a possible visual defect, while mutant *nevermind* animals have retinotectal pathfinding defects. While we did not

observe obvious synaptic connectivity defects in the lateral-line organs of mutant *stardust* animals, the lateral-line afferents follow the primordium as it migrates along the trunk and do not utilize the same retinal pathfinding mechanisms. Therefore, we plan to examine retinotectal projections to the optic tectum with neurotracer dyes in mutant *stardust* animals in order to determine wherein lies the possible visual deficits and if there is crosstalk between cytoskeleton remodeling and Rbc3α.

During the testing of the larval AEBR, I noticed that almost all auditory/vestibular mutant lines are generally more inactive than wild-type animals with regard to spontaneous activity. This observation suggests that hearing might be necessary for the development, or maintenance, of swimming and seeking behaviors in the larvae. I observed that the deafness mutant pcdh15$^{R360X}$ displayed normal optokinetic responses, which indicates that their vision is not grossly perturbed (personal communication with Weike Mo), yet they displayed an inactive phenotype. Therefore, I speculate that hearing may also contribute to spontaneous activity in the larvae. It will be interesting in the future to study the effects of various mutations that cause blindness and deafness on spontaneous activity. To this end, the ZebraBox apparatus can be modified for analyzing long periods of activity and rest (Prober et al., 2006).

In addition to the results presented here, the improved method has been used to assay the AEBR in transgenic rescue experiments and to isolate putative substrate tissues affected by various mutations (Mo et al., 2012). In the future, the ZebraBox assay can also be adapted to test lateral-line function through

analysis of rheotaxic alignment in response to directional changes in water current (Buck et al., 2012). The ZebraBox apparatus will facilitate future examination of the effects of various genetic mutations and transgenes on the function of hair cells within the auditory, vestibular and lateral-line systems.

*Rbc3α selectively enhances synaptic vesicle acidification*

We found that the mutant *stardust* had elevated pH in the synaptic vesicles of hair cells. The acidification defect was due to mis-assembly of the V-ATPase on synaptic vesicles, though a moderate level of V-ATPase activity persists in the absence of Rbc3α, which is further diminished by application of a proton pump inhibitor, bafilomycin. In contrast with reduced basal labeling in mutants with the pH-dependent dye LysoTracker, we observed that apical labeling appeared normal in the mutant hair cell. We did not identity the various apical structures labeled by LysoTracker, but the Golgi Apparatus and apical endosomes are located in the apical part of the hair cell. The normal apical organelle acidification raises the possibility that Rbc3α selectively regulates synaptic vesicles and might explain why the mutant animal's morphology is not obviously perturbed. Additionally, we observed normal polarization of the cytosolic V1 component of the V-ATPase to the plasma membrane surface of ionocytes, which supports the argument that the V-ATPase might be selectively targeted by Rbc3α in a compartment specific manner (note that we detected the *rbc3α* transcript in the skin of larvae containing several cell types including ionocytes). This finding also raises a larger question about how a cell might

precisely regulate one set of organelles without changing V-ATPase activity throughout the cell.

How might this differential regulation of the V-ATPase occur? First, it is necessary to know that while the V-ATPase is widely utilized by a variety of intracellular organelles, including lysosomes, endosomes, the Golgi, the ER and secretory vesicles (Forgac et al., 2007), there is precedence for differential regulation by a variety of mechanisms, including trafficking (Oehlke et al., 2010), ionic exchange (Goh et al., 2011), and sorting of gene- and splice- isoforms of specific subunits of the V-ATPase (Morel et al., 2003, Poea et al., 2006). With regard to the latter - regulation of the isoforms - the membrane subunit V0A is encoded by 4 genes in mammals (2 in zebrafish) and the neuronal-expressed V0A1 isoform has alternative splicing that controls where the V-ATPase resides (Poea et al., 2006): V0 A2 accumulates in the Golgi, A1-I in the axons, and A1-IV in both distal dendrites and axons. Because Rbc3α interacts with V0A1 (Li et al., 2012), it might preferentially regulate the assembly of V0A1-containing complexes. To test this prediction, we would examine whether exogenously expressed V0A1a and V0A1b proteins differentially distribute within the hair cell. V0A1a appeared to reside within the synaptic vesicles when exogenously expressed (See Chapter 4). Furthermore, we could test if over-expression of either isoform compensates for the loss of Rbc3α, though we would need to generate stable transgenic animals.

*Rbc3α does not organize the hair-cell synapse*

Previous work has shown that the Rbc3 complex associates with synaptic vesicles (Nagano et al., 2002, Kawabe et al., 2003). The peripheral membrane complex associates with synaptic vesicles by an unknown mechanism though we found that the N-terminal half of the Rbc3α is sufficient for the protein's translocation to synaptic regions of the hair cell. Rab3 GEP directly binds Rbc3β from the synaptic vesicle fraction, though it is mainly recovered from the synaptic soluble (cytosolic) fraction (Nagano et al., 2002). These findings suggest that the binding of Rab3 GEP to Rbc3 is temporally regulated and that Rbc3 likely brings Rab3 GEP to the vesicle. It was suggested that the Rbc3 complex could act as a synaptic vesicle scaffold upon which Rab3 is regulated. The molecular linkage among Rbc3, Rab3A and Rab3 GEP is important because these molecules may regulate $Ca^{2+}$-dependent exocytosis (Wang et al., 1997).

In our study we find that synaptic vesicles are normally trafficked in the mutant *stardust* to the base of hair cells and the efferent termini of the lateral-line nerve. Additionally, the levels of Rab3 and Vglut3 were similar in mutants, and pre- and post-synaptic components were normally juxtaposed, indicating normal synaptic connectivity. We also found no evidence for punctate Rab3 staining at the base of hair cells, which was present in isolated chicken hair cells (Uthaiah and Hudspeth 2010). The chicken study led to the conjecture that Rab3 organizes the ribbon synapse (Graf et al., 2009), or brings synaptic vesicles to ribbon bodies. Our findings may reflect species variation, or different antibodies used for labeling Rab3; we used a pan-Rab3 antibody versus the chicken study

that used a Rab3A isoform antibody. Our findings do not rule out the possibility that Rab3 is important for synaptic organization of the hair cell, but if it is important, it is through a Rbc3-independent mechanism.

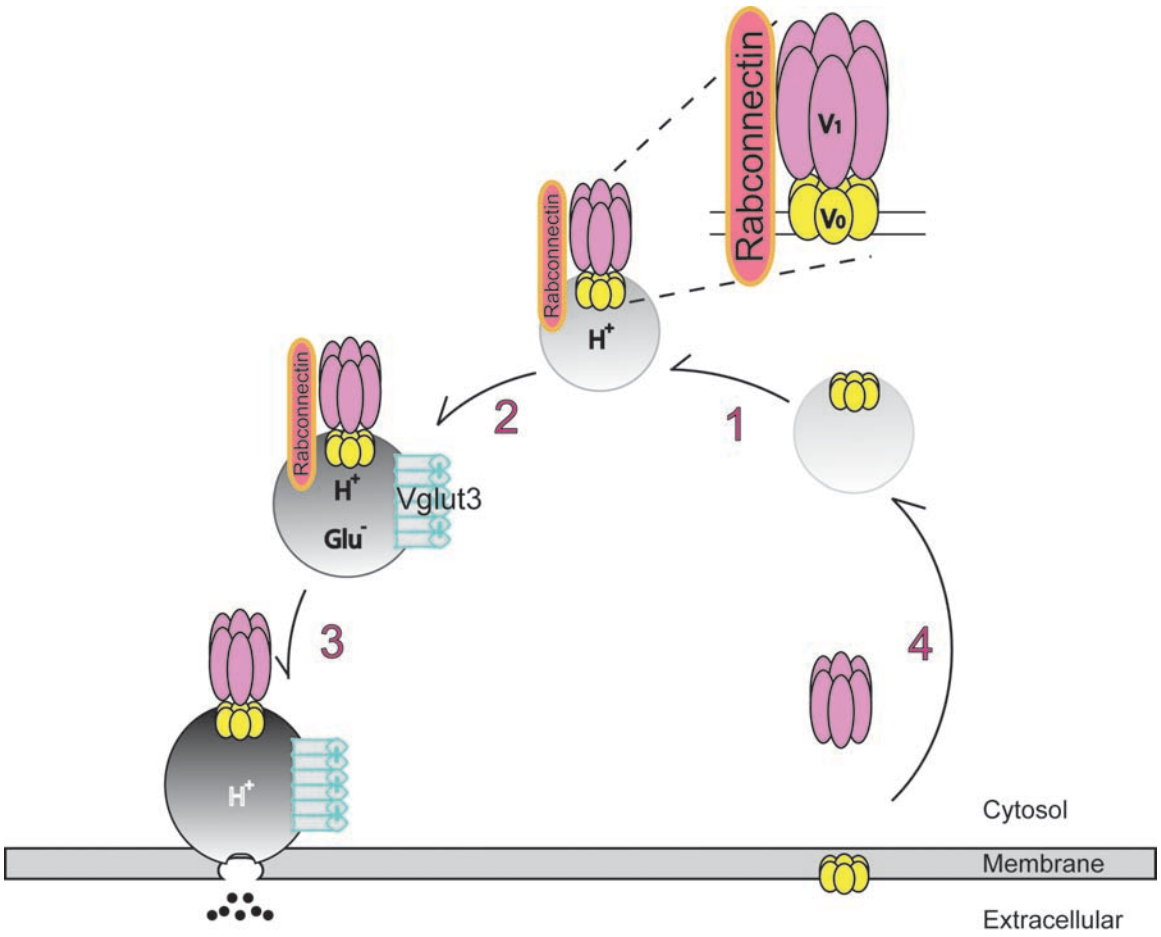


Figure 5.1 Rbc3α at the hair-cell synapse

Step 1: The hair-cell synaptic vesicle lacks a fully assembled V-ATPase holoenzyme membrane (V0 sector depicted in yellow). The Rabconnectin3 complex transiently associates with the synaptic vesicle and bridges the V1 cytosolic sector (depicted in lavender) with the V0 membrane sector to form the holoenzyme. The fully assembled V-ATPase then proceeds to pumps proton into the lumen of the synaptic vesicle by consuming ATP. Step 2: The acidified synaptic vesicle has established a proton electro-chemical gradient that is the driving for neurotransmitter glutamate transport by Vglut3. Step 3. Voltage-gated

calcium channels (not shown) that are clustered at the synapse slowly open, allowing the entry of $Ca^{2+}$ that triggers synaptic vesicle release and spilling of neurotransmitter contents into the synaptic cleft. Step 4. Through vesicle retrieval mechanisms, the process of vesicle filling is renewed. With regard to this study, it is not known whether the V-ATPase remains assembled on the plasma membrane after vesicular release, but there is evidence that it alkanizes cytosolic pH after exocytosis (Zhang et al., 2010)

## References:

Abreu BJ, Guimaraes M, Uliana LC, Vigh J, von Gersdorff H, Prado MA, Guatimosim C (2008) Protein kinase C modulates synaptic vesicle acidification in a ribbon type nerve terminal in the retina. Neurochemistry International 53: 155-164.

Baier H, Klostermann S, Trowe T, Karlstrom RO, Nüsslein-Volhard C, Bonhoeffer F (1996). Genetic dissection of the retinotectal projection. Development;123:415-25.

Bang PI, Yelick PC, Malicki JJ, Sewell WF (2002). High-throughput behavioral screening method for detecting auditory response defects in zebrafish. J Neurosci Methods.;118(2):177-87.

Binnington KC, Lane NJ (1982) Presence of T-bars, intramembranous particle arrays and exocytotic profiles in neuroendocrine terminals of an insect  Tissue Cell; 14: 463–474

Bolte S and Cordelières FP (2006) A guided tour into subcellular colocalization analysis in light microscopy. J Microsc 224: 213-32.

Buck LM, Winter MJ, Redfern WS, Whitfield TT (2012). Ototoxin-induced cellular damage in neuromasts disrupts lateral line function in larval zebrafish. Hear Res.;284(1-2):67-81.

Buran BN, Strenzke N, Neef A, Gundelfinger ED, Moser T, and Liberman MC (2010) Onset coding is degraded in auditory nerve fibers from mutant mice lacking synaptic ribbons. J. Neurosci. 30, 7587–7597.

Burgess HA, Granato M (2008). The neurogenic frontier - - lessons from misbehaving zebrafish. Brief Funct Genomic Proteomic;7(6):474-82. Review.

Dambly-Chaudière C, Sapède D, Soubiran F, Decorde K, Gompel N, Ghysen A (2003). The lateral line of zebrafish: a model system for the analysis of morphogenesis and neural development in vertebrates. Biol Cell.;95(9):579-87. Review.

Di Giovanni J, Boudkkazi S, Mochida S, Bialowas A, Samari N, Lévêque C, Youssouf F, Brechet A, Iborra C, Maulet Y, Moutot N, Debanne D, Seagar M, El Far, O (2010) V-ATPase membrane sector associates with synaptobrevin to modulate neurotransmitter release. Neuron 67: 268-79.

Dou H, Finberg K, Cardell EL, Lifton R, and Choo D (2003) Mice lacking the B1 subunit of H+ -ATPase have normal hearing. Hear Res 180: 76-84.

Edwards RH (2007) The neurotransmitter cycle and quantal size. Neuron 55: 835-58.

Einhorn Z, Trapani JG, Liu Q, Nicolson T (2012). Rabconnectin3α promotes stable activity of the H+ pump on synaptic vesicles in hair cells. J Neurosci.;32(32):11144-56.

Finberg KE, Wagner CA, Bailey MA, Paunescu TG, Breton S, Brown D, Giebisch G, Geibel JP, and Lifton RP (2005) The B1-subunit of the H(+) ATPase is required for maximal urinary acidification. Proc Natl Acad Sci U S A 102: 13616-21.

Forgac FM (2007). Vacuolar ATPases: rotary proton pumps in physiology and pathophysiology. Nat Rev Mol Cell Biol.; 8(11):917-29. Review.

Fremeau RT Jr, Burman J, Qureshi T, Tran CH, Proctor J, Johnson J, Zhang H, Sulzer D, Copenhagen DR, Storm-Mathisen J, Reimer RJ, Chaudhry FA, and Edwards RH (2002) The identification of vesicular glutamate transporter 3 suggests novel modes of signaling by glutamate. Proc Natl Acad Sci U S A 99: 14488-93.

Fukui K, Sasaki T, Imazumi K, Matsuura Y, Nakanishi H, Takai Y (1997). Isolation and characterization of a GTPase activating protein specific for the Rab3 subfamily of small G proteins. J Biol Chem.;272(8):4655-8.

Ghysen A, Dambly-Chaudière C (2007). The lateral line microcosmos. Genes Dev.;21(17):2118-30. Review.

Gillespie PG, Hudspeth AJ (1999). High-purity isolation of bullfrog hair cells and topological localization of constituent proteins. J Cell Biol.;112(4):625-40.

Glowatzki E and Fuchs PA (2002) Transmitter release at the hair cell ribbon synapse. Nature Neuroscience 5: 147-154.

Goh GY, Huang H, Ullman J, Borre L, Hnasko TS, Trussell LO, and Edwards RH (2011) Presynaptic regulation of quantal size: K+/H+ exchange stimulates vesicular glutamate transport. Nat Neurosci 14: 1285-92.

Graf ER, Daniels RW, Burgess RW, Schwarz TL, and DiAntonio A (2009) Rab3 dynamically controls protein composition at active zones. Neuron 64: 663-77.

Granato M, van Eeden FJ, Schach U, Trowe T, Brand M, Furutani-Seiki M, Haffter P, Hammerschmidt M, Heisenberg CP, Jiang YJ, Kane DA, Kelsh RN, Mullins MC, Odenthal J, Nüsslein-Volhard C (1996). Genes controlling and mediating locomotion behavior of the zebrafish embryo and larva. Development;123:399-413.

Hiesinger PR, Fayyazuddin A, Mehta SQ, Rosenmund T, Schulze KL, Zhai RG, Verstreken P, Cao Y, Zhou Y, Kunz J, and Bellen HJ (2005) The v-ATPase V0 subunit a1 is required for a late step in synaptic vesicle exocytosis in Drosophila. Cell 121: 607-20.

Higgs DM, Souza MJ, Wilkins HR, Presson JC, Popper AN (2002). Age- and size-related changes in the inner ear and hearing ability of the adult zebrafish (Danio rerio). J Assoc Res Otolaryngol. 2002 Jun;3(2):174-84.

Horng J, Lin L, and Hwang P (2009) Functional regulation of H+-ATPase-rich cells in zebrafish embryos acclimated to an acidic environment. Am J Physiol Cell Physiol 296: C682-92.

Hurtado-Lorenzo A, Skinner M, El Annan J, Futai M, Sun-Wada G, Bourgoin S, Casanova J, Wildeman A, Bechoua S, Ausiello DA, Brown D, and Marshansky V (2006) V-ATPase interacts with ARNO and Arf6 in early endosomes and regulates the protein degradative pathway. Nat Cell Biol 8: 124-36.

Ikeda A, Naggert JK, Nishina PM (2002).Genetic modification of retinal degeneration in tubby mice. Exp Eye Res.;74(4):455-61.

Kane PM (2006) The where, when, and how of organelle acidification by the yeast vacuolar H+-ATPase. Microbiol Mol Biol Rev 70: 177-91.

Karet FE, Finberg KE, Nelson RD, Nayir A, Mocan H, Sanjad SA, Rodriguez-Soriano J, Santos F, Cremers CW, Di Pietro A, Hoffbrand BI, Winiarski J, Bakkaloglu A, Ozen S, Dusunsel R, Goodyer P, Hulton SA, Wu DK, Skvorak AB, Morton CC, Cunningham MJ, Jha V, and Lifton RP (1999) Mutations in the gene encoding B1 subunit of H+-ATPase cause renal tubular acidosis with sensorineural deafness. Nat Genet 21: 84-90.

Kawabe H, Sakisaka T, Yasumi M, Shingai T, Izumi G, Nagano F, Deguchi-Tawarada M, Takeuchi M, Nakanishi H, and Takai Y (2003) A novel rabconnectin-3-binding protein that directly binds a GDP/GTP exchange protein for Rab3A small G protein implicated in Ca(2+)-dependent exocytosis of neurotransmitter. Genes Cells 8: 537-46.

Kimmel CB, Patterson J, Kimmel RO (1974). The development and behavioral characteristics of the startle response in the zebra fish. Dev Psychobiol.;7(1):47-60.

Kindt KS, Finch G, Nicolson T (2012). Kinocilia mediate mechanosensitivity in developing zebrafish hair cells. Dev Cell.;23(2):329-41.

Kohashi T, Oda Y(2008). Initiation of Mauthner- or non-Mauthner-mediated fast escape evoked by different modes of sensory input. J Neurosci.; 28(42):10641-53.

Korn H, Faber DS (2005). The Mauthner cell half a century later: a neurobiological model for decision-making? Neuron;47(1):13-28. Review.

Kwan KM, Fujimoto E, Grabher C, Mangum BD, Hardy ME, Campbell DS, Parant JM, Yost HJ, Kanki JP, and Chien C (2007) The Tol2kit: a multisite gateway-based construction kit for Tol2 transposon transgenesis constructs. Dev Dyn 236: 3088-99.

Lafourcade C, Sobo K, Kieffer-Jaquinod S, Garin J, and van der Goot FG (2008) Regulation of the V-ATPase along the endocytic pathway occurs through reversible subunit association and membrane localization. PLoS One 3: e2758.

Leibovici M, Safieddine S, and Petit C (2008) Mouse models for human hereditary deafness. Curr Top Dev Biol 84: 385-429.

Lenzi D, Runyeon JW, Crum J, Ellisman MH, Roberts WM (1999). Synaptic Vesicle Populations in Saccular Hair Cells Reconstructed by

Electron Tomography. J Neurosci. 1;19(1):119-32.

Li G, Keen E, Andor-Ardo D, Hudspeth AJ, von Gersdorf H (2009) The unitary event underlying multiquantal EPSCs at a hair cell's ribbon synapse. J Neurosci 29: 7558-7568.

Li KW, Chen N, Klemmer P, Koopmans F, Karupothula R, Smit AB (2012). Identifying true protein complex constituents in interaction proteomics: the example of the DMXL2 protein complex. Proteomics. 2012 Aug;12(15-16):2428-32.

Liégeois S, Benedetto A, Garnier J, Schwab Y, and Labouesse M (2006) The V0-ATPase mediates apical secretion of exosomes containing Hedgehog-related proteins in Caenorhabditis elegans. J Cell Biol 173: 949-61.

Mahoney TR, Liu Q,Itoh T, Luo S, Hadwiger G, Vincent R, Wang Z, Fukuda M and Nonet ML (2006) Regulation of Synaptic Transmission by RAB-3 and RAB-27 in Caenorhabditis elegans. MBOC Vol. 17, 2617–2625.

McDermott BM Jr, Baucom JM, Hudspeth AJ (2007). Analysis and functional evaluation of the hair-cell transcriptome. PNAS 10;104(28):11820-5.

Mo W, Chen F, Nechiporuk A, Nicolson T (2010).Quantification of vestibular-induced eye movements in zebrafish larvae. BMC Neurosci.;11:110.

Mo W, Nicolson T (2011). Both pre- and postsynaptic activity of Nsf prevents degeneration of hair-cell synapses. PLoS One. 2011;6(11):e27146.

Morel N, Dedieu JC, Philippe JM (2003).Specific sorting of the a1 isoform of the V-H+ATPase a subunit to nerve terminals where it associates with both synaptic vesicles and the presynaptic plasma membrane.J Cell Sci.;116(Pt 23):4751-62.

Nagano F, Kawabe H, Nakanishi H, Shinohara M, Deguchi-Tawarada M, Takeuchi M, Sasaki T, and Takai Y (2002) Rabconnectin-3, a novel protein that binds both GDP/GTP exchange protein and GTPase-activating protein for Rab3 small G protein family. J Biol Chem 277: 9629-

32.

Nagiel A, Andor-Ardo D, Hudspeth AJ (2008) Specificity of afferent synapses onto plane-polarized hair cells in the posterior lateral line of the zebrafish. Jneurosci 28: 8442-8453.

Nicolson T, Rüsch A, Friedrich RW, Granato M, Ruppersberg JP, and Nüsslein-Volhard C (1998) Genetic analysis of vertebrate sensory hair cell mechanosensation: the zebrafish circler mutants. Neuron 20: 271-83.

Nicolson T (2005). The genetics of hearing and balance in zebrafish. Annu Rev Genet. 2005;39:9-22. Review.

Niwa S, Tanaka Y, Hirokawa N (2008). KIF1Bbeta- and KIF1A-mediated axonal transport of presynaptic regulator Rab3 occurs in a GTP-dependent manner through DENN/MADD. Nat Cell Biol.;10(11):1269-79.

Nouvian R, Beutner D, Parsons TD, and Moser T (2006) Structure and function of the hair cell ribbon synapse. J Membr Biol 209: 153-65.

Nuckels RJ, Ng A, Darland T, and Gross JM (2009) The vacuolar-ATPase complex regulates retinoblast proliferation and survival, photoreceptor morphogenesis, and pigmentation in the zebrafish eye. Invest Ophthalmol Vis Sci 50: 893-905.

Obholzer N, Wolfson S, Trapani JG, Mo W, Nechiporuk A, Busch-Nentwich E, Seiler C, Sidi S, Söllner C, Duncan RN, Boehland A, and Nicolson T (2008) Vesicular glutamate transporter 3 is required for synaptic transmission in zebrafish hair cells. J Neurosci 28: 2110-8.

Oehlke O, Martin HW, Osterberg N, and Roussa E (2011) Rab11b and its effector Rip11 regulate the acidosis-induced traffic of V-ATPase in salivary ducts. J Cell Physiol 226: 638-51.

Pavlos NJ, Grønborg M, Riedel M, Chua JJE, Boyken J, Kloepper TH, Urlaub H, Rizzoli SO and Jahn R (2010) Quantitative Analysis of Synaptic Vesicle Rabs Uncovers Distinct Yet Overlapping Roles for Rab3a and Rab27b in $Ca^{2+}$ -Triggered Exocytosis. J. Neurosci. 30(40), 13441–13453.

Peri F and Nüsslein-Volhard C (2008) Live imaging of neuronal degradation by microglia reveals a role for v0-ATPase a1 in phagosomal fusion in vivo. Cell 133: 916-27.

Pittman AJ, Gaynes JA, Chien CB (2010). nev (cyfip2) is required for retinal lamination and axon guidance in the zebrafish retinotectal system. Dev Biol.;344(2):784-94.

Poëa-Guyon S, Amar M, Fossier P, Morel N (2006). Alternative splicing controls neuronal expression of v-ATPase subunit a1 and sorting to nerve terminals. J Biol Chem.;281(25):17164-72.

Prober DA, Rihel J, Onah AA, Sung RJ, Schier AF (2006). Hypocretin/orexin overexpression induces an insomnia-like phenotype in zebrafish. J Neurosci.;26(51):13400-10.

Ramakrishnan NA, Drescher MJ, Drescher DG (2009) Direct interaction of otoferlin with syntaxin 1A, SNAP-25, and the L-type voltage-gated calcium channel Cav1.3. J Biol Chem.16;284(3):1364-72.

Riley BB, Moorman SJ (2000). Development of utricular otoliths, but not saccular otoliths, is necessary for vestibular function and survival in zebrafish. J Neurobiol.;43(4):329-37.

Ruel J, Emery S, Nouvian R, Bersot T, Amilhon B, Van Rybroek JM, Rebillard G, Lenoir M, Eybalin M, Delprat B, Sivakumaran TA, Giros B, El Mestikawy S, Moser T, Smith RJH, Lesperance MM, and Puel J (2008) Impairment of SLC17A8 encoding vesicular glutamate transporter-3, VGLUT3, underlies nonsyndromic deafness DFNA25 and inner hair cell dysfunction in null mice. Am J Hum Genet 83: 278-92.

Rutherford M, Chapochnikov N, and Moser T (2012) Spike Encoding of Neurotransmitter Release Timing by Spiral Ganglion Neurons of the Cochlea. Jneurosci 32: 4773-4789.

Sakisaka T and Takai Y (2005) Purification and properties of rabconnectin-3. Methods Enzymol 403: 401-7.

Sautin YY, Lu M, Gaugler A, Zhang L, and Gluck SL (2005) Phosphatidylinositol 3-kinase-mediated effects of glucose on vacuolar H+-ATPase assembly, translocation, and acidification of intracellular compartments in renal epithelial cells. Mol Cell Biol 25: 575-89.

Schenck S, Wojcik SM, Brose N, and Takamori S (2009) A chloride conductance in VGLUT1 underlies maximal glutamate loading into synaptic vesicles. Nat Neurosci 12: 156-62.

Schmitz F, Königstorfer A, Südhof TC (2000) RIBEYE, a component of synaptic ribbons: a protein's journey through evolution provides insight into synaptic ribbon function. Neuron; 28(3):857-72.

Seal RP, Akil O, Yi E, Weber CM, Grant L, Yoo J, Clause A, Kandler K, Noebels JL, Glowatzki E, Lustig LR, and Edwards RH (2008)

Sensorineural deafness and seizures in mice lacking vesicular glutamate transporter 3. Neuron 57: 263-75.

Seol JH, Shevchenko A, Shevchenko A, and Deshaies RJ (2001) Skp1 forms multiple protein complexes, including RAVE, a regulator of V-ATPase assembly. Nat Cell Biol 3: 384-91.

Sethi N, Yan Y, Quek D, Schupbach T, and Kang Y (2010) Rabconnectin-3 is a functional regulator of mammalian Notch signaling. J Biol Chem 285: 34757-64.

Sheets L, Trapani JG, Mo W, Obholzer N, and Nicolson T (2011) Ribeye is required for presynaptic Ca(V)1.3a channel localization and afferent innervation of sensory hair cells. Development 138: 1309-19.

Shiao J, Lin L, Horng J, Hwang P, and Kaneko T (2005) How can teleostean inner ear hair cells maintain the proper association with the accreting otolith?. J Comp Neurol 488: 331-41.

Sidi S, Busch-Nentwich E, Friedrich R, Schoenberger U, Nicolson T (2004). Gemini encodes a zebrafish L-type calcium channel that localizes at sensory hair cell ribbon synapses. J Neurosci.;24(17):4213-23.

Sipos G, Brickner JH, Brace EJ, Chen L, Rambourg A, Kepes F, and Fuller RS (2004) Soi3p/Rav1p functions at the early endosome to regulate endocytic trafficking to the vacuole and localization of trans-Golgi network transmembrane proteins. Mol Biol Cell 15: 3196-209.

Smardon AM, Tarsio M, and Kane PM (2002) The RAVE complex is essential for stable assembly of the yeast V-ATPase. J Biol Chem 277: 13831-9.

Snellman J, Mehta B, Babai N, Bartoletti TM, Akmentin W, Francis A, Matthews G, Thoreson W, Zenisek D (2011). Acute destruction of the synaptic ribbon reveals a role for the ribbon in vesicle priming. Nat Neurosci.;14(9):1135-41.Smardon AM and Kane PM (2007) RAVE is essential for the efficient assembly of the C subunit with the vacuolar H(+)-ATPase. J Biol Chem 282: 26185-94.

Stover EH, Borthwick KJ, Bavalia C, Eady N, Fritz DM, Rungroj N, Giersch ABS, Morton CC, Axon PR, Akil I, Al-Sabban EA, Baguley DM, Bianca S, Bakkaloglu A, Bircan Z, Chauveau D, Clermont M, Guala A, Hulton SA, Kroes H, Li Volti G, Mir S, Mocan H, Nayir A, Ozen S, Rodriguez Soriano J, Sanjad SA, Tasic V, Taylor CM, Topaloglu R, Smith AN, and Karet FE (2002) Novel ATP6V1B1 and ATP6V0A4 mutations in autosomal recessive distal renal tubular acidosis with new evidence for hearing loss.

J Med Genet 39: 796-803.

Südhof TC (2004) The synaptic vesicle cycle. Annu Rev Neurosci 27: 509-47.

Sun-Wada G, Toyomura T, Murata Y, Yamamoto A, Futai M, and Wada Y (2006) The a3 isoform of V-ATPase regulates insulin secretion from pancreatic beta-cells. J Cell Sci 119: 4531-40.

Söllner C, Schwarz H, Geisler R, and Nicolson T (2004) Mutated otopetrin affects the genesis of otoliths and the localization of Starmaker in zebrafish. Development Genes and Evolution 214: 582-590.

Takamori S, Holt M, Stenius K, Lemke EA, Grønborg M, Riedel D, Urlaub H, Schenck S, Brügger B, Ringler P, Müller SA, Rammner B, Gräter F, Hub JS, De Groot BL, Mieskes G, Moriyama Y, Klingauf J, Grubmüller H, Heuser J, Wieland F, Jahn R (2006) Molecular anatomy of a trafficking organelle. Cell. 2006 Nov 17;127(4):831-46.

Tanaka M, Miyoshi J, Ishizaki H, Togawa A, Ohnishi K, Endo K, Matsubara K, Mizoguchi A, Nagano T, Sato M, Sasaki T, Takai Y (2001). Role of Rab3 GDP/GTP exchange protein in synaptic vesicle trafficking at the mouse neuromuscular junction. Mol Biol Cell.;12(5):1421-30.

Thisse B, Pflumio S, Fürthauer M, Loppin B, Heyer V, Degrave A, Woehl R, Lux A, Steffan T, Charbonnier XQ and Thisse C (2001) Expression of the zebrafish genome during embryogenesis. ZFIN Direct Data Submission (http://zfin.org).

Toei M, Saum R, and Forgac M (2010) Regulation and isoform function of the V-ATPases. Biochemistry 49: 4715-23.

Trapani JG, Obholzer N, Mo W, Brockerhoff SE, and Nicolson T (2009) Synaptojanin1 is required for temporal fidelity of synaptic transmission in hair cells. PLoS Genet 5: e1000480.

Trapani JG and Nicolson T (2010) Physiological recordings from zebrafish lateral-line hair cells and afferent neurons. Methods Cell Biol 100:219-31.

Trapani J and Nicolson T (2011) Mechanism of spontaneous activity in afferent neurons of the zebrafish lateral-line organ. J Neurosci 31: 1614-23.

Trombetta S, Ebersold M, Garrett W, Pypaert M, and Mellman, I (2003) Activation of lysosomal function during dendritic cell maturation. Science 299: 1400-3.

Uthaiah C and Hudspeth AJ (2010). Molecular Anatomy of the Hair Cell's Ribbon Synapse. J Neurosci;30(37):12387-99.

Wada M, Nakanishi H, Satoh A, Hirano H, Obaishi H, Matsuura Y, Takai Y (1997).Isolation and characterization of a GDP/GTP exchange protein specific for the Rab3 subfamily small G proteins. J Biol Chem.;272(7):3875-8.

Wall MA, Coleman DE, Lee E, Iñiguez-Lluhi JA, Posner BA, Gilman AG, Sprang SR (1995). The structure of the G protein heterotrimer Gi alpha 1 beta 1 gamma 2. Cell. 1995 Dec 15;83(6):1047-58.

Wang Y, Okamoto M, Schmitz F, Hofmann K, Südhof TC (1997). Rim is a putative Rab3 effector in regulating synaptic-vesicle fusion. Nature.;388(6642):593-8.

Wangemann P (2006) Supporting sensory transduction: cochlear fluid homeostasis and the endocochlear potential. J Physiol 576: 11-21.

Weisz C, Glowatzki W, and Fuchs F (2009) The postsynaptic function of type II cochlear afferents. Nature 461: 1126-1129.

Westerfield, M. (2000). The zebrafish book. A guide for the laboratory use of zebrafish (Danio rerio). 4th ed., Univ. of Oregon Press, Eugene.

Wittig JH Jr and Parsons TD (2008) Synaptic ribbon enables temporal precision of hair cell afferent synapse by increasing the number of readily releasable vesicles: a modeling study. J Neurophysiol 100: 1724-39.

Yan Y, Denef N, and Schüpbach T (2009) The vacuolar proton pump, V-ATPase, is required for notch signaling and endosomal trafficking in Drosophila. Dev Cell 17: 387-402.

Yang Q, Li G, Singh SK, Alexander EA, and Schwartz JH (2006) Vacuolar H+ -ATPase B1 subunit mutations that cause inherited distal renal tubular acidosis affect proton pump assembly and trafficking in inner medullary collecting duct cells. J Am Soc Nephrol 17: 1858-66.

Zanazzi G and Matthews G (2009) The molecular architecture of ribbon presynaptic terminals. Mol Neurobiol 39: 130-48.

Zeddies DG and Fay RR (2005) Development of the acoustically evoked

behavioral response in zebrafish to pure tones. J Exp Biol 208: 1363-72.

Zenisek D, Davila V, Wan L, Almers W. (2003). Imaging calcium entry sites and ribbon structures in two presynaptic cells. J Neurosci. 2003 Apr 1;23(7):2538-48.

Zhang Z, Nguyen KT, Barrett EF, David G (2010).Vesicular ATPase Inserted into the Plasma Membrane of Motor Terminals by Exocytosis Alkalinizes Cytosolic pH and Facilitates Endocytosis Neuron.;68(6):1097-108.

Zottoli SJ (1977). Correlation of the startle reflex and Mauthner cell auditory responses in unrestrained goldfish. J Exp Biol.;66(1):243-54.